NTNU – Trondheim
Norwegian University of
Science and Technology

Fatigue Analysis of Column-Brace Connection in a Semi-submersible Wind Turbine

Ørjan Fredheim

Marine Technology
Submission date: June 2012
Supervisor: Torgeir Moan, IMT

Norwegian University of Science and Technology
Department of Marine Technology

NTNU Trondheim
Norwegian University of Science and Technology
Department of Marine Technology – Group of Marine Structures

MSC THESIS IN MARINE TECHNOLOGY

SPRING 2012

FOR

STUD.TECHN. Ørjan Fredheim
Fatigue Analysis of Column-Brace Connection in a Semi-submersible Wind Turbine
Utmattingsanalyse av søyle-stag forbindelse i en halvt-nedsenkbar vindturbin

Background

Semi-submersible floating wind turbines have been proposed for deep water offshore wind energy application. The hull structure of semi-submersibles consists of columns connected by braces, pontoons or beams and might involve complex column-brace joints, which could potentially be susceptible for fatigue damage due to high stress concentration. Both wind and wave actions can contribute to fatigue loads for a floating wind turbine. In order to estimate the fatigue damage in such connections, it is necessary to perform a global load and motion analysis in which simultaneous wind- and wave-induced dynamic responses of member forces in columns and braces are estimated and a local stress analysis with refined finite element model to obtain the stress concentration factor.

This MSc thesis work aims at performing a detailed fatigue analysis for the connections between columns and braces in a semi-submersible floating wind turbine, and should be carried out in cooperation with the PhD candidate Chenyu Luan at CeSOS, who will design a semi-submersible floater and perform and provide the long-term statistics of global responses.

Assignment

The following tasks should be addressed in the thesis:

1. Literature review on the design of column-brace connection of semi-submersible platform, methods for stress concentration calculation, methods for time-domain fatigue analysis.

2. Considering the NREL 5MW wind turbine as a reference turbine, a preliminary design of structural dimensions should be carried out for the column-brace joints at both the central column and the side columns. Typical stiffeners and bulkheads should be considered.

3. Local stress analysis of column-brace connection:
a) Establish a detailed and refined structural model of column-brace connection for estimation of stress concentration factor (SCF) under different unit loads.
b) Carry out linear structural analysis and identify the hot spot location. Determine the relationship between the applied unit load and the hot-spot stress.
c) Software Patran will be used for modelling and Abaqus will be used for linear structural analysis.

4. Fatigue damage calculation:

a) Based on the time series obtained from the global analysis and the SCFs, estimate the time series of hot-spot stress, based on a linear combination of the applied loads.
b) Use the rainflow cycle counting method (available in the Matlab toolbox WAFO) to obtain the effective stress ranges.
c) Use the design SN curves from DNV standards to estimate the fatigue life of the column-brace connections.

5. Conclude the work and give recommendations for future work on fatigue design of semi-submersible floating wind turbines.

In the thesis the candidate shall present his personal contribution to the resolution of problem within the scope of the thesis work.

Theories and conclusions should be based on mathematical derivations and/or logic reasoning identifying the various steps in the deduction.

The candidate should utilize the existing possibilities for obtaining relevant literature.

The thesis should be organized in a rational manner to give a clear exposition of results, assessments, and conclusions. The text should be brief and to the point, with a clear language. Telegraphic language should be avoided.

The thesis shall contain the following elements: A text defining the scope, preface, list of contents, summary, main body of thesis, conclusions with recommendations for further work, list of symbols and acronyms, reference and (optional) appendices. All figures, tables and equations shall be numerated.

The supervisor may require that the candidate, in an early stage of the work, present a written plan for the completion of the work. The plan should include a budget for the use of computer and laboratory resources that will be charged to the department. Overruns shall be reported to the supervisor.

The original contribution of the candidate and material taken from other sources shall be clearly defined. Work from other sources shall be properly referenced using an acknowledged referencing system.

The thesis shall be submitted in two copies as well as an electronic copy on a CD:

- Signed by the candidate
- The text defining the scope included
- In bound volume(s)
- Drawings and/or computer prints which cannot be bound should be organized in a separate folder.

Supervisors: Professor Torgeir Moan and Dr. Zhen Gao, NTNU

Torgeir Moan

Deadline: 10.06.12.

Preface

This report presents the work done for the Master Thesis in the Discipline of Marine Structural Engineering at NTNU, Trondheim. The thesis has been carried out individually in the Spring of 2012.

The main aim has been to establish a semi-submersible wind turbine local model brace-chord connection (joint) using PATRAN and ABAQUS to find stress concentration factors, and calculate fatigue life on this using MATLAB. Meanwhile, a dynamic response analysis has been carried out for different sea states, to supply information needed to calculate the fatigue life of the joint. This has been carried out by Chenyu Luan. The finite element modelling in PATRAN, and pre- and post-processing in MATLAB have been the most time consuming subjects, and consumed more time than expected initially.

In the fall of 2011, I did a global dynamic response analyses on a similar semi-submersible wind turbine in my pre-project. It has been very rewarding to continue with a very similar structure, but with a completely different objective. I think the combination of global and local studies of a semi-submersible wind turbine has given me a good overview of some of the challenges in marine engineering.

I would like to thank Torgeir Moan for the exciting and relevant thesis suggestion and for making this thesis possible, Zhen Gao for his always open door and great effort to always give high quality answers to all of my questions, Chenyu Luan for his continuous motivation and great spirits and Martin Storheim for his contribution to my understanding of PATRAN.

I would like to give extra thanks to Chenyu Luan and Zhen Gao for a rewarding and exciting partnership. I have rarely worked with such devoted and intelligent people. Without you, this thesis would have never been possible. Also thanks for our weekly discussions, I will miss working with you both.

Last, but not least, I would like to thank my family.

Trondheim, June 9, 2012

Ørjan Fredheim

Summary

The importance of offshore renewable energy from wind is expected to increase in the future. Most offshore wind turbines are currently installed in shallow water up to 50 meter water depth on bottom mounted substructures. To harvest more wind energy at deeper waters, offshore floating support structures are needed. Semi-submersible floating wind turbine is one of the proposed floating concepts. Under simultaneous wind and wave loads, fatigue might be an important design consideration. Study of fatigue for such structures is thought to contribute to a better understanding of offshore wind turbines.

A local part of a semi-submersible wind turbine was studied. The column-brace connection, or joint, connected a wind turbine tower to a triangular semi-submersible floater. Design, stress concentration factors and fatigue damage of the part were the main topics. To calculate stress concentration factors and fatigue damage, dynamic response analyses and finite element modelling were performed. Only the fatigue limit state was considered.

Three different column-brace connection designs were analysed. For the initial design, the stress concentration factors generally were way too large - especially for out-of-plane action. For the third design a horizontal bulkhead at the brace centreline was added. This modification decreased the stress concentrations by a maximum of over 90% for out-of-plane action. The modification was only carried out for brace 1.

A long-term fatigue approximation with distribution of mean wind speed in the northern North Sea was considered, while the expected significant wave height and spectral peak period for a given mean wind speed were used, to reduce the simulation effort. The critical fatigue damage was observed for brace 2, with a life time of less than a year. For brace 1 the lowest life time was several hundred years, meaning a conservative design. By reducing and optimizing the brace thickness, one could reduce such conservatism. The critical hot-spot-stresses were found at the crown toe and heel for both brace 1 and brace 2. All fatigue calculations included a design fatigue factor of 3.

The modification of brace 1 with horizontal bulkheads as additional stiffening reduced the stress concentrations significantly, and increased the fatigue life considerably. Brace 2 still needs to be modified to decrease the stress concentrations, and thus increase the fatigue life.

Sammendrag (Norwegian Summary)

Betydningen av offshore fornybar energi fra vind forventes å øke i fremtiden. De fleste offshore vindmøller er bunnmontert på grunt vann opp til 50 meters havdyp. For å høste mer vindkraft på dypere vann, er offshore flytende støttestrukturer nødvendig. Halvt nedsenkbare flytende vindturbin er en av de foreslåtte flytende konseptene. Under belastninger fra både vind og bølger, kan utmatting være en viktig designvurdering. Studier av utmatting for slike strukturer er tenkt å bidra til en bedre forståelse av offshore vindturbiner.

En lokal del av en halvt nedsenkbar vindmølle ble studert. Kolonne-stag-tilkoblingen kobler et vindturbintårn til en halvt nedsenkbar plattform. Design, spenningskonsentrasjonsfaktorer og utmatting var de viktigste temaene. For å beregne spenningskonsentrasjonsfaktorer og utmatting, ble dynamiske respons analyser og finite element modellering utført.

Tre forskjellige kolonne-stag forbindelser ble analysert. For det første designet, var spenningskonsentrasjonsfaktorerene generelt altfor store - spesielt for ut-av-plan utbøyning. For det tredje designet ble et horisontal skott på stagets midtlinje lagt til. Denne endringen reduserte spenningskonsentrasjonene med maksimalt over 90 % for ut-av-plan utbøyning. Modifikasjonen ble bare utført for stag nummer 1.

En langsiktig utmattingsanalyse med gjennomsnittlig vindhastighet fra den nordlige Nordsjøen ble vurdert, mens forventet signifikant bølgehøyde og spektral peak periode for en gitt vindhastighet ble brukt, for å redusere simuleringstiden. Den kritiske utmattingsskaden ble observert for stag 2, med en levetid på mindre enn ett år. For stag 1 var lavest levetid flere hundre år, noe som betyr en konservativ design. Ved å redusere og optimalisere stagenes platetykkelse, kan man redusere slik konservatisme. De kritiske hot-spot-påkjenninger ble funnet på kronene for både stag 1 og stag to. Alle utmattingsberegninger inkluderte en designutmattingsfaktor på 3.

Modifikasjonen av stag 1 med horisontale skott reduserte spenningskonsentrasjonene betydelig, og økte utmattinsliv betraktelig. Stag 2 må likevel bli endret for å redusere spenningskonsentrasjonen.

Contents

List of Figures

List of Tables

Nomenclature

$\Delta\sigma_1$	Principal stress in direction 1
$\Delta\sigma_2$	Principal stress in direction 2
α	Detail classification dependent factor for effective stress calculation
α	Parameter in Weibull distribution
α_h	Parameter in Weibull PDF for h
α_w	Parameter in Weibull PDF for W
β	Parameter in Weibull distribution
β_h	Parameter in Weibull PDF for h
β_w	Parameter in Weibull PDF for W
$\Delta\sigma_\perp$	Stress perpendicular to the weld
$\Delta\sigma$	Stress range
$\Delta\tau_\parallel$	Shear stress parallel to weld
$\Delta\sigma_{Eff}$	Effective hot spot stress
ω	Angular frequency [rad/s]
σ	Stress amplitude
σ_I	Turbulence standard deviation
σ_{max}	Maximum Stress
σ_N	Nominal Stress
A	Cross-sectional area of brace
a	Constant value in S-N curve
a	Left limit in integration of Weibull PDF block for the wind speed
b	Right limit in integration of Weibull PDF block for the wind speed

D	Fatigue Damage
d	Damage per second
$D(t)$	Total Damage at time t
D_b	Brace diameter
D_m	$\sum_{t_k \leq t} (\Delta\sigma)^m$
D_{tot}	Total fatigue damage
$E(H_s)$	Expected value of the significant wave height
$E(T_p)$	Expected value of the significant wave height
$F(W)$	CDF for the mean wind speed, W
F_i	Force unit load
F_{D_i}	Fatigue damage in sea state i
H	Hub Height [m]
h	Significant wave height [m]
H_s	Significant wave height [m]
I	Moment of inertia $[mm^4]$
I_{ref}	Expected value of the turbulence intensity at 15 m/s mean wind speed
IF	Influence Factor. [Pa/N] or [Pa/Nm]
k	Read out point
k	Thickness exponent used together with S-N curve
$L(t)$	Constant amplitude oscillating load
$log\bar{a}$	intercept of log N-axis by S-N curve $loga - 2S_{logN}$
$loga$	Intercept of mean S-N curve with the log N axis
log	The logarithmic function with base 10
m	Meter
m	Negative inverse slope of the S-N curve
m^3	metric volume
M_i	Moment unit load
M_{IP}	In-plane bending
M_{OP}	Out-of-plane bending
N	Axial force

N	Newton (force)
N	predicted number of cycles to failure for stress range $\Delta\sigma$
$N(\Delta\sigma)$	Number of cyles to failure at stress range $\Delta\sigma$
Nm	Newton-Meter (moment)
p_i	Probability of sea state i occurring
Pa	Pascal $[N/m^2]$
r_{in}	Inner radius of brace
r_{out}	Outer radius of brace
S_{logN}	standard deviation of log N.
sec	seconds
t	Plate thickness [mm]
t	Time
t	metric tons
t_f	Time to failure/fatigue life time
T_I	Turbulence intensity factor
T_p	Peak spectral period [s]
t_{ref}	reference thickness. For tubular joints the reference thickness is 32 mm
T_{sea}	Sea-state duration [s]
W	1-hour mean wind speed at 10 m aswl [m/s]
w	1-hour mean wind speed at 10 m aswl [m/s]
x	Distance from the load (perpendicular) to the ROP of interest
y	Maximum distance from the neutral axis
z	coordinate above sea level [m]
$\bar{T_p}(w,h)$	Expected value of the significant wave height
$f_W(w)$	PDF for mean wind speed, W
$f_{WH_sT_p}(w,h,t)$	Joint conditional PDF for mean wind speed, significant wave height and peak spectral period
*.odb	ABAQUS database file extension
ALS	Accidental limit state
aswl	**A**bove **s**ea **w**ater **l**evel
B1	Brace 1

B1C	Brace 1, chord side of weld
B2	Brace 2
B2C	Brace 2, chord side of weld
BXY	Brace-side of weld on brace X read-out point Y
C	Chord
CDF	Cumulative Distribution Function
CXY	Chord-side of weld on brace X read-out point Y
DFF	Design Fatigue Factor
DNV	Det norske Veritas
FEA	Finite Element Analysis
FEM	Finite Element Method
FLS	Fatigue limit state
G	Giga (10^9)
GPa	Giga-Pascal
IEC	International Electrotechnical Commission
JONSWAP	Joint North Sea Wave Project
LCX	Load Case X
Mega	10^6
MIT	Massachusetts Institute of Technology
MPa	Mega-Pascal
MPC	Multi-Purpose Constraint
MW	Mega-Watt
NREL	National Renewable Energy Laboratory
PDF	Probability Density Function
PM	Palmgreen-Miner
ROP	Read-out-point
S-N	Stress Cycle Curve (also known as the Wöhler Curve)
SCF	Stress Concentration Factor. Dimensionless factor
SLS	Serviceability limit state
STD	Standard Deviation

TLP Tension-Leg Platform

ULS Ultimate limit state

WAFO Wave Analysis for Fatigue and Oceanography

Chapter 1

Introduction

1.1 Background & Motivation

The importance of offshore renewable energy from wind is expected to increase in the future. There are numerous challenges associated with providing sufficient amount of clean energy and energy security.

According to the European Wind Energy Association, the International Energy Agency, the EU Ocean Energy Association and Greenpeace Advanced Energy, the 2050 targets for offshore wind and wave energy in Europe are approximately 460 and 188 GW, respectively. The international targets are approximately 2 and 4 times greater than the respective European targets.

Large wind turbines optimised to withstand rough weather and a corrosive environment are needed to reach the offshore wind power targets. Huge challenges are accompanied by the emerging status of offshore wind energy technologies, including development of concepts, design criteria, analytical methods to explore manufacturability, installability, operability, survivability, reliability and affordability. Experiments and in-service experience are necessary to validate the design and analyses. Research is needed to reduce the costs of offshore wind power, so that the technology becomes competitive. [Moan et al., 2011]

Most offshore wind turbines are currently installed in shallow water up to 50 meter water depth on bottom mounted substructures, including gravity bases, mono-piles and jackets. To harvest more wind energy at deeper waters, offshore floating support structures are needed [Robertson and Jonkman, 2011]. The first floating wind turbine prototypes are already being tested [Moan et al., 2011]. Several floating support platform configurations have been suggested, including

- Barge
- Semi-submersibles

- Spars
- Tension-leg platforms (TLP)

Recent concepts include the MIT/NREL TLP, the HyWind Spar, the ITI Energy Barge, the UMaine TLP, the Umaine semi-submersible, the Umaine Spar, (see [Robertson and Jonkman, 2011]) the Principle Power's WindFloat (5 MW, Semi), [PrinciplePower, 2012] and the Olav Olsen's HiPRWind (Semi), [Bard et al., 2012].

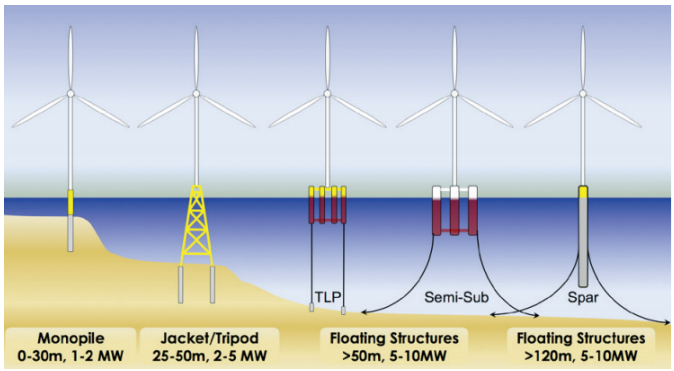

Figure 1.1: Concepts [Roddier et al., 2011]

Offshore wind structures are considered advantageous, as they are not visible from land, and do not impact the aesthetics of the landscape. Offshore wind currents are more frequent, stable and powerful, than their counterpart. Into the bargain, there are large areas available for wind farm installations, which is important for countries with limited land based area available.

Determining which one is the best concept depends on environmental conditions, has proved to be a demanding task [Luan, 2010, Lygren, 2010, Solberg, 2010]. It is thought that the study of fatigue of these structures is one of several topics that will contribute to a better understanding of offshore wind turbines.

1.2 Objectives

Fatigue on regular semi-submersibles are well documented, although it often is a case-to-case study. Fatigue on semi-submersible wind turbines, however, is less elaborated.

The objectives of this thesis are listed in the following:

1. Preliminary design of the semi-submersible wind turbine column-brace connections

2. Local stress analysis
    - Establish a detailed structural model of column-brace connection
    - Carry out linear static finite element analysis on the model
    - Find relation between applied unit load and hot-spot stress (stress concentration factor, SCF)
3. Fatigue damage calculation
    - Use established global response time series and SCFs to estimate the time series of hot spot stress
    - Estimate fatigue life of column-brace connection using DNV standard S-N curves

To calculate stress concentration factors and fatigue damage, dynamic response analyses and finite element modelling were carried out.

1.3 Method

The SESAM software package together with TDHMill were used to do the dynamic response analyses. This was done in time-domain, and therefore the fatigue analyses were also done in time-domain. The finite element programs PATRAN and ABAQUS were used to calculate SCFs. The commercial freeware MATLAB script package WAFO ([WAFO-group, 2000]) was used for the fatigue analysis, while all other necessary pre-processing, post-processing and programming was done in MATLAB.

42 PATRAN/ABAQUS analyses were conducted for the hot spot calculations, while 18 additional PATRAN/ABAQUS analyses were conducted for verification and sensitivity studies. 150 sea states were simulated for fatigue long term approximation, where each sea state produced 42 force time series. The time series together with the hot spot results were used for fatigue damage calculation.

Several software packages were used:

- Dynamic Response Analysis for Timeseries (SESAM, TDHMill)
- Finite Element Modelling for SCF (PATRAN)
- Finite Element Analysis for SCF (ABAQUS)
- Fatigue Damage Analysis (MATLAB/WAFO)
- Pre- and post-processing (MATLAB)

Normally, ULS, ALS and SLS (Ultimate-, accidental- and serviceability limit states) need to be considered - only FLS (fatigue limit state) was considered in this thesis.

1.4 Context

A local part of a semi-submersible wind turbine was analysed. The part is a joint connecting the floater to the wind turbine tower. Design, stress concentration factors and fatigue life of the part were the main topics.

The semi-submersible was based on the 5 MW semi-submersible wind-turbine from the University of Maine DeepCwind project, [Robertson and Jonkman, 2011]. In a pre-project, the dynamic response of Umaine DeepCwind was analysed, [Ørjan Fredheim, 2011]. The design has now been modified by Ph.D. candidate Chenyu Luan, who was responsible for the semi-submersible wind turbine design and dynamic response analysis. His dynamic response analysis of the new design was used for the fatigue analysis of the local part.

This report is focusing on the upper (white) work and results presented in Figure 1.2.

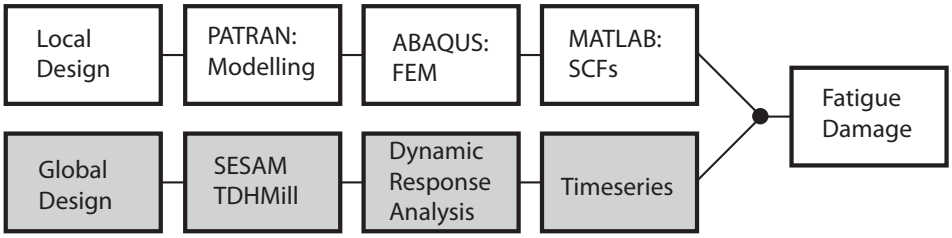

Figure 1.2: White: Ørjan Fredheim, Grey: Chenyu Luan

1.5 Contributions

The following has been done:

- Preliminary design of column-brace connection for a semi-submersible wind turbine
- SCF-study of the design
- Modifications and suggestions to designing of such a joint
- Fatigue analysis of the joint
- Conclusion and recommendations for future work

A suggestion for a preliminary column-brace connection design was presented. The design still needs modifications to reduce stress concentrations and optimizations to achieve a more reasonable design.

1.6 Thesis overview

Chapter 2 presents the design and geometry of the semi-submersible and of the brace-chord connection. Chapter 3 gives a presentation of some theory relevant to the thesis. A short presentation of what computer programs were used, and flow charts of programming and modelling work are presented in Chapter 4. In Chapter 5 the procedure for stress concentration calculation, boundary condition and interaction studies are presented together with relevant findings and results. Chapter 6 contains the procedure for the fatigue damage calculation based on the findings from Chapter 5 and the fatigue calculation results. Chapter 7 discusses the work done, the results and concluding remarks. Chapter 8 presents recommendations for future work.

Chapter 2

Design and Geometry

This chapter describes the preliminary geometry and design for the semi-submersible. At the end of the chapter, a preliminary design for the column-brace connection was suggested. The semi-submersible has several joints - only the joint connecting the wind turbine tower to the semi-submersible was studied.

2.1 Semi-submersible concept

The catenary moored semi-submersible was based on University of Maine's UMaine Semi-submersible 5 MW Wind Turbine DeepCwind project, [Robertson and Jonkman, 2011].

In 2011, the author did a dynamic response analysis of the UMaine semi-submersible concept in the NTNU project thesis, [Ørjan Fredheim, 2011]. The findings made clear that the concept needed to be modified, especially concerning heave natural period (17.5 sec) and displacement (14340 ton). Chenyu Luan made a new design based on UMaine. The overall design is very similar to the original, however the displacement was reduced to 6938 ton, and it was added heave plates to deal with the heave natural period resonance problem. The semi-submersible has a 3-line catenary mooring system and an NREL 5 MW wind turbine, [Jonkman et al., 2009].

Figure 2.1: Umaine Semi-submersible [Robertson and Jonkman, 2011]

2.2 Preliminary Design of a Semi-submersible Wind Turbine

In this section, the preliminary design of the semi-submersible is presented.

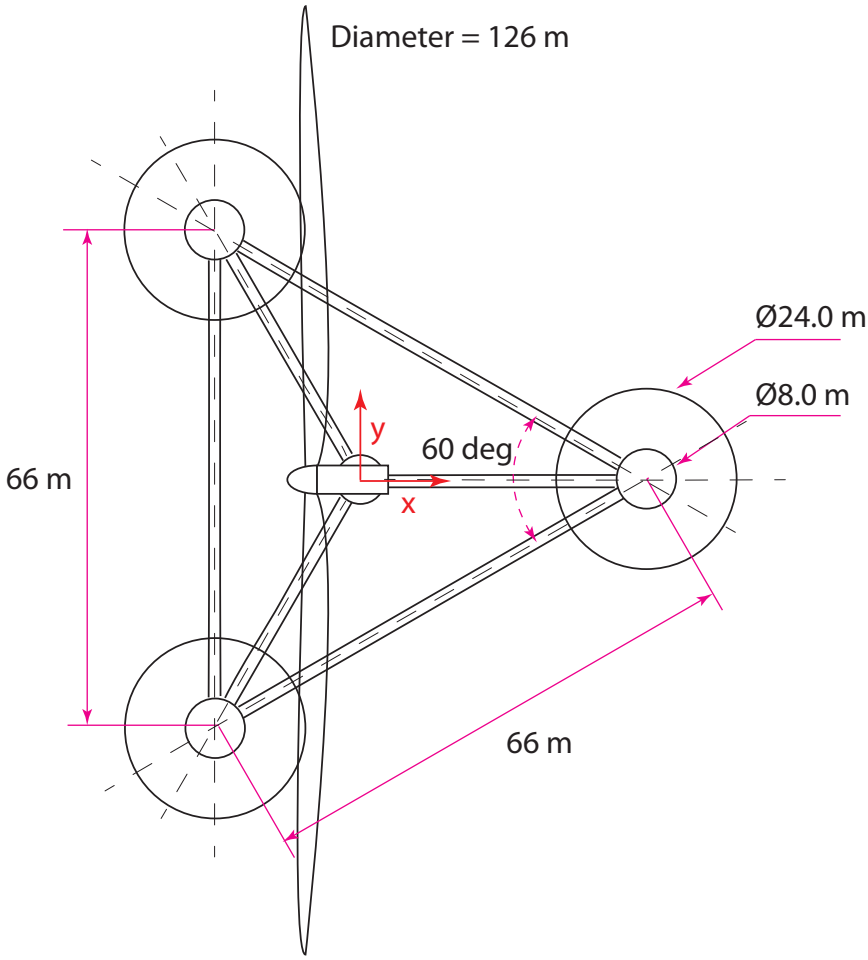

Figure 2.2: Geometry (Top View). The blades and nacelle are illustrative only. The wind turbine diameter is to scale (126 m).

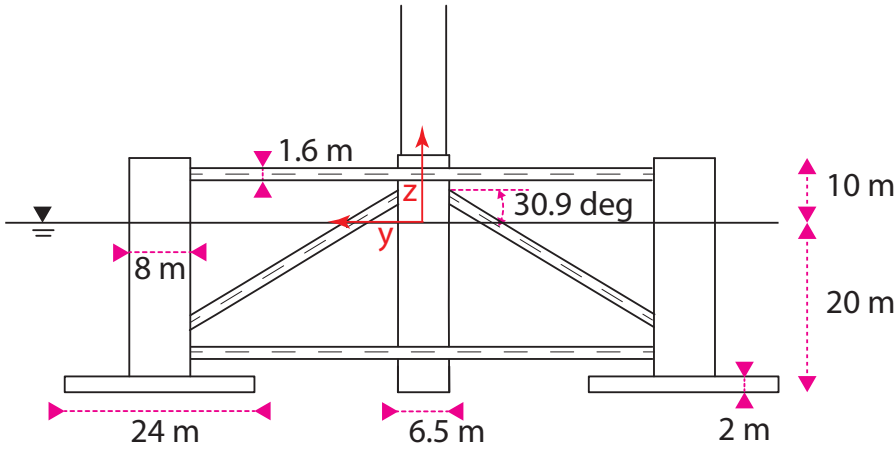

Figure 2.3: Geometry (Side view)

Table 2.1: Preliminary design for a 5 MW turbine

Turbine dimensions	
Turbine rated power	5 MW
Rotor diameter	126 m
Hub height above SWL	90 m
Floater dimensions	
Operating draft	20 m
Operating displacement	6938 ton
Column-center distance	38 m
Column-column distance	66 m
Mooring lines	3
Surge period	80 sec
Sway period	80 sec
Heave period	22 sec
Roll period	39 sec
Pitch period	39 sec
Yaw period	57 sec

2.2.1 Global Design as Modelled in DeepC

In this section the DeepC-model is presented.

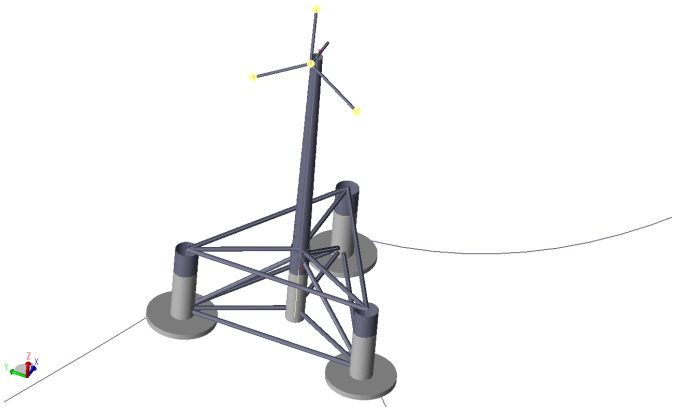

Figure 2.4: Semi-Sub Design (as modelled in DeepC)

The wind turbine blades are longer than they appear in the figure.

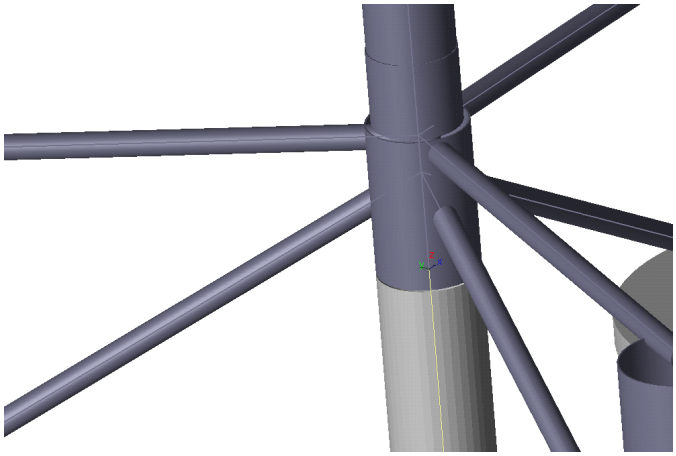

Figure 2.5: Joint in Global Model

The light grey parts of the structure were modelled as SIMO-bodies (rigid), while the darker grey were modelled as RIFLEX-elements (flexible). This was to be able to model the flexibility of the braces, so the forces could be obtained. Normally the whole structure is modelled as SIMO-elements, but then the joint would be completely rigid, and the fatigue analysis approach would not be possible.

2.3 Preliminary design of column-brace connection

This section describes the designing process and finally the preliminary design for the column-brace connection.

Designing is an iteration procedure, where a better and better solution is obtained after alterations to the initial design. In the following, "the joint" will also be used to refer to the column-brace connection. The procedure to design such a joint is case-to-case. The joint connecting the semi-submersible to the wind tower is also based on the UMaine Semi-Submersible design. The joint is a complex tubular joint attaching the 3 outer columns of the platform with the mid column. The joint consists of a 6.5 meter in diameter chord with 6 incoming 1.6 meter in diameter braces from 3 different planes. 3 of the braces are horizontal, while the remaining 3 are inclined.

2.3.1 Brace-chord connection

A three-symmetric vertical bulkhead system was proposed for the brace-chord connection, which works both as a stiffener and connection. The braces was split at the end, and welded to the bulkhead along the splits. This was done for all the braces. The length of the weld (or split) was set to 2250 mm for the horizontal brace, meaning that the gap between the column centre line and the brace is equal to 1000 mm. This gives sufficient space for inspection, and at the same time the braces are not overlapping for the different planes. The weld lengths of the inclined brace are 1664 and 2620 mm. The three bulkheads were connected through a solid steel 200 mm diameter rod in the centre line of the chord.

Initially, it was suggested to make the centreline of the horizontal and inclined braces to coincide at the column centre line to create a smooth stress transition. After closer inspection, this was not possible for this design if brace overlapping was to be avoided (which could lead to new SCFs). The inclined brace was instead translated in negative z-direction. Welder access was considered, and the distance from horizontal to inclined brace was set to 1 times the brace diameter. Based on the platform model, the inclination angle then became 30.9 [deg].

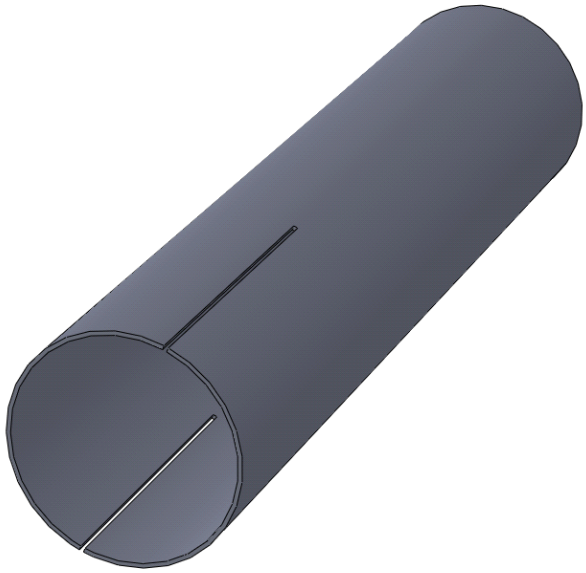

Figure 2.6: Horizontal brace with split

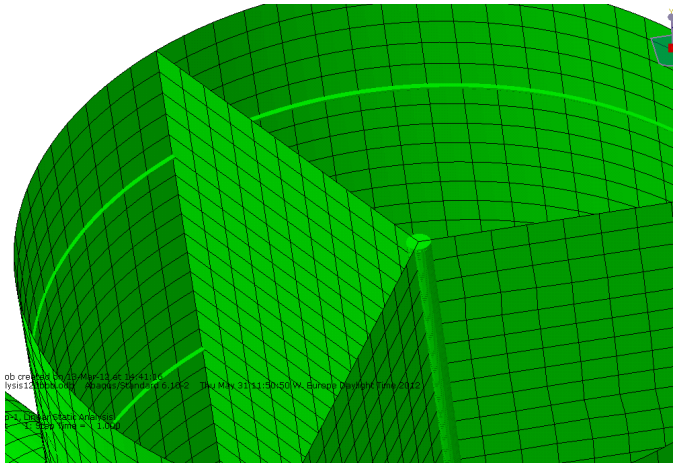

Figure 2.7: Bulkheads, stiffeners, steel rod and outer shell

2.3.2 Stiffening

Ring-stiffeners were added in addition to the vertical bulkheads. 5 ring stiffeners were added at heights 1830, 6600, 11400, 14400 and 17400 mm from bottom cut

of the chord. The exact selection of locations of the ring stiffeners were somewhat arbitrary, but the 3 lower stiffeners were added to reduce the displacement of the chord due to the braces - one below the lower brace, one in-between and one over the upper brace. The stiffeners have rectangular cross section with height $1 \times t = 30mm$ and length $3 \times t = 90mm$.

No horizontal bulkheads were installed at this point, because it was expected that the axial action would be the dominating degree of freedom.

2.3.3 Plate thickness

A constant steel thickness of 30 mm was chosen, which was based on a given total weight of the UMaine Semi-Submersible, and transferred to the new design. The steel thickness is therefore somewhat arbitrary, and needs more concern - especially close to the brace/chord intersection, where the largest stress concentrations occur.

2.3.4 Cuts

Cut: where the braces were cut for applying loads and boundary conditions.

The locations of the cuts were chosen to avoid distorted stress contributions from the geometric discontinuities. Thus, the cuts are far away from the places where stress concentrations (and complicated stress distributions) were expected to occur. Distances of $(2 - 3) \times D_b$ were chosen, where D_b is the diameter of the brace = 1600 mm.

The upper and lower braces were cut at 8250 and 7950 mm from the longitudinal centre line of the chord, respectively. See Figure 2.8. The lower chord cut is in the waterline-plane.

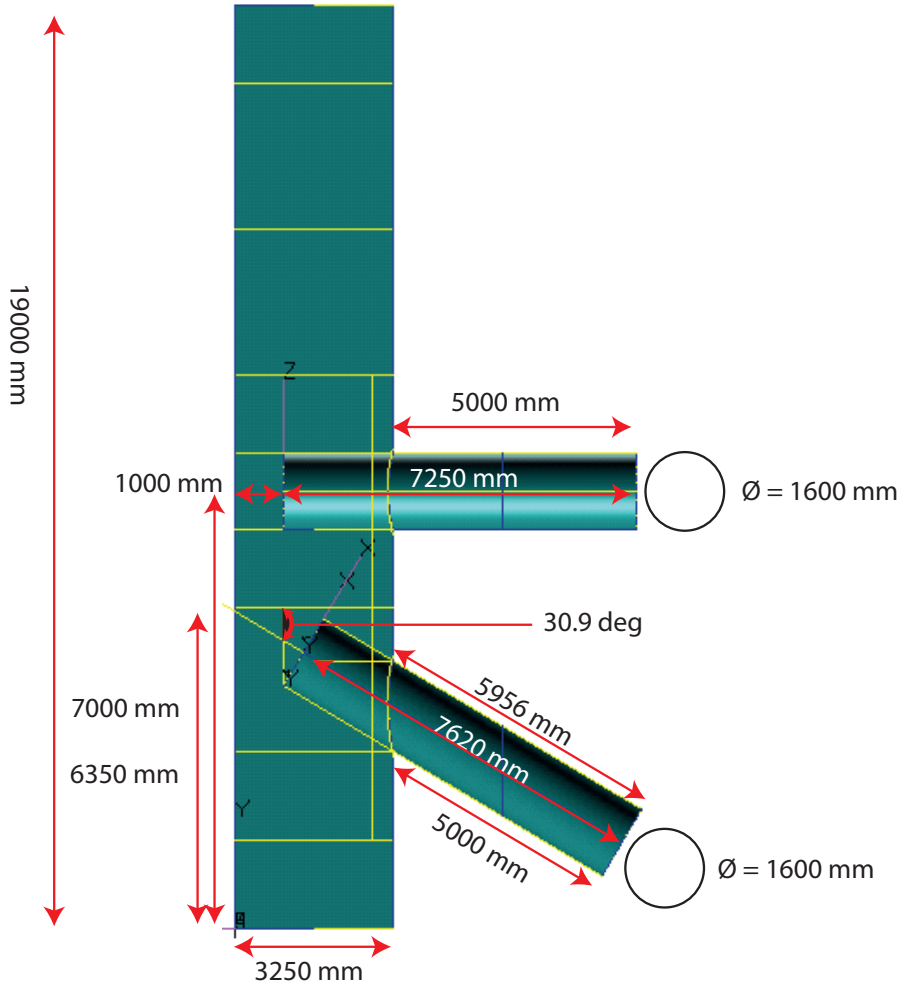

Figure 2.8: Dimensions

Here the dimensions of one bulkhead with braces are presented. All three bulkheads are identical with 120 degrees angle between them, and surrounded by an outer shell, as illustrated in Figure 2.9.

2.4 Preliminary Design

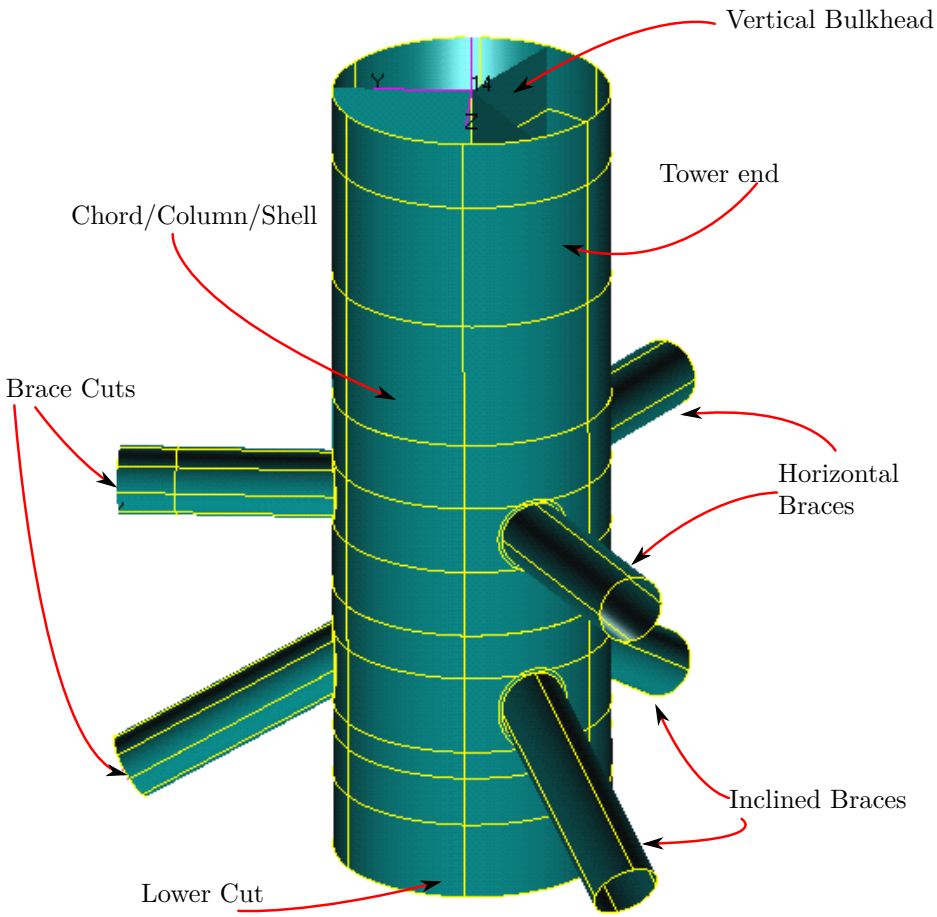

Figure 2.9: Proposed Preliminary Joint Design

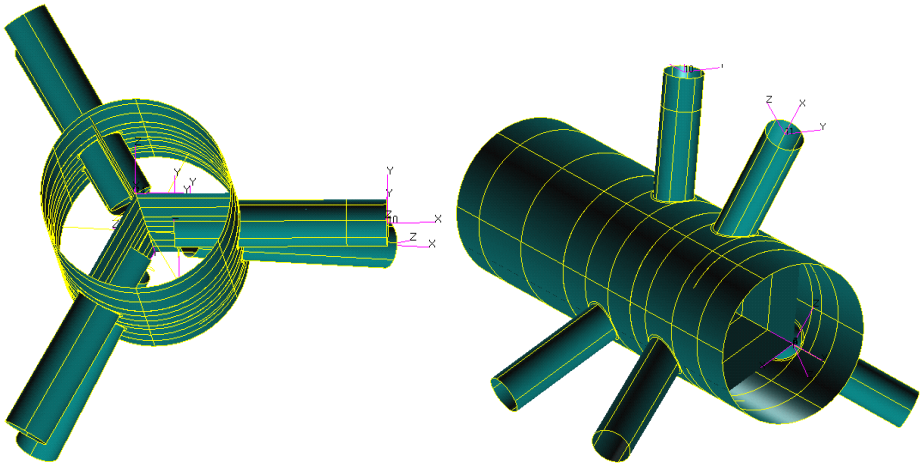

(a) Top **(b)** Bottom

Figure 2.10: Geometry of local joint

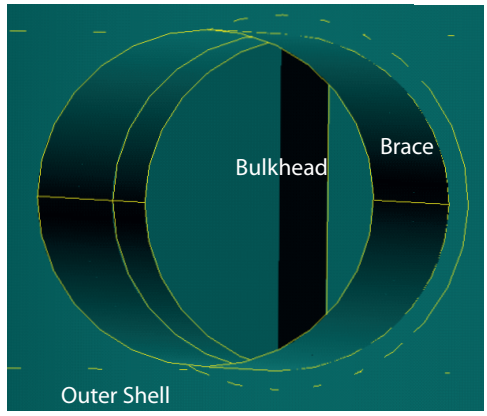

Figure 2.11: Inside of Brace seen from outside

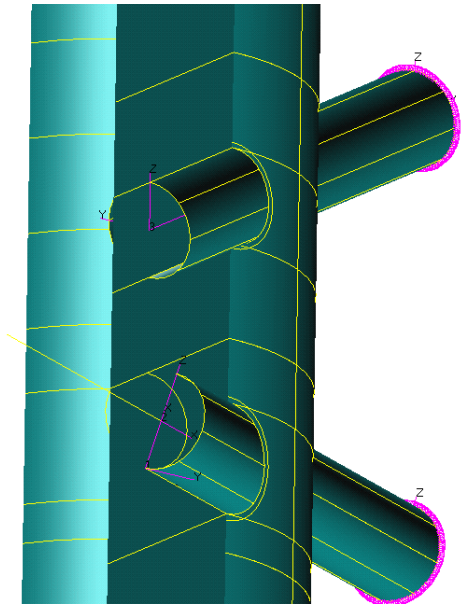

Figure 2.12: Inside

Chapter 3

Theory

This chapter briefly presents some relevant theory.

3.1 Short introduction to Wind Power

The concept of wind power is the capture of the kinetic energy in the wind, normally using a wind turbine. Wind power is renewable, and one of the cleanest and most environmentally friendly energy sources. [European Wind Energy Association, 2010].

Wind energy is extracted using airfoils. Airfoils are formed in such a way that the wind that travels over the foil, has to travel a longer distance than the wind that travels under the foil. Consequently, the air above the foil has to speed up to catch up with the air that is flowing below (conservation of mass). Referring to Bernoulli's equation, we know that when the speed increases, the pressure is lowered. Thus it will be induced a pressure difference over the foil, which again gives rise to a net lift force. This leads to the rotation of the wind turbine. The mechanical energy is converted to electrical energy using a generator. [Minsaas and Steen, 2008].

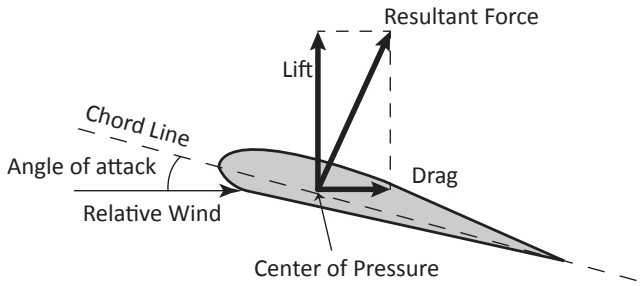

Figure 3.1: Airfoil

3.2 Tubular Joints

A tubular joint is a connection between a main load carrying member and one or more secondary members. The largest member is denoted chord, and the smaller members brace. The in plane intersection between brace and chord is called the crown, while the out of plane intersection is called the saddle.

Tubular joints are not regulated by official standards, and the configurations and dimensions can be freely chosen to suit structural needs, [Næss et al., 1985]. There is a large variety of shapes and designs.

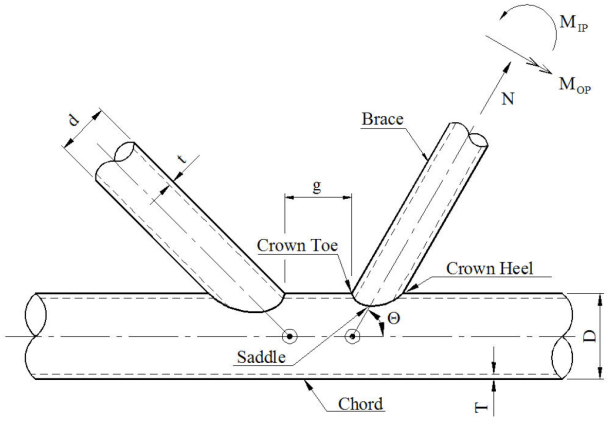

Figure 3.2: Tubular joint, [DNV-RP-C203, 2010]

Braces are frequently used in marine structural design. Because of their circular and geometric shape, the drag forces are minimized, the tubes exhibit minimal stress concentrations, have outstanding buckling strength, and are insensitive to

lateral load direction. A drawback of tubular structures is that the joints tend to be complicated, leading to discontinuities and thus large stress concentrations (SCF) in the brace-chord intersection. For welded tubular joints, the latter is the main problem and is very important when designing for fatigue strength.

[Næss et al., 1985] mentions 4 categories of tubular joints:

- Simple welded joints
- Overlapping joints
- Complex joints
- Cast steel nodes

The 3 latter categories are also called heavy duty joints. There are many definitions and classifications of tubular joints - The reader is recommended to read [Næss et al., 1985] for a more detailed overview.

3.2.1 Complex Tubular Joints

Offshore steel platforms are usually constructed as truss frameworks utilizing tubular joints as structural elements. Bracing of semi-submersibles may be viewed as complex tubular structures. Complex joints can be built with internal or/and external stiffening, and are often multi-plane joints. This joint type was for these reasons used for the preliminary joint design.

3.3 Stiffening

Stiffening of tubular joints should be applied and designed with great care. In many cases stiffening may lead to hard points which increase SCFs, and thus decrease fatigue life. [Berge, 2006]

The most common form of stiffening is by internal ring stiffeners in the chord. This may only be applied to large joints due to welding access. Large reductions of stress concentrations may be obtained using this technique. Large joints, like in a semi-submersible bracing, may be heavily stiffened with ring as well as longitudinal stiffeners. Such complex joints are designed from case to case. [Berge, 2006].

In an unstiffened simple joint, the SCFs normally occur outside of the joint, while for internal stiffened joints the fatigue hot spot is likely to be on the inside, leading to harder in-service inspection. External stiffening or wing plates are possible for further reduction of fatigue damage.

3.4 Hot Spots

The locations at which the highest stresses occur, are called **hot spots**. The location of maximum stress normally occurs at the saddle or the crown of the intersection. For example, in-plane bending of a so-called T-joint will create a maximum stress will be at the crown, while out of plane bending will give a maximum stress at the saddle. The maximum stress value may be at either of these dependent on geometry and design of the joint.

The hot spots for tubular joints are in the weld toe at the hot spots, where small irregularities and discontinuities exist. The hot spot stress should therefore be calculated based upon the true stress at the weld toe. However, it is difficult to quantify this stress because of the localized weld irregularities and discontinuities. In addition, the fatigue life of tubular joints is largely determined by the growth of a crack in a region where the peak stress from the weld geometry is of minor significance, [Berge, 2006]. For these reasons, the so-called geometric stress has been taken as the characteristic stress for fatigue design of a tubular joint.

The geometric stress, often termed the hot spot stress, is determined by the global stress concentration of a given joint, including stress concentrations due to geometric effects, and excluding stress concentrations of the weldment itself. The standard procedure for assessment of this stress is an extrapolation on the basis of an assumed linear variation of stress at some distance from the weld, [Næss et al., 1985]. The only effect of the weldment to be accounted for is the contribution to stiffness in the tube wall. However in most design analyses this effect is neglected, [Berge, 2006].

3.5 Stress Concentration Factor

The stress concentration factor is dimensionless and defined as the ratio between the hot spot stress and the nominal stress in the brace:

$$SCF = \frac{\sigma_{max}}{\sigma_N} \tag{3.1}$$

In the process of design evaluation, the hot spot stresses on the chord and brace side of the weld must be considered individually. SCF_b and SCF_c denote the SCF on the chord and brace side respectively. They are both multiplies of the same nominal brace stress.

The most influential factors deciding the fatigue strength of a tubular joint are the values of the SCFs. Reliable and accurate knowledge about the SCFs are therefore very important in order to be able to design for fatigue strength. An underestimation of 18% of the value of the SCF may cause a 100% overestimation of the fatigue life prediction [Næss et al., 1985].

Simple joints are well documented, and are relatively easy to analyse. Parametric dimensionless formulas have been established for SCFs and can be found in e.g. [DNV-RP-C203, 2010]. These parametric equations are however only valid for simple joint configurations. For more complex joints, this is not possible. Several methods are available for stress analysis, among them the finite element analysis which is the most popular one, [Berge, 2006, Næss et al., 1985].

3.5.1 Influence Coefficient

It is sometimes preferable to work with a different factor than the SCF, sometimes called the influence coefficient:

$$IF_i = \frac{\sigma_{max}}{F_i} \tag{3.2}$$

F_i is load in degrees of freedom 1-6.

The IF is not dimensionless, and have dimension $[Pa/N]$ or $[Pa/Nm]$, dependent on if the load is force or moment. The results from the dynamic response analyses have dimension Newton [N] or Newton-meter [Nm] (and not [Pa]). The influence factor is thus easier to work with.

3.6 Finite Element Method (FEM)

The finite element method is a versatile, economical and effective tool, and a common approach to do stress analysis to determine the stress distribution and hot spot stress in e.g. tubular joints. The method is not straight forward. Great care and skill are required in order to obtain relevant results for the hot spot stress, like for example choice of element type and element size in the region of intersection [Berge, 2006].

There are several sources of error in a FE analysis that may lead to poor approximation of the real situation as outlined by [Moan, 2003]:

- simplified assumptions in the mathematical model
- Discretization error
- numerical round-off error in the computer
- Poor input data due to lack of information about geometry, material etc. to describe the mathematical model
- Error in interpreting the results

The results from such an analysis should therefore be carefully investigated.

ABAQUS was used to do finite element analysis, assuming a linear system.

The finite element method is a well documented method, and will not be further elaborated on here.

3.7 Fatigue

Fatigue is the progressive and localized structural damage that occurs when a material is subjected to cyclic loading. The stress values are below the ultimate tensile stress limit, and even below the yield stress limit. If the loads are above a certain threshold, small cracks will begin to form in the material. Under repeated loading and unloading, the crack will grow, and eventually the material will fracture.

The shape of the structure greatly affects the fatigue life, and sharp corners and discontinuities should be avoided.

3.7.1 The Hot Spot Method

From detailed finite element analyses it may be difficult to identify the "nominal stress" to be used together with the S-N curves. In many cases it may be more convenient to use a different approach using an appropriate S-N curve:

- The stress concentration factor due to the weld itself is included in the D-curve
- The SCFs is calculated using a fine mesh model using shell elements.

This procedure is denoted the hot spot method and is the basis for this thesis. [DNV-RP-C203, 2010]. Thus no welds were modelled in the joint.

3.7.2 S-N Curves

In laboratory experiments, one often subjects a specimen of a material to a constant amplitude oscillating load, say $L(t) = \sigma sin(\omega t)$, and counts the number of cycles until the specimen breaks, N. The number of cycles N, as well as the value of the stress range σ are recorded. Using these results it is possible to create a relation between N and σ:

$$N = a(\sigma)^{-m} \tag{3.3}$$

The stress range of the load is often used instead of the amplitude:

$$N = a(\Delta\sigma)^{-m} \tag{3.4}$$

where a is a constant and m the negative inverse slope of the S-N curve, [Berge, 2006]. On log-log scale equation (3.4) becomes a straight line,

$$logN = loga - mlog\Delta\sigma \tag{3.5}$$

Actually, in design, $log\bar{a}$ is used instead of $loga$, where $log\bar{a} = loga - 2S_{logN}$, and S_{logN} is the standard deviation of log N. These curves are called design S-N curves. The reason is to account for the uncertainty in the obtained experimental data in the S-N curves. A design S-N curve was used in this thesis.

$$logN = log\bar{a} - mlog\Delta\sigma \tag{3.6}$$

The values for $log\bar{a}$ and m are given in [DNV-RP-C203, 2010] for different geometries, scenarios, weld types etc.

[DNV-RP-C203, 2010] has some modifications to eq. (3.5) to account for the fatigue strength of welded joints, which to some extent is dependent on plate thickness. This modification if referred to as the thickness effect:

$$logN = log\bar{a} - mlog(\Delta\sigma(\frac{t}{t_{ref}})^k) \tag{3.7}$$

For tubular joints, the reference thickness $t_{ref} = 32mm$. k is dependent on the S-N curve used, and t is the plate thickness.

Haibach

For small amplitudes the fatigue life is often very large, and is in some cases set to infinity, $N = \infty$. Completely ignoring the cycles smaller than the fatigue limit may be non-conservative. Haibach suggested using a different slope (m) for the SN-curve in the regions above and below the fatigue limit. This model is called the "Haibach Model" (1970) [Berge, 2006] and is more conservative and accurate than assuming that cycles below the original fatigue limit are non-damaging.

The S-N curves are a powerful tool, and are often combined with the Palmgren-Miner linear damage accumulation theory to predict fatigue failure time.

3.7.3 Palmgren-Miner Rule

Almost all available fatigue data for design purposes is based on constant-amplitude tests. In practice, however, fatigue stresses are variable amplitude or random. The key issue is how to use the massive amounts of constant-amplitude data to predict fatigue in a component. Many different cumulative damage theories have been proposed for purposes of assessing fatigue damage caused by operation at any

given stress level. Even so, the original model, a linear damage rule originally suggested by Palmgren (1924) and later developed by Miner (1945), maintains its popularity principally because of its simplicity, [Wirsching et al., 1995]. The P-M summation has proved to be no worse than any other method, and much simpler, [Berge, 2006]. The model is referred to as the Palmgren-Miner rule or the linear damage rule. Life estimates may be made by employing Palmgren-Miner rule along with a cycle counting procedure.

If the $k'th$ cycle of a load has stress range $\Delta\sigma_k$, then it is assumed that it causes a damage equal to $1/N(\Delta\sigma_k)$. The total damage at time t is then

$$D(t) = \sum_{t_k \leq t} \frac{1}{N(\Delta\sigma_k)} \overset{eq.(3.4)}{=} \frac{1}{\bar{a}} \sum_{t_k \leq t} (\Delta\sigma)^m = \frac{1}{\bar{a}} D_m \tag{3.8}$$

where the sum contains all cycles up to time t. The fatigue life time t_f, say, is shorter than t if the total damage at time t exceeds unity. t_f is thus defined as the time when $D(t) > 1$ for the first time.

We are interested in the damage caused per second of the entire life-time of the structure, to be able to calculate the fatigue life time. It is time-consuming to realize a sea state of say 20 years. Using several sea state realizations of 1-3 hours is much more convenient, and for a high-cycle fatigue, and stationary and ergodic process, the total damage can be approximated using a time series of length, say, T_{sea}. Thus the damage per second, d, will be approximated by

$$d \equiv \frac{D(t)}{t} \approxeq \frac{D(T_{sea})}{T_{sea}} [1/s] \tag{3.9}$$

The time to failure will be when $D(t)$ equals one, and thus the time to failure, t_f equals:

$$\underline{\underline{t_f = \frac{1}{d}[s]}} \tag{3.10}$$

[Brodtkorb et al., 2000]

As mentioned in section 3.5 the SCF is an influential fatigue strength factor, which is justified by looking at equation (3.8). The total stress has the power of m, which is either 3 or 5 (Haibach, [Berge, 2006]). An increase of the SCF by a factor of 2, means that the stress is increased by a factor of 8 or 32, dependent on m.

3.7.4 Rainflow Counting

Counting methods have been developed for the study of fatigue damage. A number of algorithms for identifying stress cycles have been proposed. Methods include

level crossing counting, peak counting, simple range counting and rainflow counting. A review of these methods is provided by [Næss et al., 1985]. The method now widely accepted as providing the most accurate results is the rainflow method, [Wirsching et al., 1995].

The counting procedure is designed to count reversals in accordance with the material's stress-strain response, [Næss et al., 1985].

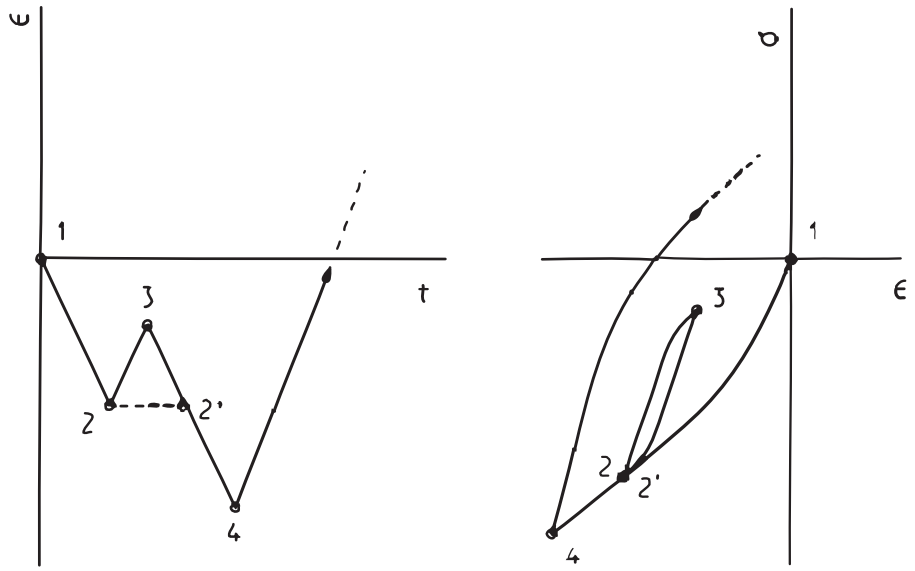

(a) Part of a strain history **(b)** Stress-strain response

Figure 3.3: Rainflow Principle. The small cycle 2-3-2' forms a closed hysteresis loop within the large cycle 1-4, the latter being undisturbed by the interruption [Næss et al., 1985, Fig. 4.46]

Chapter 4

Software

There are several fatigue software-packages available. However, the author have no access to one single software-package that can include both dynamic response from waves and wind on a wind turbine on an offshore vessel. In addition, a finite element program is necessary for SCF calculations. Consequently several software-packages were used to obtain the fatigue damage results.

To analyze the fatigue life of the joint, 3 computer programs were used:

1. PATRAN
2. ABAQUS
3. MATLAB

PATRAN is a pre- and post-processing package for the finite element program ABAQUS. It is also capable of doing finite element analysis (FEA). However, ABAQUS was used for this purpose. PATRAN is very efficient and usable for modelling structures, and have a very good element mesher (by experience). Thus, all modelling work, meshing, properties, materials, boundary conditions and loading were specified in PATRAN. The output from PATRAN is the input file for ABAQUS. The linear static analyses were carried out in ABAQUS/Standard by running a batch through a MATLAB script. Later all relevant data (ROPs, stresses) were extracted from ABAQUS using python-scripting. ABAQUS/Viewer was also used for visualization and verification.

MATLAB is a coding language and software which was used for pre-processing for analyses in ABAQUS, post-processing of results, and calculating fatigue life using the free and commercially available toolbox "WAFO" (Wave Analysis for Fatigue and Oceanography, [WAFO-group, 2000]) coded for MATLAB. MATLAB was used as a bridge between PATRAN and ABAQUS, and was thus a very powerful tool when running analyses. MATLAB was also used for small tasks like plotting/making illustrative figures.

The force/moment time-series needed for fatigue analysis were obtained from analyses done by Chenyu Luan. For the dynamic response analyses of the semi-submersible wind turbine, 5 computer programs were used:

1. GeniE
2. HydroD
3. SIMO
4. RIFLEX
5. TDHMill

SIMO and RIFLEX are included in the interactive application "DeepC". GeniE, HydroD and DeepC are all programs in DNV's SESAM-package, [DeepC, 2010, Simo, 2010, Simo, 2009, Riflex, 2008, Riflex, 2010]. TDHMill is a program using simplified methods to calculate wind thrust on a turbine.

Analysis of offshore floating structures is well established in the SESAM package, except the modelling of the wind turbine. External software like TDHMill is then used.

4.1 Modelling Procedure

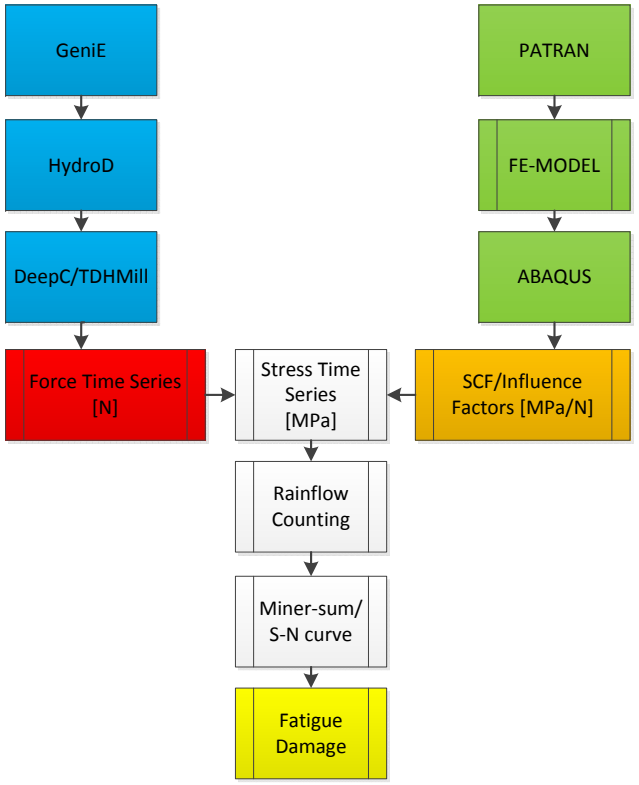

Figure 4.1: Modelling procedure

Both dynamic response analysis and finite element modelling were carried out. The influence factors from the finite element model were combined with the force time series from the dynamic response analyses to obtain a stress series for the hot spot locations on the joint. Rainflow counting together with the Palmgreen-Miner accumulated damage rule and a DNV S-N curve gave the fatigue damage for the joint.

4.2 Script for finding SCF/IF

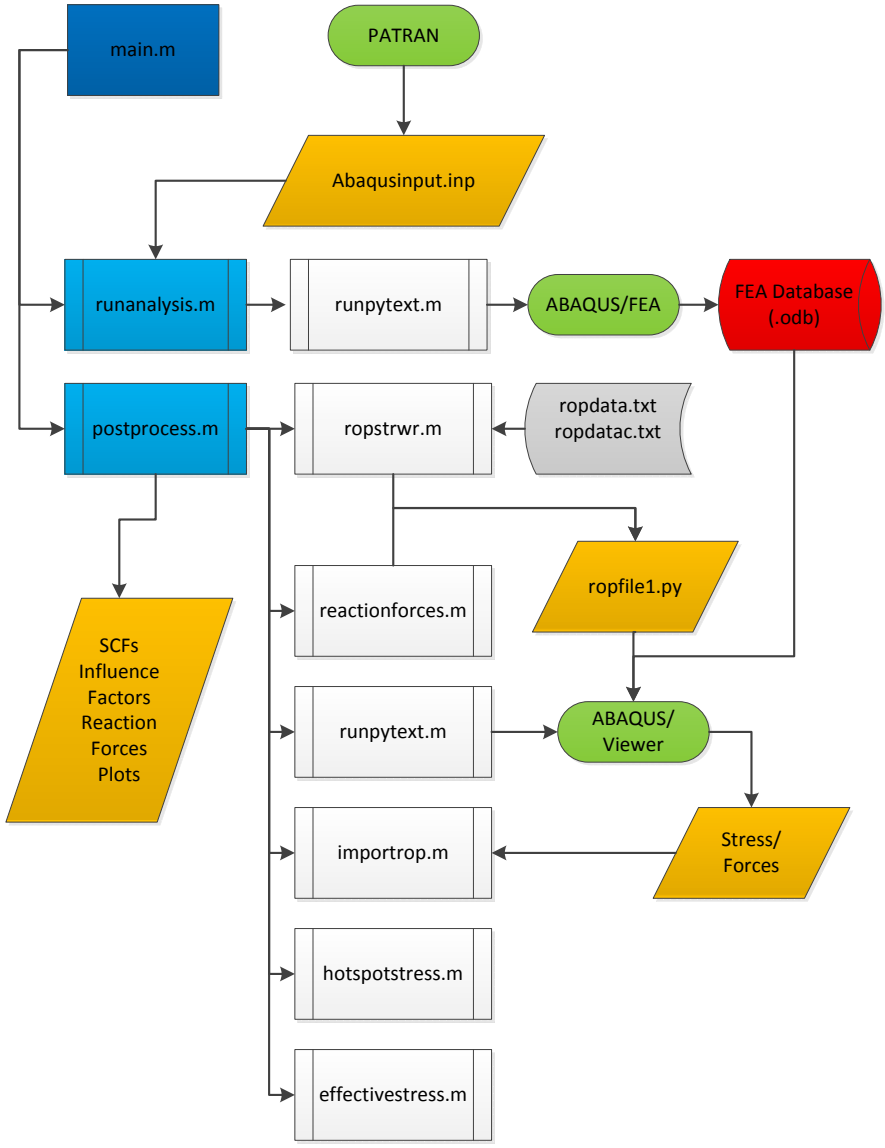

Figure 4.2: Flowchart SCF/IF Calc.

1. First, the output from PATRAN creates several input files for ABAQUS.

2. The MATLAB script main.m runs ABAQUS through runanalysis.m, which creates a database (*.odb) that contains all FEA-results needed. runpytext.m is a script which calls ABAQUS from MATLAB.
3. postprocess.m is then called to extract the relevant data from the database. This is done by ropstrwr.m and reactionforces.m which are writing several python-scripts. These scripts are sent to ABAQUS which exports the data needed.
4. importrop.m imports the data exported from ABAQUS back into MATLAB.
5. hotspotstress.m extrapolates to obtain the hot spot stresses.
6. effectivestress.m calculates the effective stresses as specified in [DNV-RP-C203, 2010].
7. main.m/postprocess.m outputs graphs, plots, SCFs, influence factors and reaction forces.

Several other MATLAB-scripts for plotting purposes were created, but are excluded from the flowchart for space.

4.3 Script for finding damage/fatigue life

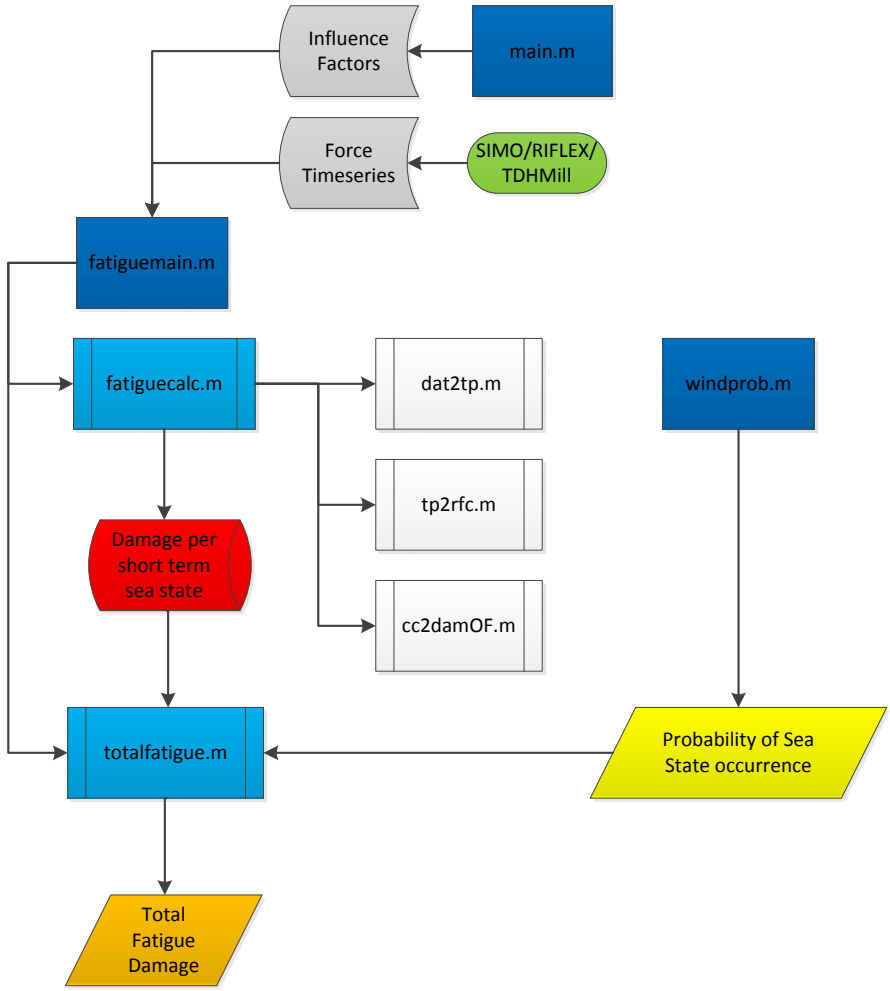

Figure 4.3: Flowchart Fatigue Calc.

WAFO was used for fatigue calculation.

1. The already calculated influence factors and force time series are imported by fatiguemain.m.
2. fatiguecalc.m calls WAFO-scripts for rainflow counting: dat2tp.m and

tp2rfc.m. cc2damOF.m calculates fatigue damage. The latter was edited by the author to comply with the [DNV-RP-C203, 2010] S-N curve fatigue limit.

3. fatiguemain.m/fatiguecalc.m outputs total fatigue damage, damage per second and fatigue life for all ROPs for every short term sea state.

4. totalfatigue.m calculates the total fatigue damage for every member on all brace planes, with input from windprob.m which calculates the probability of all short term sea states occurring.

Chapter 5

Stress Concentration Factors

The stress concentration factors are crucial in designing a joint with sufficient fatigue life. This chapter presents the modelling, calculation and results for the stress concentration factor study.

5.1 Coordinate System

The local coordinate systems are right hand coordinate systems with the x-axis along the cylinders, pointing away from the joint. For the braces the z-axis are pointing upwards, and the y-axis is found using the right hand rule. For the chord, the y-axis is along the global x-axis, while the z-axis is found using the right hand rule.

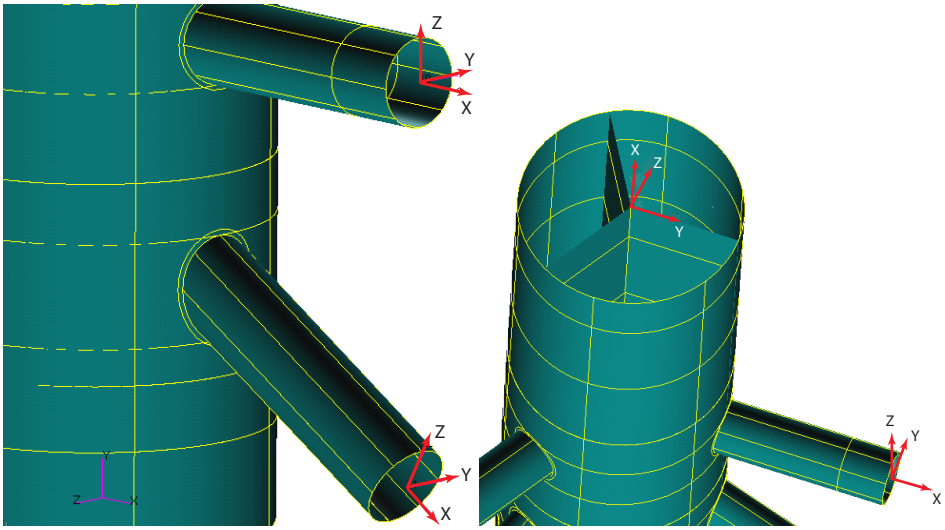

(a) Braces **(b)** Chord

Figure 5.1: Local Coordinate Systems

The global coordinate system was defined in Figure 2.2 and Figure 2.3.

5.2 Critical Part for Fatigue Damage

Because this is a complex joint, and there is internal stiffening, the hot spots may occur inside the joint. This was investigated to see what parts of the joint is most critical for fatigue damage.

By inspection, it was seen that the largest stresses occurred at the brace/chord-intersections, and at the brace/bulkhead intersections. The brace/bulkhead intersection's highest stress values in these cases were observed at the intersection end nodes. It was assumed that these high stresses occurred because of the discontinuity in the model at these locations. At a later stage is possible to remove these localized stresses by smoothing the local structural arrangement, e.g. making holes. Disregarding the end-nodes, the highest stresses were observed occurring at the brace/chord circumference intersection.

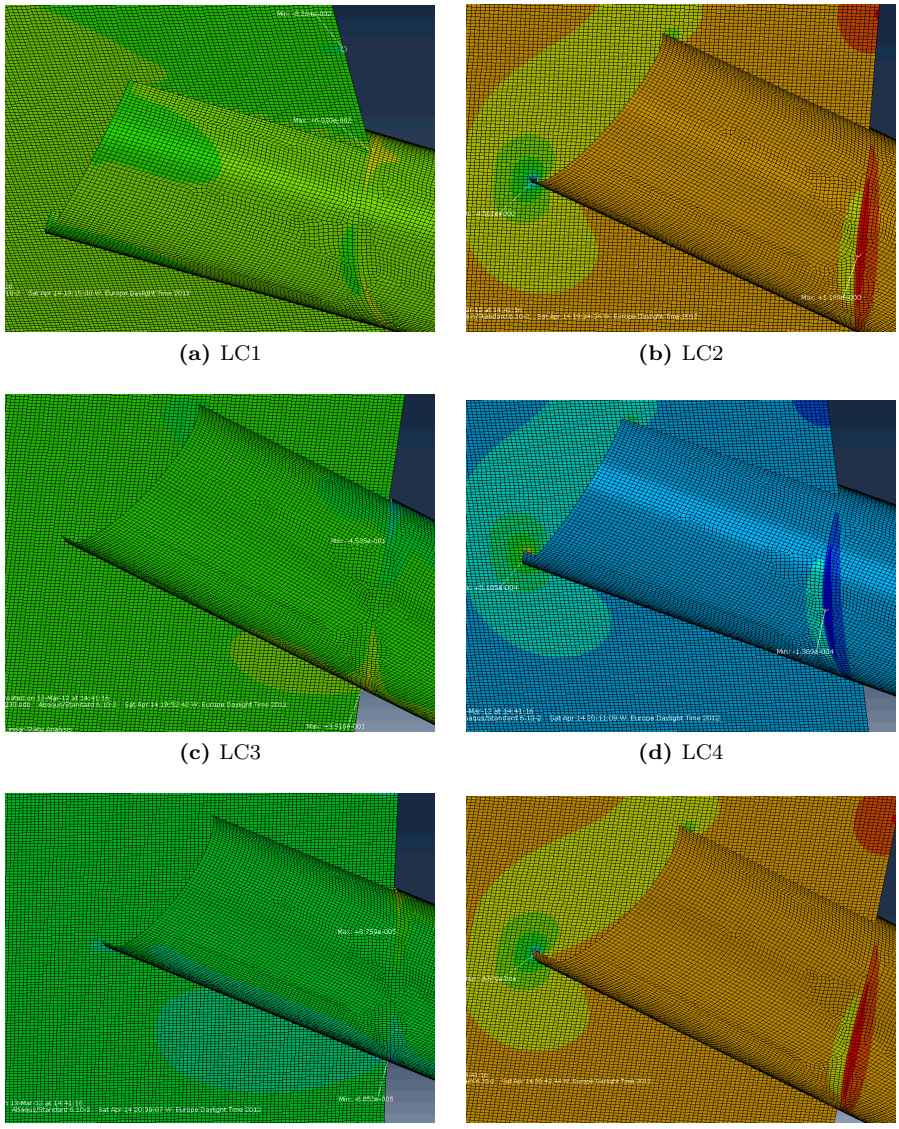

(a) LC1 **(b)** LC2

(c) LC3 **(d)** LC4

(e) LC5 **(f)** LC6

Figure 5.2: Brace/Bulkhead intersection as presented by ABAQUS/Viewer, Brace 2. Notice the high stress concentration at the end nodes, most visible for the out-of-plane cases

5.3 Loads & Boundary Conditions

This section presents the boundary condition defined, and the loads applied to the structure.

5.3.1 Loading

As discussed earlier, there are no SCF-parametric equations for complex tubular joints. Instead it is possible to load one brace at a time, later referred to as *the load cases (LC)*, and find the corresponding SCFs. For each load case there is a specific stress distribution, and a stress concentration for fatigue analysis. 3 load cases are normally used, but in this thesis, 6 were used to comply with the RIFLEX output.

- axial force (LC1)
- out-of-plane force (LC2)
- in-plane force (LC3)
- torsion (LC4)
- out-of-plane bending (LC5)
- in-plane bending (LC6)

Only 2 of the braces were loaded because of symmetry. These braces are the horizontal and inclined braces along the global x-axis. This saves time as well as elements. The chord was also loaded to see the stress concentration on the brace/chord intersection.

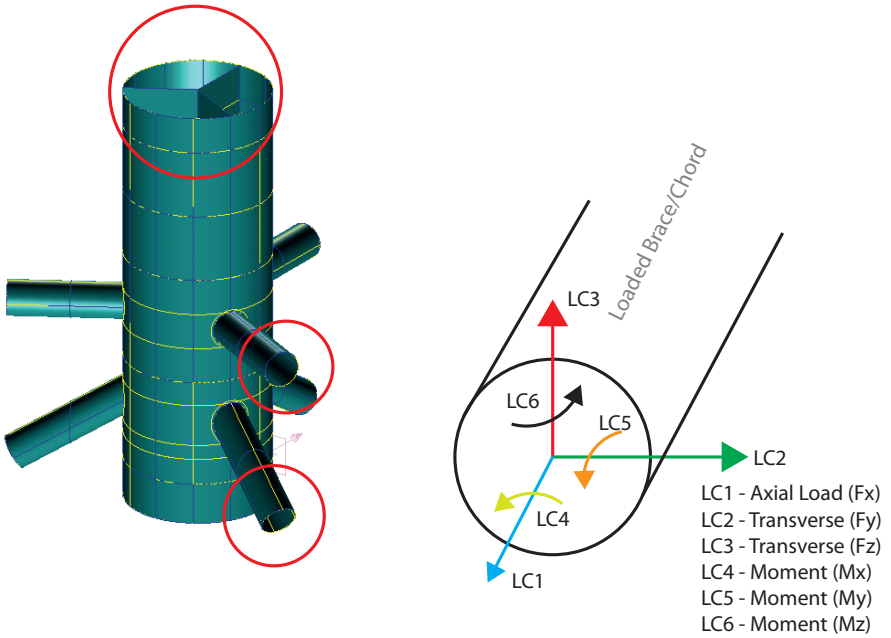

(a) Load locations

(b) Definition of Load Cases/Unit forces in local model

Figure 5.3: Loading

Braces

For each of the two braces, 3 forces and 3 moments were applied in the local X, Y and Z-direction respectively, to simulate the brace behaviour. Because it is a linear system superposition is possible, thus the loads were applied separately, giving $6 \times 2 = 12$ load cases/analyses in PATRAN. For each load case, read-out-points at 8 positions around the circumference intersection for the loaded brace were obtained, extrapolating from brace to chord and from chord to brace because the hot spot stresses on the chord and brace side of the weld must be considered individually [DNV-RP-C203, 2010, 3.3.2].

Chord

For the chord, the same procedure was applied. 3 forces and 3 moments were applied at the top of the chord to simulate the wind turbine tower behaviour. 6 loads give 6 load cases/analyses in PATRAN. For each load case, read-out-points at 8 positions around the circumference intersection for the braces were obtained, extrapolating from chord to brace.

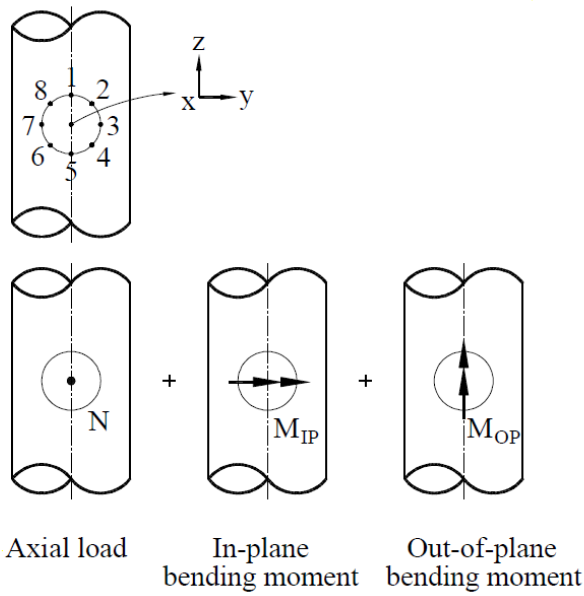

Figure 5.4: ROPs and superposition [DNV-RP-C203, 2010]. DNV operate with 3 load cases, whereas 6 were used in this thesis.

5.3.2 Boundary Conditions

The extent of the model is defined in [DNV-RP-C203, 2010]:

> "The extent of the local model has to be chosen such that effects due to the boundaries on the structural detail considered are sufficiently small and reasonable boundary conditions can be formulated"

The boundary conditions for the joint were difficult to predict. For that reason the whole joint was modelled.

The lower cut of the joint was fixed to avoid rigid body motion.

Boundary Conditions when loading the braces

To investigate the SCFs sensitivity to boundary conditions, analyses were made with the other 4 (unloaded) braces pinned and free. The ratio between SCFs from cases with free braces and pinned braces were for most cases below 1%. However, there were some ratios which nearly reached $\pm$ 20%, but this was never for the highest stress in the respective case (see section 5.8).

The conclusion was that the sensitivity of boundary conditions for the other 4 unloaded braces were negligible. The braces were thus modelled as free. The top of the chord (representing the wind turbine tower base) was not restrained, because the wind turbine tower is free.

Boundary Conditions when loading the chord

The real boundary conditions for the braces are governed by the attachment to the stabilization columns. Letting the braces have free ends would create something similar to rigid body motion for the braces, and thus too small SCFs would occur - this was too non-conservative. Fixing the braces would not account for the flexibility in the braces, and thus too large SCFs would occur - this was too conservative. Pinning the braces would give something in between a highly conservative and a highly non-conservative boundary condition, but would still be too conservative. A good way to model this boundary condition would be to create all the braces in full length, and then apply the boundary conditions at the end. In this thesis however, the braces were pinned at the cut, as recommended in [Næss et al., 1985].

5.3.3 MPC

Because the time series were obtained using RIFLEX beam elements in the SESAM software DeepC/SIMO-RIFLEX, the joint braces were loaded in a centre master node connected to slave nodes at the brace edges. The MPC RBE2 (**M**ulti-**P**urpose **C**onstraint) was used for this purpose.

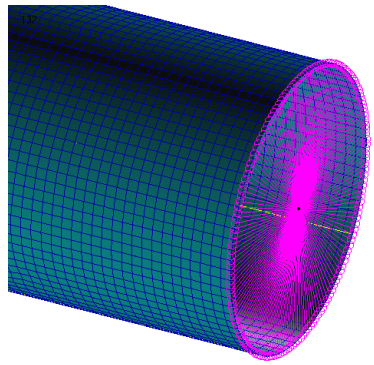

Figure 5.5: MPC. Master node (black dot) and slave nodes (purple circles)

5.4 Material

The same material (steel) was used for the whole joint. The material input data for PATRAN were the Young's modulus of 210 GPa, and Poisson's ratio of 0.3.

5.5 Extrapolation

The extrapolation procedure which should be used when not including the weld in the FE model is discussed in this section.

In certain literature [Næss et al., 1985] and [Berge, 2006], extrapolation to the weld toe is recommended. [DNV-RP-C203, 2010] suggests either extrapolating to the weld toe, or extrapolating to the intersection between shell elements. From [DNV-RP-C203, 2010, 4.3.3 and 4.3.4 (Method A)]:

> "Recommended stress evaluation points are located at distances 0.5 t and 1.5 t away from the hot spot, where t is the plate thickness at the weld toe. These locations are also denoted as stress read out points."
>
> "For modelling with shell elements without any weld included in the model a linear extrapolation of the stresses to the intersection line from the read out points at 0.5t and 1.5t from the intersection line can be performed to derive hot spot stress."

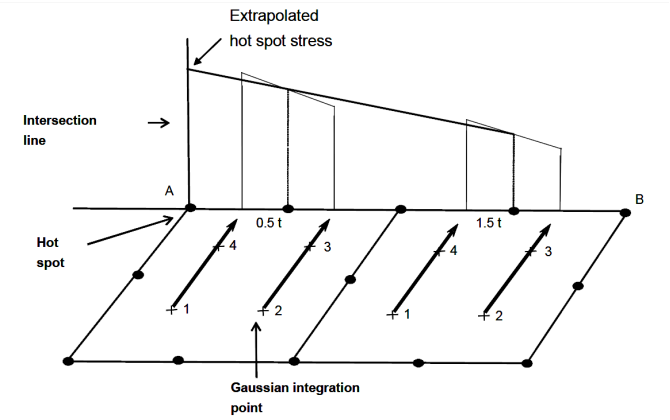

Figure 4-2
Example of derivation of hot spot stress

Figure 5.6: DNV RP-C203 [DNV-RP-C203, 2010, Figure 4-2]

[ABS, 2005], on the other hand, suggests extrapolating to the weld toe, without weld modelled, and using shell elements from the weld boundary.

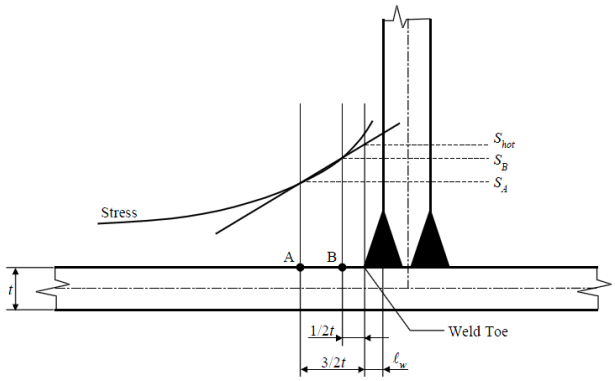

Figure 5.7: ABS-procedure, [ABS, 2005]

The most effective approach would be the one suggested by [DNV-RP-C203, 2010]. This approach is also supported by [Fricke, 2001]. His results found that better agreement between analyses and model measurements were achieved if the distances of the read-out-points were measured to the hot spot as modelled, i.e. to the weld toe if the weld is modelled or to the structural intersection point if the weld is not modelled. The same applies to the point where the stress is extrapolated to. What justifies this procedure without weld representation is that the stress at the fictitious weld toe position is in many cases too low due to the reduced stiffness compared to the real structure. Extrapolation to the structural intersection may thus give conservative results.

In conclusion, read-out-points were set $0.5t$ and $1.5t$ from the intersection line, and the stresses were extrapolated to the structural intersection line.

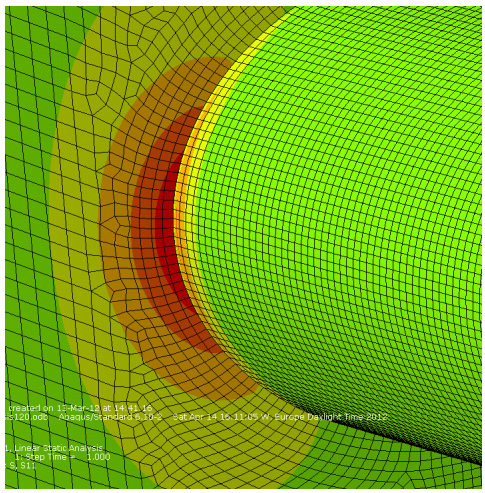

(a) Perpendicular Stress from ABAQUS

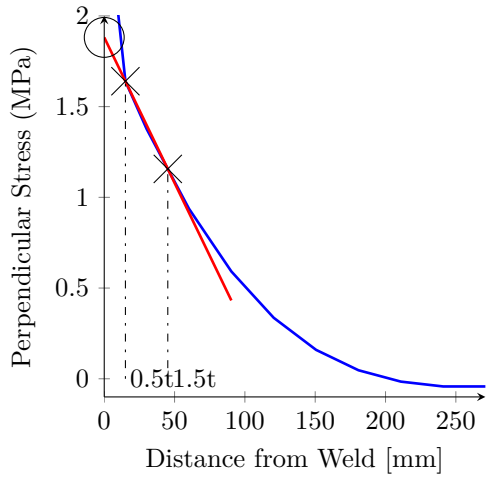

(b) Extrapolation of Figure 5.8a along brace

Figure 5.8: Extrapolation Procedure (here for OPB, LC2 Brace 1, ROP B17)

5.6 SCF

The nodal stresses at the position of interest was used to extrapolate to the intersection. This was done for read-out-points at 8 positions around the circumference intersection, as specified in [DNV-RP-C203, 2010].

From [DNV-RP-C203, 2010, 4.3.3]

> "If the element size at a hot spot region of size $t \times t$ is used, the stresses may be evaluated as follows: — In case of plate or shell elements the surface stress may be evaluated at the corresponding mid-side points. **Thus the stresses at mid side nodes along line A-B in Figure 4-2 may be used directly as stress at read out points 0.5 t and 1.5 t.**"

The nominal stress, σ_N, were taken some distance away from the brace/chord intersection, and compared with hand calculations, and there were found no deviations.

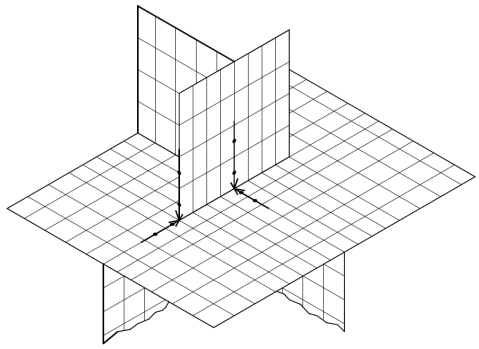

Figure 4-4
Stress extrapolation in a three-dimensional FE model to the weld toe

Figure 5.9: Shell Structural Intersection ROPs, DNV Figure 4-4

5.6.1 Nominal Stress Calculation

The nominal stresses were calculated as follows:

$$\sigma_{N_1} = \frac{F_1}{A} \tag{5.1}$$

$$\sigma_{N_i} = \frac{F_i \times x}{I} y \quad i = 2, 3 \tag{5.2}$$

$$\sigma_{N_i} = \frac{F_i}{I} y \quad i = 4, 5, 6 \tag{5.3}$$

The calculation of the nominal stress for the out-of- and in-plane forces are perhaps too simple. A cantilever beam approximation was used.

y is the distance from the brace centerline to the brace edge, and is equal to half the brace radius. x is the distance from the load (perpendicular) to the ROP of interest. I is the moment of inertia of the brace. A is the cross sectional area of the brace. F_i is the force/moment unit load.

$$I = \frac{\pi}{4}(r_{out}^4 - r_{in}^4) \tag{5.4}$$

5.7 Elements

This section presents the element types and meshing size.

5.7.1 Element Type

[DNV-RP-C203, 2010] recommends thin shell elements. 8-noded elements were used, which also gives easier access to stress values at the read-out-points in ABAQUS. Triangular elements were used in transitions. For the stiffeners and steel rod, linear beam elements were used.

Table 5.1: Element Data

Number of nodes	390063
Number of elements	131202
Element types	S8R5, STRI65, B21

5.7.2 Element Size

The element size were chosen as $t \times t$ in the hot spot area to be able to deal with the complicated stress distribution in these regions. The mesh at the rest of the model transitions to $2t \times 2t$ and then to $10t \times 10t$.

Several attempts were made to create the model in such a way that the meshing would obey the boundaries - the model was divided in several substructures to keep the meshing under control, and to be able to remove excessive nodes automatically, thus merging coherent surfaces.

The mesh was made very fine over a very large area on the model. The bulkhead, shell and braces have refined mesh. This was not really necessary, as the parts around the braces were the most interesting areas. However, it was difficult to make a nice transition between the two braces without meshing with very small elements.

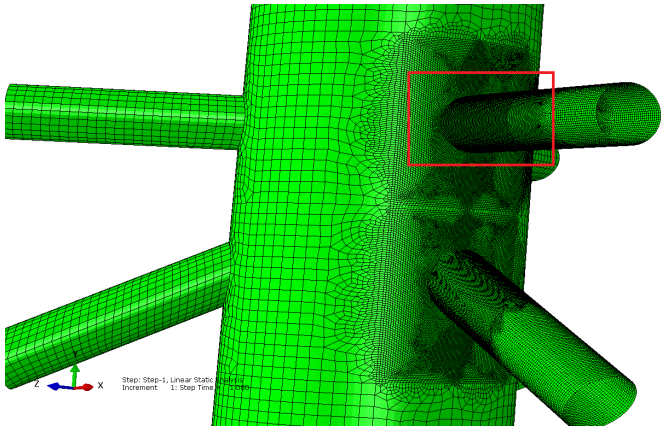

(a) Overview

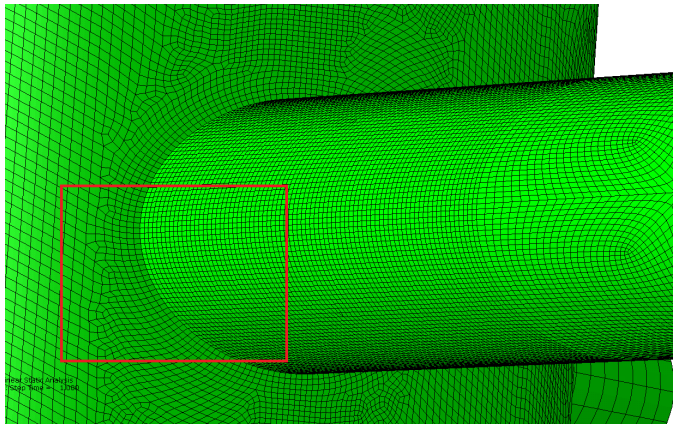

(b) Zoom in #1

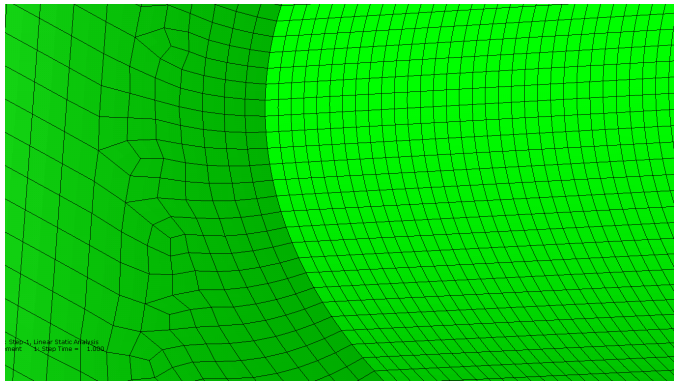

(c) Zoom in #2

Figure 5.10: Refined Mesh Outside

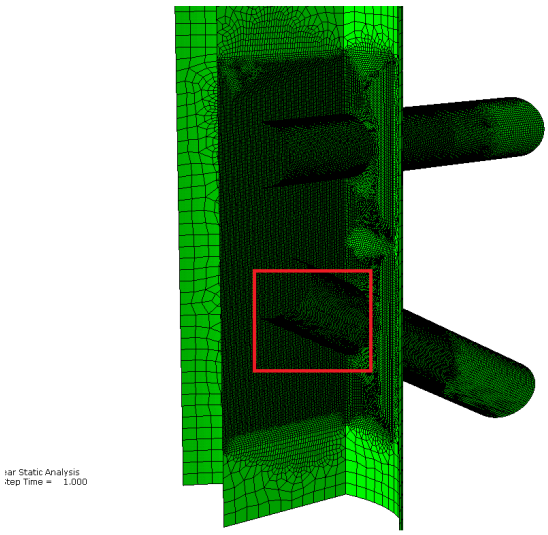

(a) Overview

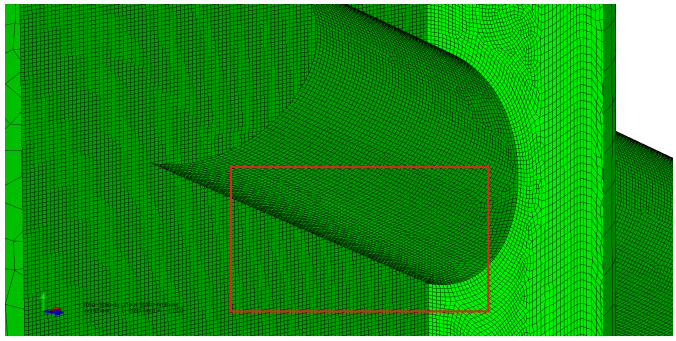

(b) Zoom in #1

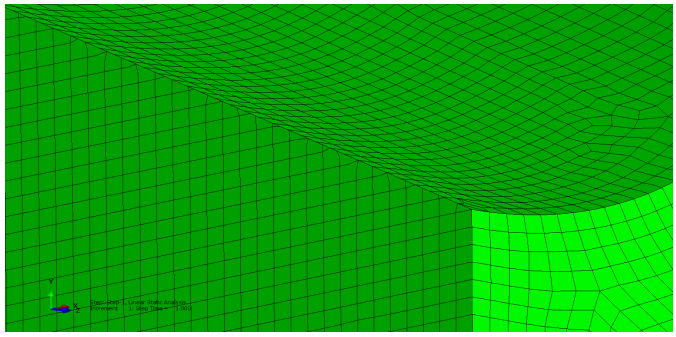

(c) Zoom in #2

Figure 5.11: Refined Mesh Inside

5.8 Boundary Condition Study

A comparison of the obtained stress concentration factors with pinned and free boundary conditions for the unloaded braces was carried out. ROP to ROP was compared.

Table 5.2: SCF_{Free}/SCF_{Pinned}, Brace 1

	LC1	LC2	LC3	LC4	LC5	LC6
B11	4.76%	0.63%	0.31%	-0.85%	0.22%	0.09%
B12	13.99%	0.26%	0.98%	1.55%	0.71%	0.03%
B13	18.69%	0.15%	-17.99%	0.65%	-6.70%	0.15%
B14	15.06%	-0.01%	-1.05%	1.80%	-0.78%	0.27%
B15	4.07%	-0.28%	-0.20%	-1.08%	-0.13%	0.38%
B16	15.06%	-0.01%	-1.05%	1.80%	-0.79	0.27%
B17	18.69%	0.14%	-18.04%	0.65%	-6.70%	0.15%
B18	13.99%	0.26%	0.98%	1.54%	0.71%	0.03%

Table 5.3: SCF_{Free}/SCF_{Pinned}, Brace 2

	LC1	LC2	LC3	LC4	LC5	LC6
B21	3.40%	-0.26%	0.37%	0.30%	0.44%	-0.42%
B22	4.51%	-0.09%	0.07%	0.09%	0.29%	-0.19%
B23	-4.90%	-0.05%	7.52%	-0.04%	-16.91%	-0.06%
B24	6.36%	0.19%	-0.31%	-0.05%	-0.64%	0.30%
B25	8.32%	0.69%	-0.75%	-0.06%	-0.93%	0.72%
B26	6.31%	0.20%	-0.31%	-0.04%	-0.64%	0.31%
B27	-4.60%	-0.01%	7.21%	0.00%	-15.89%	-0.01%
B28	4.49%	-0.08%	0.08%	0.10%	0.30%	-0.18%

Load case 2, 4 and 6 seem to be fairly unaffected by the change of boundary conditions.

Load case 1 (axial loading) for brace 1 have about 18% larger SCFs for free vs. pinned BCs, but only to 4% for the largest hot spot stresses in this case, which is ROPs B11 and B15. For reference see section 5.12.

Load case 1 for brace 2 have about 4-8% increase in SCFs, but a reduction for the hot spot stresses ROPs B22 and B25.

Load case 3 (In plane load) has a very small change in SCFs. However, for the lowest SCFs for this case, ROPs B13, B17, B23 and B27 the difference increases a lot, to about -18% and 7% respectively. Load case 5 (moment about y-axis/in plane bending) have very similar results.

It seems to be a tendency that the ROPs with lowest SCFs were most sensitive to change of boundary conditions, while the ROPs where largest hot spot stress occur, change very little. In other words, the governing stress concentration factors change very little. There was a big difference in SCFs for ROPs with small SCFs, and these may be disregarded. Disregarding ROPs with the lowest SCFs, the conclusion is that the largest change in SCFs when changing boundary conditions occurred for axial loading of the braces. For this case the maximum was ∼5% for an influence factor of ∼31 = 1.55, and ∼15% for an influence factor of ∼23 = 3.45, which is a small relative difference.

Based on this, it can not be said which model is most realistic. The other braces were thus modelled as free.

5.9 Interaction

There may be some interactions between the braces, as the SCF of a loaded brace may be influenced by the presence and loading of other braces. [Berge, 2006].

The ratio between SCF for unloaded brace vs. loaded brace are presented in Table 5.4 and Table 5.5. ROP to ROP are compared.

Table 5.4: Interaction, Brace 1 is loaded. $SCF_{Brace2}/SCF_{Brace1}$

ROP	LC1	LC2	LC3	LC4	LC5	LC6
1	10.69%	29.07%	1.35%	7.37%	0.47%	17.61%
2	8.04%	1.73%	6.00%	14.53%	5.25%	3.47%
3	31.87%	1.11%	219.53%	2.73%	119.42%	1.20%
4	9.09%	2.22%	4.94%	8.16%	3.89%	1.02%
5	28.72%	9.46%	0.45%	3.63%	0.52%	1.42%
6	9.01%	2.19%	4.90%	8.14%	3.87%	0.98%
7	31.77%	1.07%	221.39%	2.66%	120.44%	1.15%
8	8.08%	1.69%	5.96%	14.55%	5.23%	3.46%

Table 5.5: Interaction. Brace 2 is loaded. $SCF_{Brace1}/SCF_{Brace2}$

ROP	LC1	LC2	LC3	LC4	LC5	LC6
1	1.43%	1.96%	0.03%	1.19%	0.07%	2.27%
2	7.39%	2.43%	3.51%	0.64%	1.98%	2.84%
3	14.39%	0.49%	9.92%	0.58%	63.76%	0.66%
4	8.53%	1.45%	1.03%	3.20%	0.54%	1.97%
5	1.66%	24.38%	0.02%	8.78%	0.13%	14.96%
6	8.41%	1.47%	1.02%	3.21%	0.54%	1.99%
7	13.92%	0.50%	9.79%	0.59%	63.35%	0.66%
8	7.28%	2.42%	3.53%	0.63%	1.98%	2.83%

There seem to be great interaction for the ROPs where the SCFs are lowest, which may be disregarded as concluded in section 5.9. Disregarding these, the axial load seem to be the one that causes the largest interaction.

The interaction is negligible, thus interaction was not included in the analyses.

5.10 Joint with horizontal bulkheads (Design 2)

The results from the cases with stiffeners only, showed that the out-of-plane loading gave very high SCFs. The earlier assumption that the axial action would be dominating were not longer valid, due to the high SCFs. The ring-stiffeners were replaced by simple horizontal bulkheads to try to reduce the out-of-plane loading stress concentration factors.

The bulkheads were placed at the same positions as the ring-stiffeners, with radius 3250 mm, and a hole in the middle with a radius of 500 mm. This hole was created to control the meshing, and avoid very small elements. It was also necessary for welder and inspection access. However, for later optimizing of the bulkheads, the holes for this purpose would maybe have been placed elsewhere. The thickness of the bulkheads was set to 30 mm.

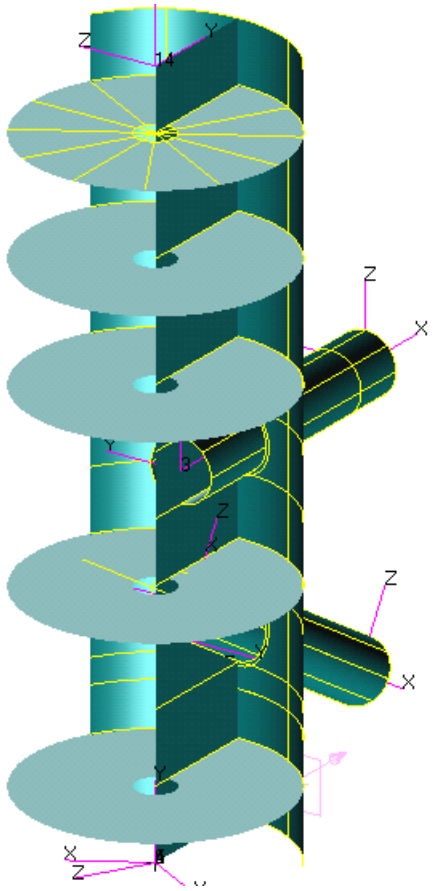

Figure 5.12: Joint with horizontal bulkheads. Only 1/3 of the other parts of the joint is presented

5.11 Joint with horizontal bulkhead at Brace 1 (Design 3)

Because there were small changes in the SCFs when adding the horizontal bulkheads, they were replaced by the original ring-stiffeners. A horizontal bulkhead was placed at the upper brace/vertical bulkhead-intersection as shown in Figure 5.13

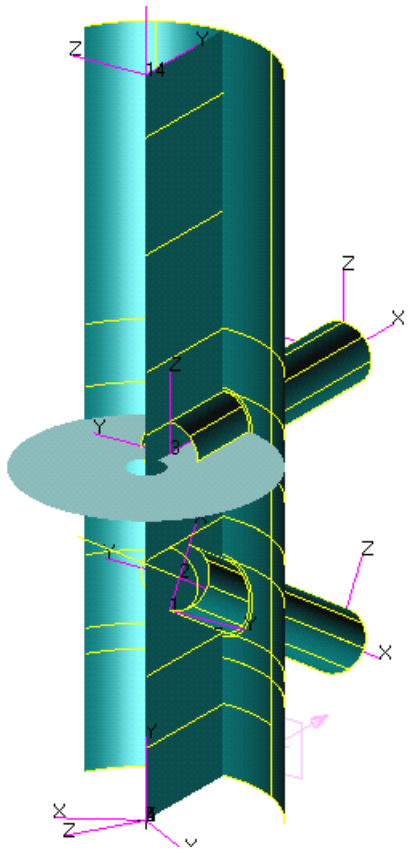

Figure 5.13: Joint with horizontal bulkhead at brace/vertical bulkhead-intersection. Only 1/3 of the other parts of the joint is presented

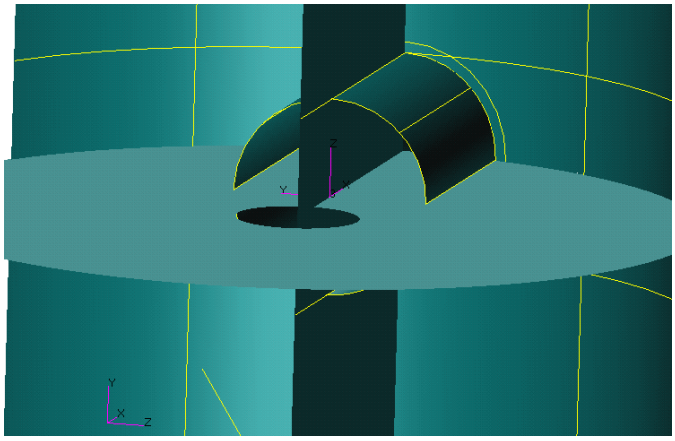

Figure 5.14: Joint with horizontal bulkheads and bulkhead at brace/vertical bulkhead-intersection.

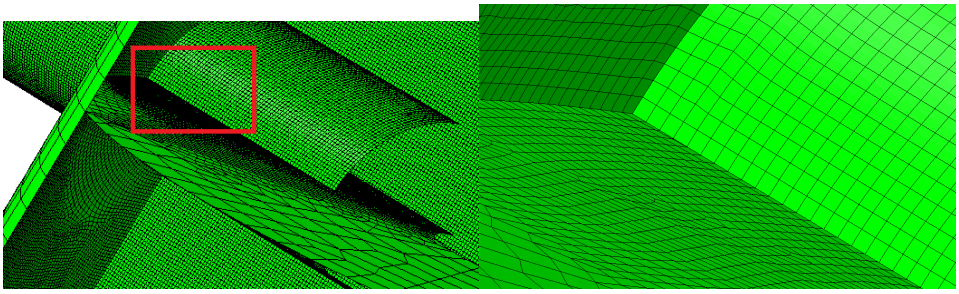

(a) Bulkhead **(b)** Bulkhead zoom

Figure 5.15: Bulkhead at brace/vertical bulkhead-intersection mesh

5.12 Results

Here the SCFs and influence factors are presented for all load cases. First, the results for the joint without horizontal bulkheads are presented, and then for the joints with horizontal bulkhead(s). A comparison of the two latter joint configurations is presented in the end. The results are presented in tables and in histograms. Two illustrative circumference-plots was also provided.

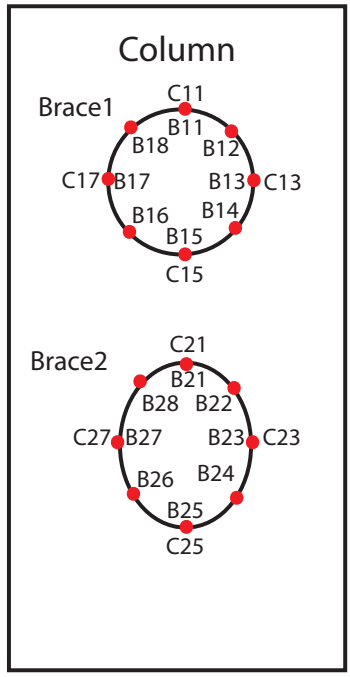

Figure 5.16: Definition of hot-spot locations/Read-Out-Point IDs. CXY means chord-side of weld on brace X read-out point Y. BXY means brace-side of weld on brace X read-out point Y.

Notice that the influence factors for moments (LC4,-5,-6) are small relative to the influence factors for forces (LC1,-2,-3). This is because of different dimensions: [Pa/N] and [Pa/Nm]. It is better to look at the SCFs for comparing.

ROP IDs are referred to Figure 5.16.

For calculation purposes, only the influence factor is necessary. However, the SCFs are useful for comparing action from moment load and the ones from force load. For these reasons, SCFs are presented for brace loading. For the chord loading the influence factors are presented only, because of the difficulty of finding the correct nominal stress to be used.

5.12.1 Stress Concentration Factors. Brace loaded

Brace side of weld, SCF_b

Table 5.6: SCFs for Brace 1

Load/ROP	B11	B12	B13	B14	B15	B16	B17	B18
LC1 (Fx)	4.69	2.45	3.43	2.52	4.62	2.52	3.44	2.45
LC2 (Fy)	0.81	10.97	21.01	10.63	0.74	10.62	21.02	10.98
LC3 (Fz)	3.89	1.49	0.11	1.54	3.95	1.54	0.11	1.49
LC4 (Mx)	0.40	1.25	0.47	1.24	0.40	1.24	0.47	1.25
LC5 (My)	3.70	1.36	0.12	1.38	3.73	1.38	0.12	1.36
LC6 (Mz)	0.96	10.93	21.49	10.85	0.94	10.84	21.50	10.94

Table 5.7: SCFs for Brace 2

Load/ROP	B21	B22	B23	B24	B25	B26	B27	B28
LC1 (Fx)	4.26	1.92	2.23	2.16	6.17	2.19	2.30	1.96
LC2 (Fy)	0.80	8.13	13.45	7.78	0.44	7.73	13.46	8.14
LC3 (Fz)	3.24	1.12	0.32	1.68	5.20	1.69	0.33	1.12
LC4 (Mx)	0.25	6.32	8.41	3.66	0.90	3.63	8.42	6.32
LC5 (My)	3.27	1.19	0.06	1.25	4.53	1.26	0.06	1.19
LC6 (Mz)	0.96	8.46	13.68	7.54	0.63	7.49	13.69	8.47

Chord side of weld, SCF_c

Table 5.8: SCF_c Brace 1

	C11	C13	C15	C17
LC1 (Fx)	1.47	3.26	1.52	3.30
LC2 (Fy)	0.96	30.03	0.86	30.34
LC3 (Fz)	1.40	0.06	1.41	0.06
LC4 (Mx)	0.29	0.54	0.29	0.55
LC5 (My)	1.28	0.07	1.28	0.07
LC6 (Mz)	1.08	30.85	1.05	31.16

Table 5.9: SCF_c Brace 2

	C21	C23	C25	C27
LC1 (Fx)	3.05	2.20	0.65	2.34
LC2 (Fy)	0.87	18.63	0.40	19.02
LC3 (Fz)	1.64	0.26	0.92	0.27
LC4 (Mx)	0.36	11.58	0.75	11.83
LC5 (My)	1.79	0.04	0.76	0.05
LC6 (Mz)	1.03	19.10	0.57	19.50

Below, the influence factors are presented for Brace 1 and Brace 2.

5.12.2 Influence Factors, Brace loaded

Brace side of weld, IF_b

Table 5.10: Influence Factors Brace 1

Load Type	B11	B12	B13	B14	B15	B16	B17	B18
LC1 (Fx)	31.72	16.55	23.20	17.01	31.24	17.01	23.21	16.55
LC2 (Fy)	71.12	972.08	1 879.17	941.72	65.10	941.15	1 880.57	972.55
LC3 (Fz)	341.10	132.35	10.20	136.39	346.13	136.36	10.17	132.35
LC4 (Mx)	0.007	0.022	0.008	0.022	0.007	0.022	0.008	0.022
LC5 (My)	0.065	0.024	0.002	0.024	0.065	0.024	0.002	0.024
LC6 (Mz)	0.017	0.192	0.377	0.190	0.016	0.190	0.377	0.192

Table 5.11: Influence Factors Brace 2

Load Type	B21	B22	B23	B24	B25	B26	B27	B28
LC1 (Fx)	28.76	12.96	15.07	14.60	41.67	14.77	15.58	13.24
LC2 (Fy)	83.47	837.87	1319.90	709.39	38.47	704.88	1321.06	838.25
LC3 (Fz)	338.58	115.51	31.67	152.81	455.96	153.76	32.08	115.16
LC4 (Mx)	0.004	0.111	0.147	0.064	0.016	0.064	0.148	0.111
LC5 (My)	0.057	0.021	0.001	0.022	0.079	0.022	0.001	0.021
LC6 (Mz)	0.017	0.148	0.240	0.132	0.011	0.131	0.240	0.149

Chord side of weld IF_c

Table 5.12: Influence Factors Brace 1

Load Type	C11	C13	C15	C17
LC1 (Fx)	9.94	22.06	10.27	22.33
LC2 (Fy)	84.23	2686.79	75.29	2713.79
LC3 (Fz)	122.62	5.38	123.32	5.35
LC4 (Mx)	0.005	0.009	0.005	0.010
LC5 (My)	0.022	0.001	0.022	0.001
LC6 (Mz)	0.019	0.541	0.018	0.547

Table 5.13: Influence Factors Brace 2

Load Type	C21	C23	C25	C27
LC1 (Fx)	20.64	14.84	4.41	15.84
LC2 (Fy)	90.43	1828.23	35.12	1866.56
LC3 (Fz)	171.15	25.09	80.28	26.43
LC4 (Mx)	0.006	0.203	0.013	0.207
LC5 (My)	0.031	0.001	0.013	0.001
LC6 (Mz)	0.018	0.335	0.010	0.342

Circumference plot

Circumference plots for influence factors for Brace 1, LC1 and LC2 are presented.

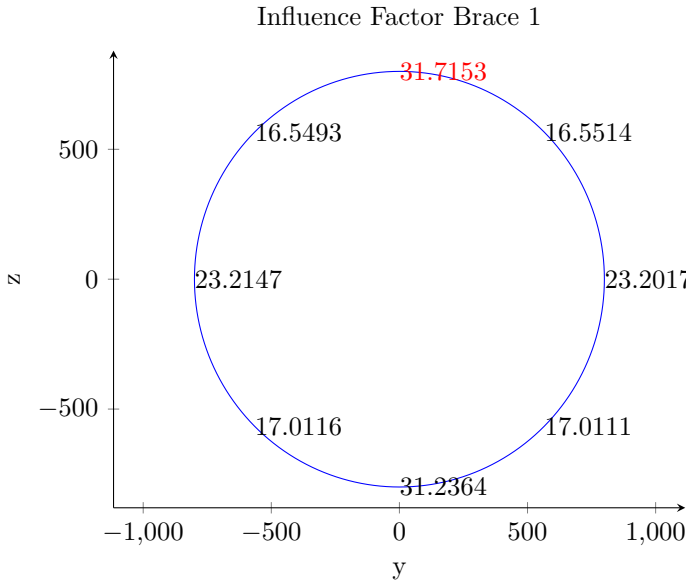

Figure 5.17: Influence factors, Brace 1 circumf., LC1

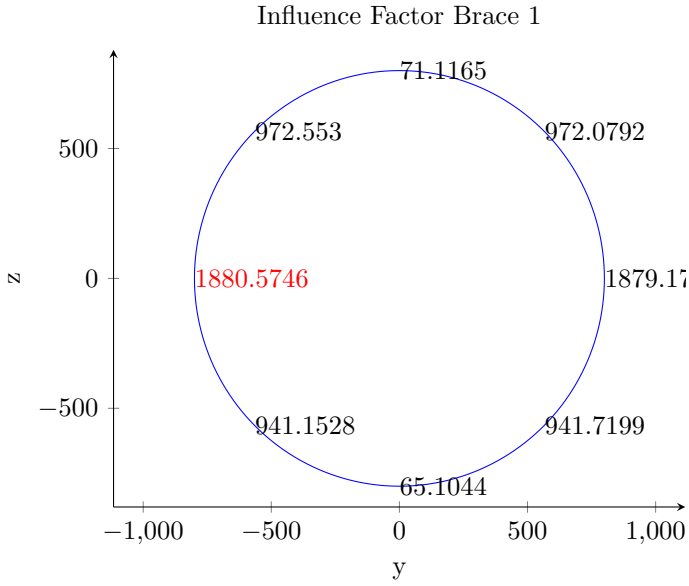

Figure 5.18: Influence factors, Brace 1 circumf., LC2

5.12.3 Comments

In Table 5.6 and 5.7 the SCFs for brace to chord extrapolation are presented. For LC1 the SCFs have values ∼1-5, where the highest values appear at the crowns, and the smallest at the saddles. For LC2 the SCFs range from ∼1-22, where the smallest values are located at the crowns, and largest values at the saddles, as expected. LC3 have SCF-values in the region ∼0-5 with the highest values at the crowns. LC4 (torsion) have small SCFs for Brace 1: 0-1.25, and larger for Brace 2: 0-9, which probably is because of the non-symmetric cross section of the brace/chord intersection. LC5 have values from 0-4 and have the largest SCFs at the crowns. LC6 have very large SCFs for both braces, ∼1-22, with the largest values at the saddles.

Notice that LC2 and LC6 (Out-of-plane-action), and LC2 and LC5 (in-plane-action) almost gives the same SCF-values. This is because the load cases are close to identical.

For the chord-to-brace extrapolation, LC2 and LC6 are the dominating load cases. Brace 1 is most exposed with a maximum SCF of 31.16, while Brace 2 maxes at 19.50.

Brace 1 have larger SCFs for LC2 and LC6 compared to brace 2, while Brace 2 have larger SCFs for LC1 and LC4. LC3 and LC5 are very close for both cases, but slightly larger for Brace 2 for LC3. The differences are caused because of the non-symmetric attachment of brace 2.

The SCF-values are on average very large, which indicates that the design needs modifications. The worst load case is out-of-plane-action, LC2 and LC6, which in reality is caused by torsion of the tower/mid-column. When looking at Figure 2.9, it is clear that it should have been included some sort of horizontal stiffening e.g. bulkheads at the brace centrelines. The stiffening of the joint is at this point not sufficient.

5.12.4 Influence Factors, Chord loaded

Chord side of weld, IF_c

Table 5.14: Influence Factors Brace 1

Load Type	C11	C13	C15	C17
LC1 (Fx)	0.65	1.11	0.57	1.13
LC2 (Fy)	20.89	29.18	3.40	29.58
LC3 (Fz)	1.78	5.58	2.54	5.64
LC4 (Mx)	0.000	0.001	0.001	0.001
LC5 (My)	0.000	0.000	0.000	0.000
LC6 (Mz)	0.001	0.002	0.000	0.002

Table 5.15: Influence Factors Brace 2

Load Type	C21	C23	C25	C27
LC1 (Fx)	2.35	1.42	0.16	1.47
LC2 (Fy)	7.19	11.88	0.76	12.31
LC3 (Fz)	2.11	2.78	2.32	2.89
LC4 (Mx)	0.00	0.00	0.00	0.00
LC5 (My)	0.00	0.00	0.00	0.00
LC6 (Mz)	0.00	0.00	0.00	0.00

5.12.5 Comments

The influence factors for the braces when the chord is loaded are negligible compared to when the braces are loaded. The chord loading was not presented for the 2 remaining joint designs.

5.12.6 Histogram Presentation

Here a histogram presentation of the results are presented for a better overview.

SCFs

Brace 1

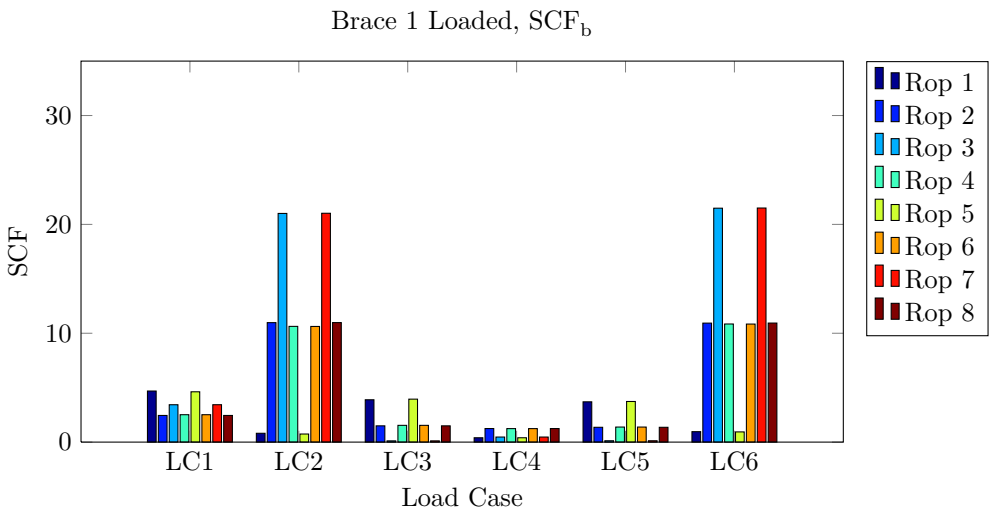

Figure 5.19: SCF for brace 1, brace side of weld

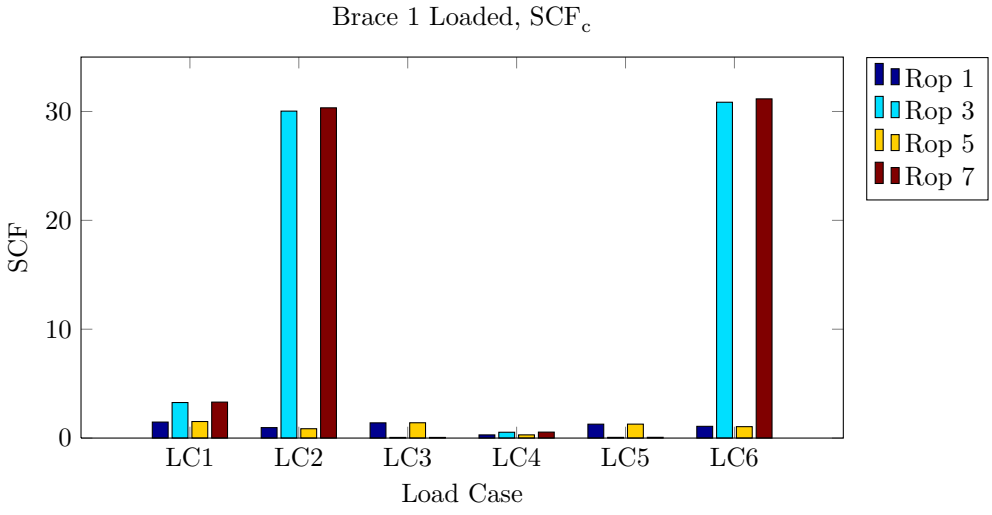

Figure 5.20: SCF for brace 1, chord side of weld

Brace 2

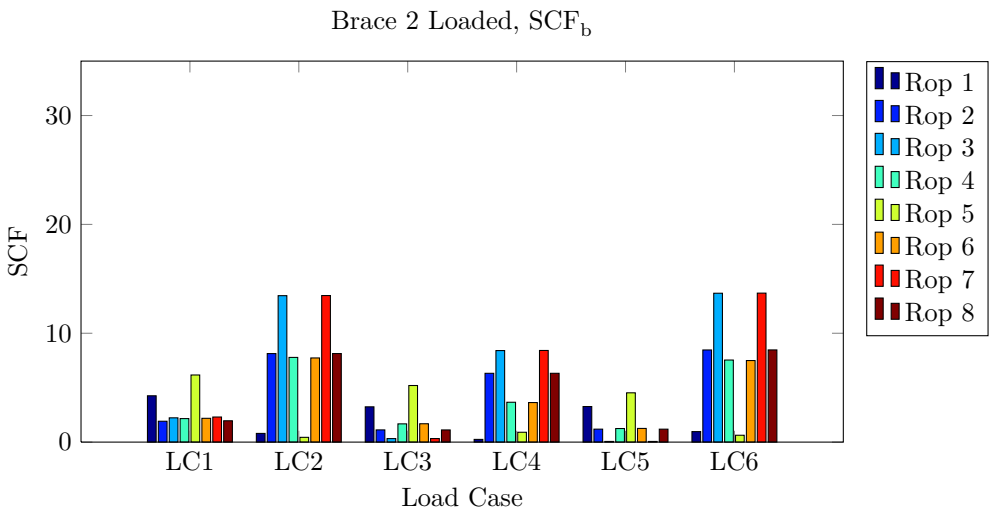

Figure 5.21: SCF for brace 2, brace side of weld

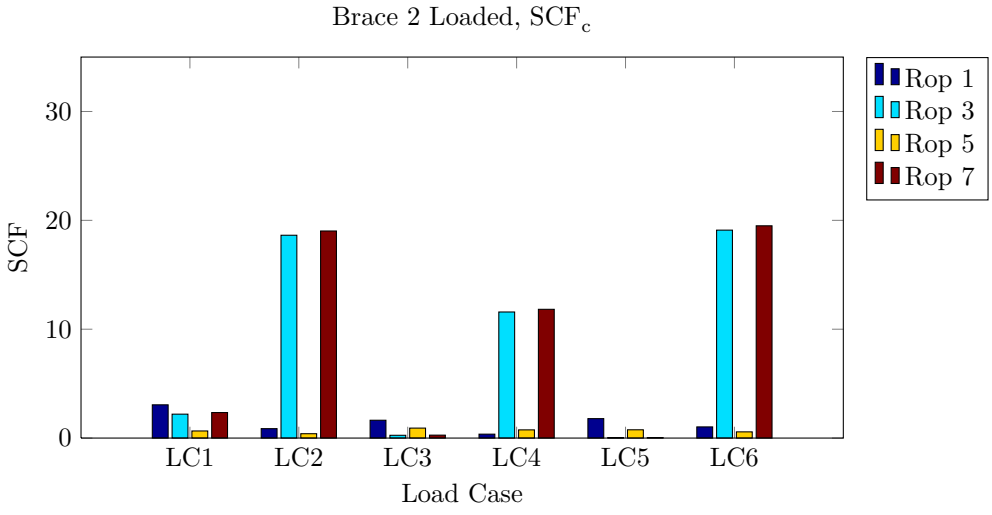

Figure 5.22: SCF for brace 2, chord side of weld

IFs

Brace 1

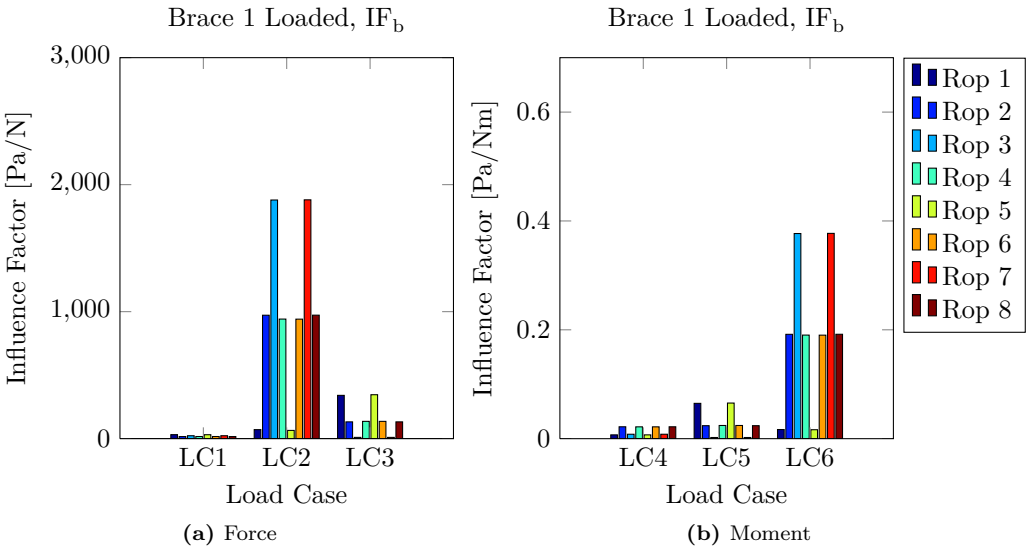

(a) Force **(b)** Moment

Figure 5.23: IF for brace 1, brace side of weld

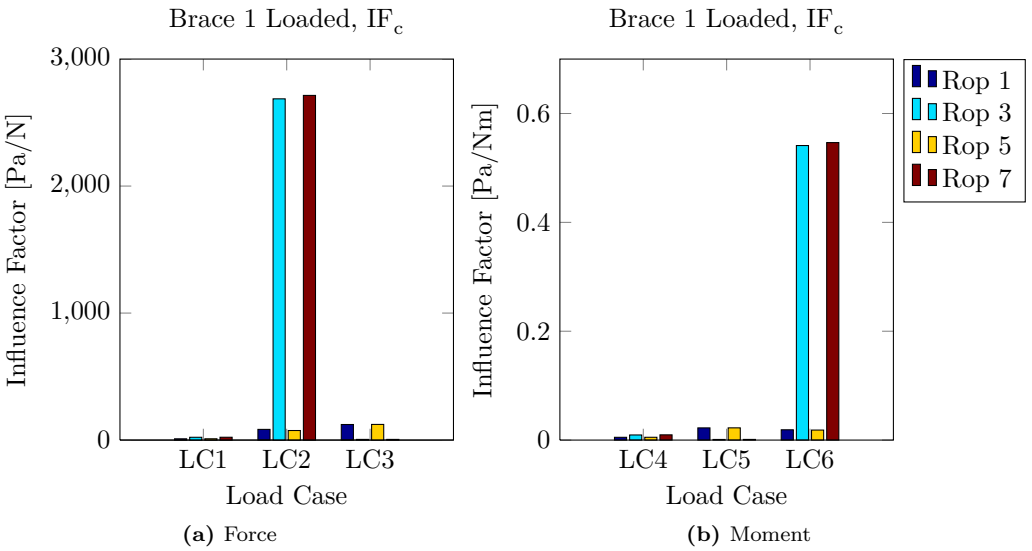

(a) Force **(b)** Moment

Figure 5.24: IF for brace 1, chord side of weld

Brace 2

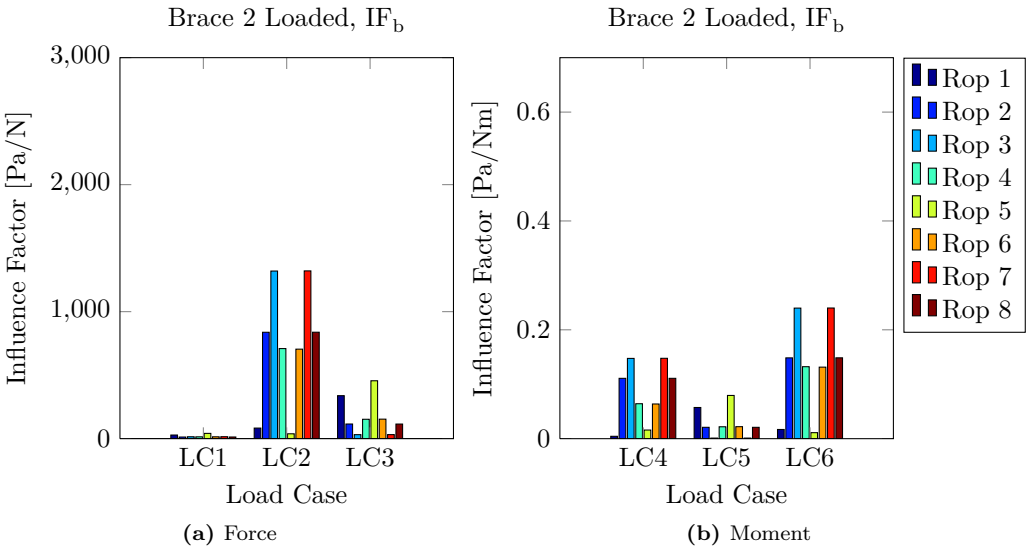

(a) Force **(b)** Moment

Figure 5.25: IF for brace 2, brace side of weld

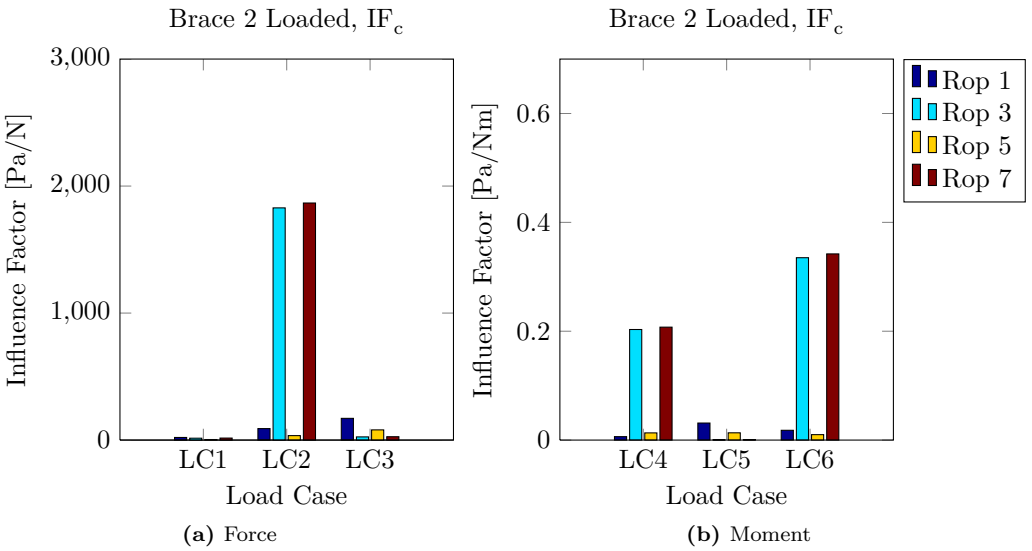

(a) Force **(b)** Moment

Figure 5.26: IF for brace 2, chord side of weld

Chord

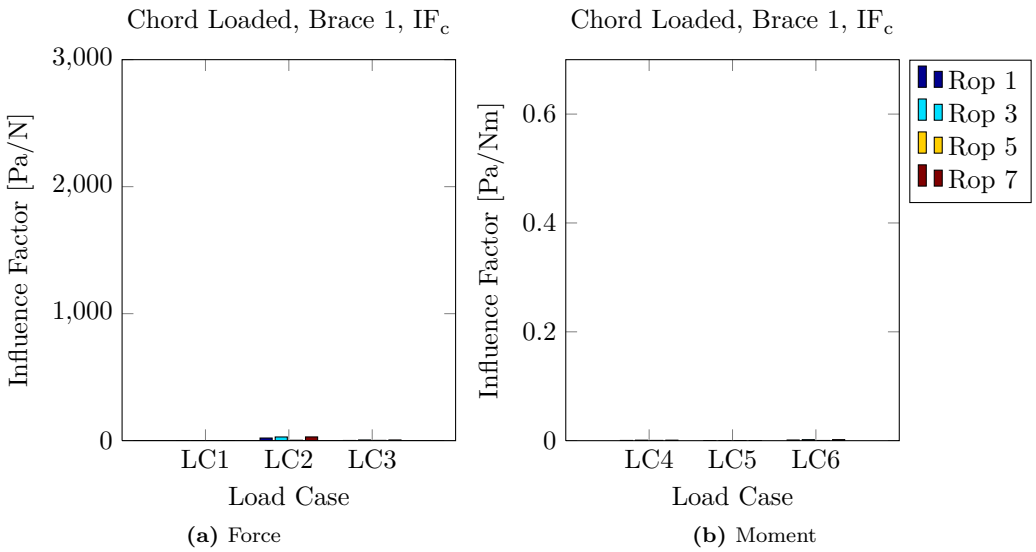

(a) Force **(b)** Moment

Figure 5.27: IF for brace 1, chord loaded, chord side of weld

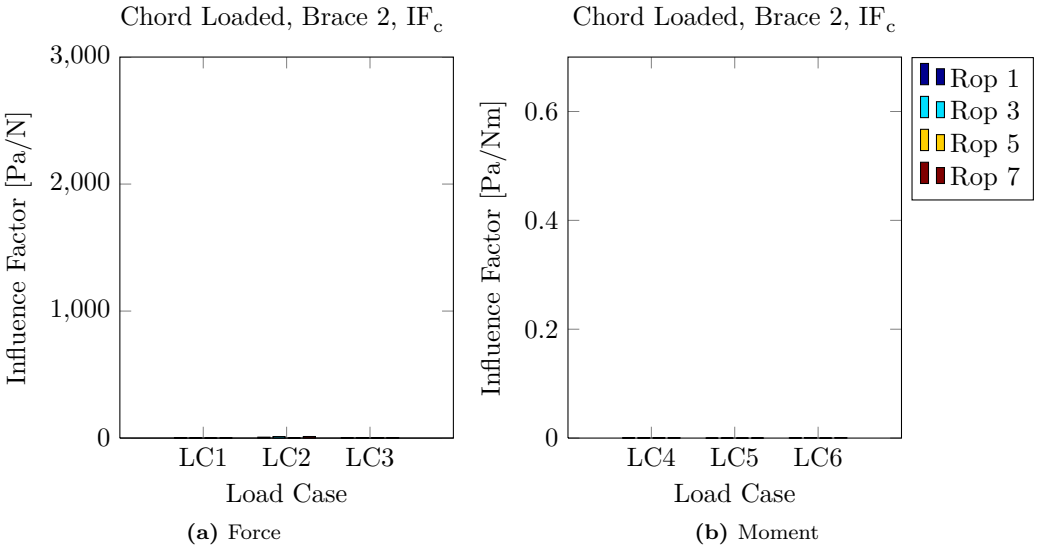

(a) Force **(b)** Moment

Figure 5.28: IF for brace 2, chord loaded, chord side of weld

As the histograms show, LC2 and LC6 are by far the dominating cases.

5.12.7 Load Cases from ABAQUS/Viewer

The perpendicular stresses are presented for the six load cases.

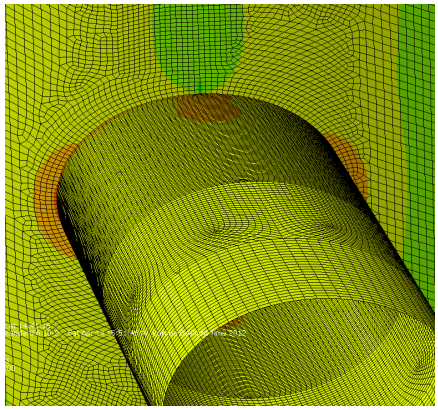

(a) LC1

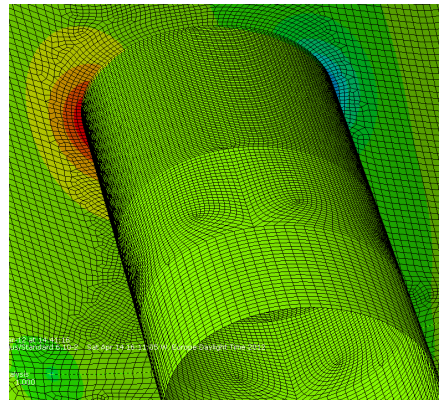

(b) LC2

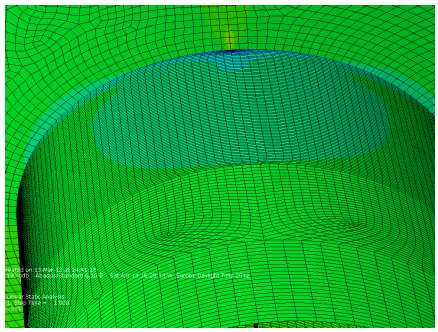

(c) LC3

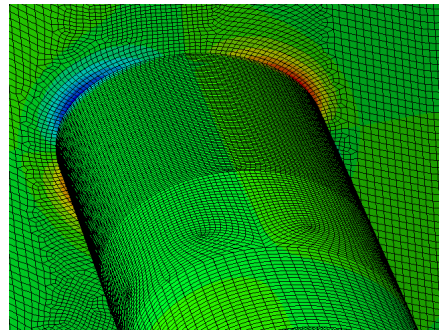

(d) LC4

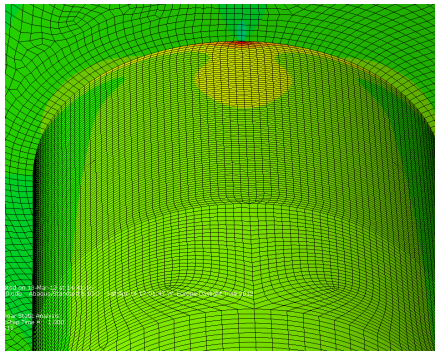

(e) LC5

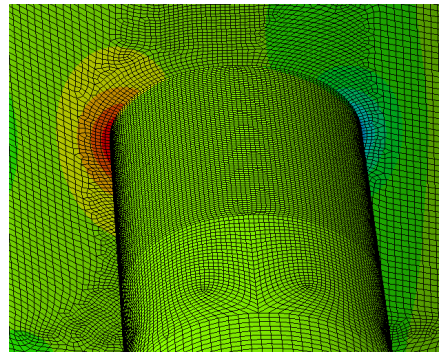

(f) LC6

Figure 5.29: Brace/Chord intersection as presented by ABAQUS/Viewer, Brace 1. Red is tension, blue is compression. Deformation view is turned off.

5.13 Results from joint with horizontal bulkheads

5.13.1 Stress Concentration Factors. Brace loaded

Brace side of weld, SCF_b

Table 5.16: SCFs for Brace 1

Load/ROP	B11	B12	B13	B14	B15	B16	B17	B18
LC1 (Fx)	4.68	2.46	3.28	2.54	4.60	2.54	3.28	2.46
LC2 (Fy)	0.85	11.33	20.65	10.72	0.72	10.71	20.67	11.33
LC3 (Fz)	3.89	1.50	0.12	1.56	3.95	1.56	0.12	1.50
LC4 (Mx)	0.43	1.05	0.45	1.05	0.43	1.05	0.45	1.05
LC5 (My)	3.70	1.36	0.13	1.39	3.73	1.39	0.13	1.36
LC6 (Mz)	1.00	11.32	21.13	10.97	0.91	10.96	21.15	11.32

Table 5.17: SCFs for Brace 2

Load/ROP	B21	B22	B23	B24	B25	B26	B27	B28
LC1 (Fx)	4.31	2.00	2.18	2.13	5.99	2.15	2.23	2.04
LC2 (Fy)	0.79	8.45	12.00	6.80	0.36	6.76	12.00	8.45
LC3 (Fz)	3.24	1.12	0.33	1.69	5.21	1.70	0.33	1.12
LC4 (Mx)	0.20	6.30	7.54	3.30	0.89	3.28	7.54	6.29
LC5 (My)	3.27	1.19	0.06	1.26	4.54	1.27	0.06	1.19
LC6 (Mz)	0.97	8.90	12.17	6.56	0.55	6.52	12.17	8.90

Chord side of weld, SCF_c

Table 5.18: SCF_c Brace 1

	C11	C13	C15	C17
LC1 (Fx)	1.46	3.17	1.52	3.21
LC2 (Fy)	0.98	28.91	0.82	29.20
LC3 (Fz)	1.40	0.07	1.41	0.07
LC4 (Mx)	0.33	0.51	0.33	0.52
LC5 (My)	1.28	0.07	1.28	0.07
LC6 (Mz)	1.10	29.69	1.01	29.99

Table 5.19: SCF_c Brace 2

	C21	C23	C25	C27
LC1 (Fx)	2.91	2.16	0.62	2.29
LC2 (Fy)	0.85	16.27	0.29	16.62
LC3 (Fz)	1.64	0.27	0.92	0.28
LC4 (Mx)	0.29	10.14	0.73	10.36
LC5 (My)	1.78	0.05	0.76	0.05
LC6 (Mz)	1.02	16.66	0.45	17.01

Below, the influence factors are presented for Brace 1 and Brace 2.

5.13.2 Influence Factors, Brace loaded

Brace side of weld, IF_b

Table 5.20: Influence Factors Brace 1

Load Type	B11	B12	B13	B14	B15	B16	B17	B18
LC1 (Fx)	31.61	16.66	22.19	17.15	31.11	17.14	22.20	16.65
LC2 (Fy)	74.38	1003.30	1847.61	949.33	62.84	948.78	1848.99	1003.70
LC3 (Fz)	341.10	132.71	10.61	138.10	346.30	138.07	10.58	132.71
LC4 (Mx)	0.008	0.018	0.008	0.018	0.007	0.018	0.008	0.018
LC5 (My)	0.065	0.024	0.002	0.024	0.065	0.024	0.002	0.024
LC6 (Mz)	0.018	0.198	0.371	0.192	0.016	0.192	0.371	0.199

Table 5.21: Influence Factors Brace 2

Load Type	B21	B22	B23	B24	B25	B26	B27	B28
LC1 (Fx)	29.11	13.54	14.71	14.41	40.46	14.55	15.05	13.81
LC2 (Fy)	82.15	870.60	1177.42	619.99	31.30	616.04	1177.67	870.39
LC3 (Fz)	338.66	115.59	32.38	154.11	456.77	154.99	32.62	115.26
LC4 (Mx)	0.003	0.110	0.132	0.058	0.016	0.057	0.132	0.110
LC5 (My)	0.057	0.021	0.001	0.022	0.080	0.022	0.001	0.021
LC6 (Mz)	0.017	0.156	0.213	0.115	0.010	0.114	0.213	0.156

Chord side of weld IF_c

Table 5.22: Influence Factors Brace 1

Load Type	C11	C13	C15	C17
LC1 (Fx)	9.90	21.41	10.25	21.67
LC2 (Fy)	86.05	2585.88	71.49	2612.26
LC3 (Fz)	122.65	6.09	123.70	6.09
LC4 (Mx)	0.006	0.009	0.006	0.009
LC5 (My)	0.022	0.001	0.023	0.001
LC6 (Mz)	0.019	0.521	0.018	0.526

Table 5.23: Influence Factors Brace 2

Load Type	C21	C23	C25	C27
LC1 (Fx)	19.65	14.57	4.22	15.47
LC2 (Fy)	88.35	1596.45	25.34	1630.76
LC3 (Fz)	170.98	26.07	80.45	27.35
LC4 (Mx)	0.005	0.178	0.013	0.182
LC5 (My)	0.031	0.001	0.013	0.001
LC6 (Mz)	0.018	0.292	0.008	0.298

5.13.3 Comments

Replacing the stiffeners with bulkheads gave a very small reduction, and at some places an increase in SCFs.

5.13.4 Histogram presentation

Here a histogram presentation of the results are presented for a better overview.

Brace 1

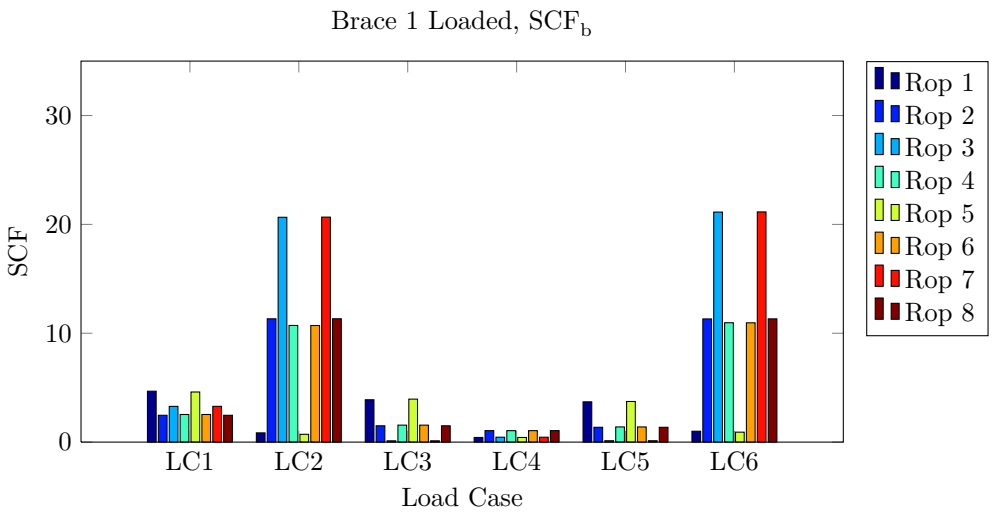

Figure 5.30: SCF for brace 1, brace side of weld

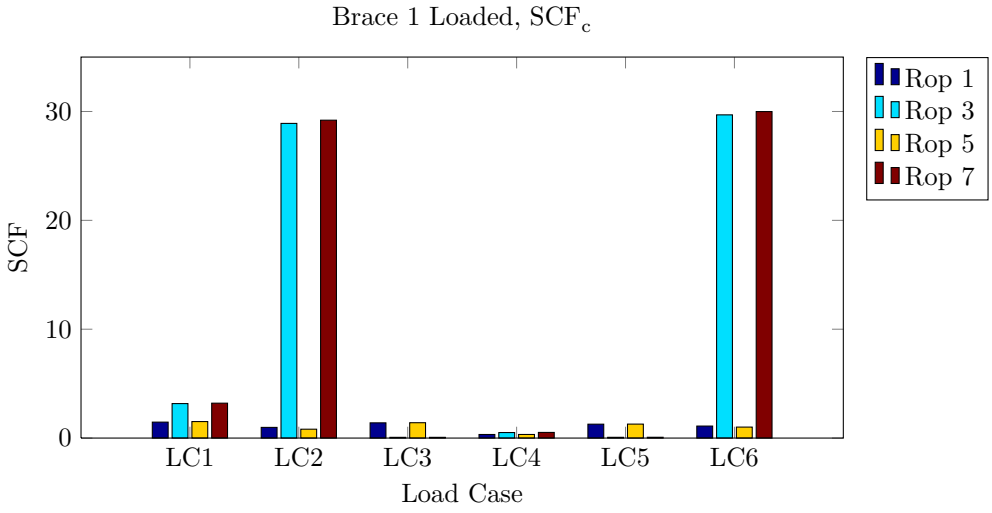

Figure 5.31: SCF for brace 1, chord side of weld

Brace 2

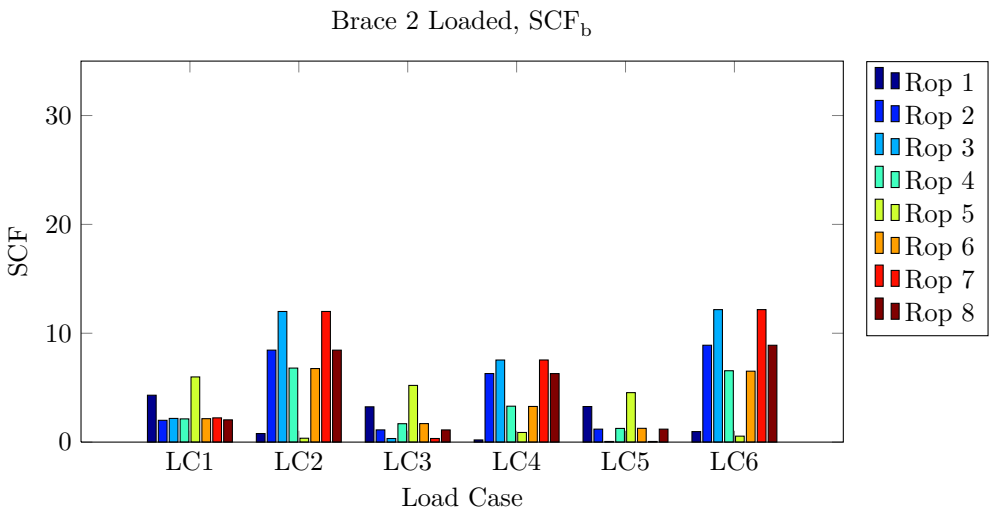

Figure 5.32: SCF for brace 2, brace side of weld

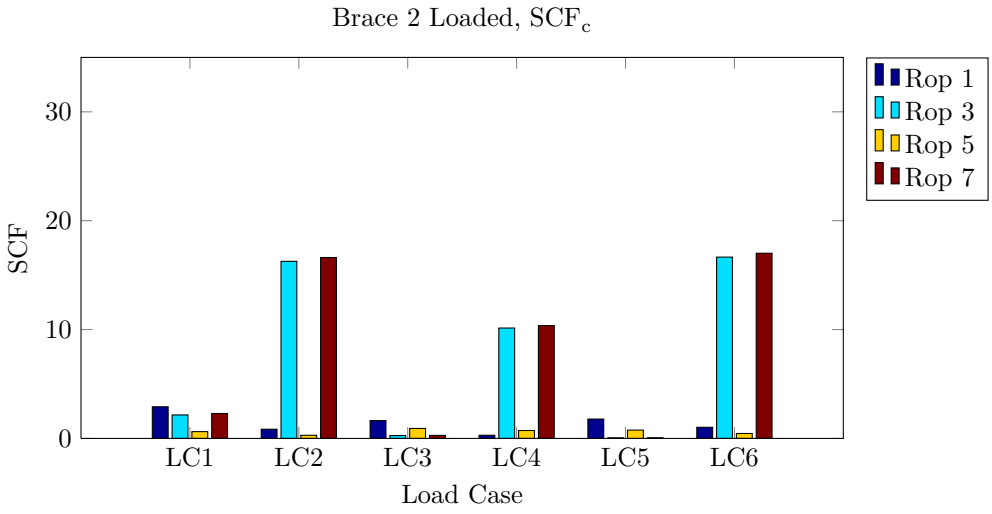

Figure 5.33: SCF for brace 2, chord side of weld

5.14 Results from joint with bulkhead at brace 1 centerline

In this section, the results from Brace 1 SCF and IF are presented only, as the bulkhead was placed at the Brace 1 position.

5.14.1 Stress Concentration Factors. Brace loaded

Brace side of weld, SCF_b

Table 5.24: SCFs for Brace 1

Load/ROP	B11	B12	B13	B14	B15	B16	B17	B18
LC1 (Fx)	3.76	2.47	3.58	2.55	3.71	2.55	3.53	2.46
LC2 (Fy)	0.03	1.44	3.53	1.14	0.09	1.14	3.49	1.44
LC3 (Fz)	3.76	1.44	0.07	1.56	3.83	1.55	0.07	1.44
LC4 (Mx)	0.40	1.12	0.55	1.17	0.39	1.17	0.54	1.12
LC5 (My)	3.57	1.33	0.11	1.39	3.61	1.38	0.11	1.32
LC6 (Mz)	0.08	1.03	3.38	0.94	0.06	0.94	3.33	1.03

Chord side of weld, SCF_c

Table 5.25: SCF_c Brace 1

Load/ROP	C11	C13	C15	C17
LC1 (Fx)	1.34	1.13	1.40	1.11
LC2 (Fy)	0.03	1.38	0.11	1.37
LC3 (Fz)	1.32	0.06	1.35	0.06
LC4 (Mx)	0.29	0.55	0.29	0.55
LC5 (My)	1.20	0.06	1.22	0.06
LC6 (Mz)	0.03	1.36	0.01	1.34

5.14.2 Influence Factors, Brace loaded

Brace side of weld, IF_b

Table 5.26: Influence Factors Brace 1

Load Type	B11	B12	B13	B14	B15	B16	B17	B18
LC1 (Fx)	25.40	16.67	24.18	17.23	25.08	17.22	23.84	16.66
LC2 (Fy)	2.77	127.59	315.95	100.96	7.91	100.79	311.78	127.44
LC3 (Fz)	329.53	128.00	6.11	137.81	336.16	137.56	6.07	127.72
LC4 (Mx)	0.007	0.020	0.010	0.021	0.007	0.021	0.009	0.020
LC5 (My)	0.063	0.023	0.002	0.024	0.063	0.024	0.002	0.023
LC6 (Mz)	0.001	0.018	0.059	0.017	0.001	0.016	0.058	0.018

Chord side of weld IF_c

Table 5.27: Influence Factors Brace 1

Load Type	C11	C13	C15	C17
LC1 (Fx)	9.04	7.64	9.49	7.52
LC2 (Fy)	2.87	123.65	10.04	122.31
LC3 (Fz)	116.13	5.53	118.26	5.54
LC4 (Mx)	0.005	0.010	0.005	0.010
LC5 (My)	0.021	0.001	0.021	0.001
LC6 (Mz)	0.001	0.024	0.000	0.024

5.14.3 Comments

There seem to be a great reduction of SCFs/IFs after adding the horizontal bulkhead at the brace location. The largest SCF is now for LC3 at the crown with a value of 3.83. The out-of-plane cases LC2 and LC6 have a maximum SCF of 3.53 at the saddle, compared to a value of 32 for Design 1. Now the brace side of the weld has the largest SCF-values, opposed to Design 1, where the chord side of the weld was the most critical.

The adding of a horizontal bulkhead was found to be a huge improvement for the joint design, and the out-of-plane action is no longer the critical load case.

5.14.4 Histogram presentation

Here a histogram presentation of the results are presented for a better overview.

Brace 1

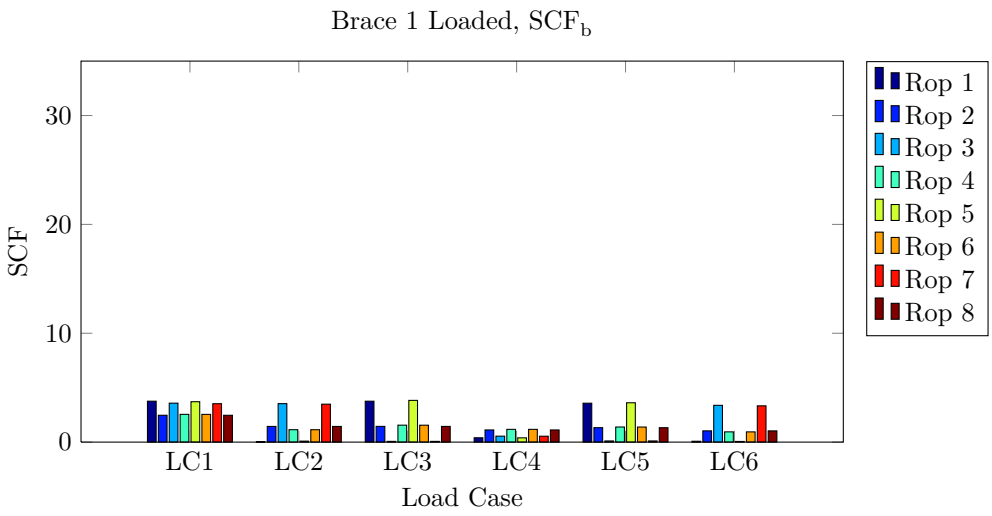

Figure 5.34: SCF for brace 1, brace side of weld

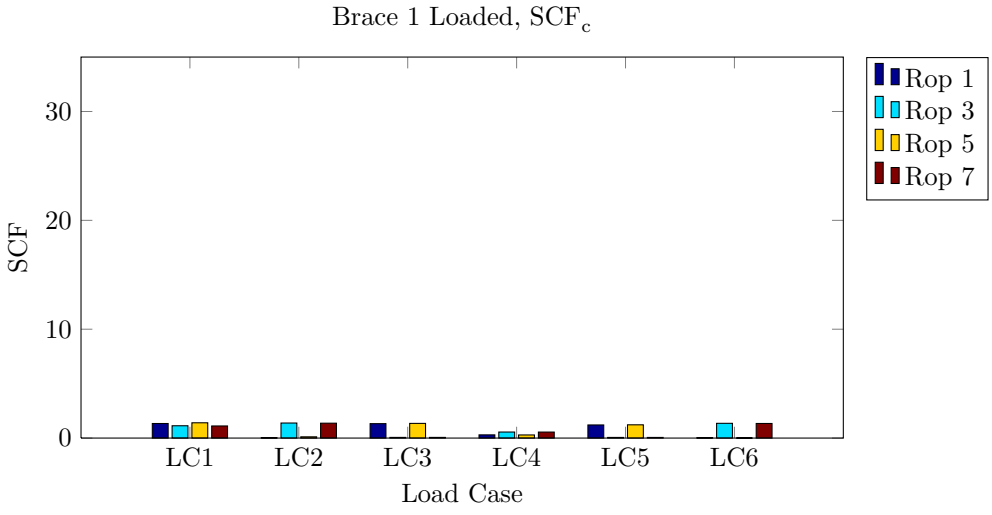

Figure 5.35: SCF for brace 1, chord side of weld

5.15 Comparing w/ and w/o bulkheads

Comparisons of the SCFs from the original design (Design 1) with the two new designs (Design 2 and 3) are presented in this section. Only the brace's SCFs were

compared. The chord loading was not compared because the values were found negligible compared to the brace loadings.

5.15.1 Design 2 / Design 1

Brace side of weld, brace loaded

Table 5.28: $SCF_{b_{Des2}}/SCF_{b_{Des1}}$ Brace 1

Load Type	B11	B12	B13	B14	B15	B16	B17	B18
LC1 (Fx)	100%	101%	96%	101%	100%	101%	96%	101%
LC2 (Fy)	105%	103%	98%	101%	97%	101%	98%	103%
LC3 (Fz)	100%	100%	104%	101%	100%	101%	104%	100%
LC4 (Mx)	107%	85%	97%	85%	107%	85%	97%	85%
LC5 (My)	100%	100%	102%	101%	100%	101%	102%	100%
LC6 (Mz)	104%	104%	98%	101%	98%	101%	98%	104%

Table 5.29: $SCF_{b_{Des2}}/SCF_{b_{Des1}}$ Brace 2

Load Type	B21	B22	B23	B24	B25	B26	B27	B28
LC1 (Fx)	101%	104%	98%	99%	97%	98%	97%	104%
LC2 (Fy)	98%	104%	89%	87%	81%	87%	89%	104%
LC3 (Fz)	100%	100%	102%	101%	100%	101%	102%	100%
LC4 (Mx)	80%	100%	90%	90%	98%	90%	90%	100%
LC5 (My)	100%	100%	96%	101%	100%	101%	97%	100%
LC6 (Mz)	100%	105%	89%	87%	87%	87%	89%	105%

Chord side of weld, brace loaded

Table 5.30: $SCF_{c_{Des2}}/SCF_{c_{Des1}}$ Brace 1

Load Type	C1	C3	C5	C7
LC1 (Fx)	99.6%	97.0%	99.7%	97.0%
LC2 (Fy)	102.2%	96.2%	95.0%	96.3%
LC3 (Fz)	100.0%	113.3%	100.3%	113.7%
LC4 (Mx)	113.3%	94.8%	112.7%	94.7%
LC5 (My)	99.9%	107.4%	100.2%	106.9%
LC6 (Mz)	102.3%	96.2%	96.2%	96.3%

Table 5.31: $SCF_{c_{Des2}}/SCF_{c_{Des1}}$ Brace 2

Load Type	C9	C11	C13	C15
LC1 (Fx)	95.2%	98.1%	95.7%	97.7%
LC2 (Fy)	97.7%	87.3%	72.1%	87.4%
LC3 (Fz)	99.9%	103.9%	100.2%	103.5%
LC4 (Mx)	81.2%	87.6%	96.6%	87.6%
LC5 (My)	99.6%	115.8%	100.2%	113.3%
LC6 (Mz)	99.9%	87.2%	79.6%	87.2%

Comments

As discussed earlier, there were found no large changes in SCFs for Design 2. This ratio comparison confirms this. The objective was to reduce the out-of-plane action SCFs, and this was obtained to some extent. The largest reduction were seen for Brace 2 with a reduction of 13%. For Brace 1 the reduction was at maximum with 5%. But the SCFs also increased with a max. of 5% for some cases for Brace 1.

Design 2 was concluded as unsuccessful.

5.15.2 Design 3 / Design 1

Table 5.32: $SCF_{b_{Des3}}/SCF_{b_{Des1}}$ Brace 1

Load Type	B11	B12	B13	B14	B15	B16	B17	B18
LC1 (Fx)	80%	100%	109%	101%	81%	100%	107%	100%
LC2 (Fy)	4%	13%	17%	11%	13%	11%	17%	13%
LC3 (Fz)	97%	96%	58%	100%	97%	100%	57%	96%
LC4 (Mx)	93%	106%	121%	111%	92%	111%	120%	106%
LC5 (My)	97%	97%	84%	99%	97%	99%	85%	97%
LC6 (Mz)	8%	9%	16%	9%	7%	9%	16%	9%

Table 5.33: $SCF_{c_{Des3}}/SCF_{c_{Des1}}$ Brace 1

Load Type	C1	C3	C5	C7
LC1 (Fx)	91.3%	35.7%	92.6%	34.7%
LC2 (Fy)	3.3%	4.8%	14.0%	4.7%
LC3 (Fz)	94.7%	90.8%	95.6%	91.0%
LC4 (Mx)	89.0%	109.1%	86.5%	106.3%
LC5 (My)	94.4%	84.3%	95.0%	79.3%
LC6 (Mz)	2.9%	4.6%	0.9%	4.5%

Comments

The comparison shows that the horizontal bulkhead at Brace 1 position had a great reduction effect for the SCFs, especially in out-of-plane action. The SCFs for LC2 and LC6 were reduced by 83-99.1%. SCFs for other load cases were also reduced by 3-65.3%.

For LC4 and LC1, however, there are seen some increasing SCF-values, with a minimum of 1% and a maximum increase of 9.1%. This may be explained with the increased (overly) stiffness in the 1 and 4 degree of freedom.

LC3 and LC5 did not experience a great SCF reduction, which can be explained by that the horizontal bulkhead only give stiffness in the horizontal direction, and thus no large change should be expected.

Overall, Design 3 is by far the best design, and was chosen as the final preliminiray design. Fatigue analyses were carried out for Design 3 in Chapter 6.

Chapter 6

Fatigue Calculation

The fatigue calculation was carried out as described in section 3.7. Some more assumptions and calculations are presented in this chapter, together with the fatigue results.

6.1 Superposition for Total Stress

The stresses were first calculated at the defined read out points, see Figure 5.4. Then the hot spot stresses at these points were derived by summation of the single stress components from axial, in-plane and out of plane action. [DNV-RP-C203, 2010, 3.3.2].

If the influence factors for each load case is multiplied by the corresponding force time series from the global dynamic response analysis, the total stress time series at each read-out-point, k, can be defined:

$$\sigma_{total_k} = \sum_{i=1}^{6} F_i \times IF_{i_k} \tag{6.1}$$

F_i has dimension $[N]$ or $[Nm]$, while IF_i has dimension $[Pa/m]$ or $[Pa/Nm]$. Thus, the total stress has dimension $[Pa]$ or $[N/m^2]$

6.2 Effective Stress Range

According to [DNV-RP-C203, 2010, 4.3.4] an effective hot spot stress range is to be used together with the hot spot S-N curve to account for the situation with

fatigue cracking along a weld toe:

$$\Delta\sigma_{Eff} = \max \begin{cases} \sqrt{\Delta\sigma_{\perp}^2 + 0.81\Delta\tau_{\parallel}^2} \\ \alpha\Delta\sigma_1 \\ \alpha\left|\Delta\sigma_2\right| \end{cases} \tag{6.2}$$

where $\Delta\sigma_{\perp}$ is the stress perpendicular to the weld and $\Delta\tau_{\parallel}$ is the shear stress parallel to the weld. $\Delta\sigma_1$ and $\Delta\sigma_2$ are the principal stresses in direction 1 and 2 respectively, defined as:

$$\Delta\sigma_{1,2} = \begin{cases} \frac{\Delta\sigma_{\perp}+\Delta\sigma_{\parallel}}{2} + \frac{1}{2}\sqrt{\left(\Delta\sigma_{\perp} - \Delta\sigma_{\parallel}\right)^2 + 4\Delta\tau_{\parallel}^2} \\ \frac{\Delta\sigma_{\perp}+\Delta\sigma_{\parallel}}{2} - \frac{1}{2}\sqrt{\left(\Delta\sigma_{\perp} - \Delta\sigma_{\parallel}\right)^2 + 4\Delta\tau_{\parallel}^2} \end{cases} \tag{6.3}$$

α is a factor dependent on the detail classification with stress parallel to the weld.

The first effective stress in equation (6.2) was expected to be the dominating one, because the main force component is acting along the brace (axial force), in other words perpendicular to the weld. The latter was verified by force time series inspection.

To decide what effective stress to use, the upper brace was loaded with a force of 1000 [N] in the axial direction. An α of 0.9 was used.

Table 6.1 shows the effective stress (included stress concentration) at the 8 hot spots around the horizontal brace.

Table 6.1: Effective Stress (MPa), max. in **bold**

ROP	eq. (6.2) 1)	eq. (6.2) 2)	eq. (6.2) 3)
1	**0.0317**	0.0286	0.0053
2	**0.0164**	0.015	0.0065
3	**0.0232**	0.0209	0.0111
4	**0.0173**	0.0157	0.007
5	**0.0312**	0.0281	0.0039
6	**0.0173**	0.0157	0.007
7	**0.0232**	0.0209	0.0111
8	**0.0164**	0.015	0.0065

Thus, the top equation in eq. (6.2) was used for effective stress calculation.

6.2.1 Effective stress for chord side of weld

The perpendicular and parallel stress output were for the chord side of the weld not consistently defined from the ABAQUS output. Therefore, it was for simplicity calculated 4 (of 8) effective stress ranges for the chord side of the weld for each brace.

6.3 S-N Curve to be used

The joint is located above the sea surface, and "Table 2-1 S-N curves in air"([DNV-RP-C203, 2010]) was used. The joint was regarded as a non-tubular joint because of its complex design, and because the SCFs were obtained by FEM, the D-curve was used.

Table 6.2: D-curve

S-N Curve	m_1	$log\bar{a}_1$	m_2	$log\bar{a}_2$	Fat. Lim.	Thick. Exp.
D	3	12.164	5	15.606	52.63	0.2

6.4 Design Fatigue Factor

[NORSOK-N-001, 2010] and [DNV-RP-C203, 2010] uses a design fatigue factor (DFF) as a safety factor for fatigue design. The DFF is to be multiplied with the accumulated damage and has a value based on position and inspection accessibility of the structural part considered.

> [[NORSOK-N-001, 2010]] "Structures shall be designed to withstand the presupposed repetitive (fatigue) actions during the life span of the structure. Design fatigue factors shall be applied for safety and with the objective to minimise life cycle costs, taking into account the need for in-service inspection, maintenance and repair."

Table 3 - Design fatigue factors (DFFs)

Classification of structural components based on damage consequence	Not accessible for inspection and repair or in the splash zone	Accessible for inspection, maintenance and repair, and where inspections or maintenance is planned	
		Below splash zone	Above splash zone or internal
Substantial consequences	10	3	2
Without substantial consequences	3	2	1

Figure 6.1: Design Fatigue Factors as stated in [NORSOK-N-001, 2010]

[[NORSOK-N-005, 1997]] "Splash zone: The part of the load-bearing structure which is subjected to repeated sea water wetting and drying."

- The joint is as mentioned earlier designed to be accessible for inspection, maintenance and repair.
- The upper brace is positioned 9 meters aswl and the lower brace connection is positioned 4 meters aswl, so the joint is somewhat in the limit region. Being conservative, it was assumed the joint is within the splash zone.
- There is no information available whether the joint is redundant if one of the braces collapses, and the joint was therefore conservatively assumed as non-redundant. Failure of one part would thus lead to "substantial consequences" (financial).

In conclusion, the DFF was set to 3.

$\underline{DFF = 3}$

6.5 Dynamic Response Parameters

This section presents the approximation of the full long-term fatigue analysis.

6.5.1 Sea states

In reality, the ideal method is to do a full long-term fatigue analysis for fatigue design. It is necessary to consider the fatigue damage for every possible combination of mean wind speed, significant wave height and peak spectral period and their probability of occurrence. This means that numerous time-domain dynamic response analyses should be simulated for all (short term) sea states, and for every sea state, several analyses should be done to reduce statistical uncertainties in the

limited sea state duration. Due to limited time, the long-term fatigue analysis was for simplicity approximated by using the expected significant wave height and peak spectral period given mean wind speed, for the range of mean wind speed. This method is also proposed in [IEC61400-3, 2009] for some fatigue analyses for bottom fixed offshore wind turbines. The accuracy of this way of doing this approximation for a floater however, is uncertain. The method might not give good results.

A joint distribution of 1 hour mean wind speed, W, significant wave height, H_s, and peak spectral period, T_p, proposed by [Johannessen et al., 2001] was used to find the sea states to be applied to the structure. Wind and wave measurements from 1973-1999 from the Northern North Sea were used as a database. Because

> "the wind is assumed to have the strongest influence on the loads on the mooring lines [...], the significant wave height is assumed to have second most influence and the peak spectral period is assumed to have least influence of the loads [...] of a semi-submersible structure"[Johannessen et al., 2001]

the wind speed was chosen as the primary parameter. The joint distribution suggested is defined as:

$$f_{WH_sT_p}(w,h,t) = f_W(w) \cdot f_{H_s|W}(h|w) \cdot f_{T_p|H_sW}(t|h,w) \tag{6.4}$$

Here, the marginal distribution for mean wind speed was assumed be Weibull-distributed (see Figure 6.4). [Johannessen et al., 2001] found that if the mean wind speed, w follows a Weibull distribution, the conditional distribution of H_s given w also follows a Weibull distribution. If the latter is true, the conditional distribution of T_p given H_s and W follows a log-normal distribution.

The values for the primary parameter, mean wind speed, were chosen. The mean significant wave height and the mean peak spectral period were calculated. From [Johannessen et al., 2001], the model is defined in the following equations:

Mean Wind Speed:

$$\begin{aligned} \alpha_w &= 1.708 \\ \beta_w &= 8.426 \end{aligned} \tag{6.5}$$

$$F(W) = 1 - exp\left[-\left(\frac{W}{\beta_w}\right)^{\alpha_w}\right] \tag{6.6}$$

Expected Significant Wave Height:

$$\begin{aligned} \alpha_h &= 2.0 + 0.135w \\ \beta_h &= 1.8 + 0.100w^{1.322} \end{aligned} \tag{6.7}$$

$$E(H_s) = h = \beta_h \cdot \Gamma\left(\frac{1}{\alpha_h} + 1\right) \tag{6.8}$$

Expected Peak Spectral Period:

$$E(T_p) = \bar{T}_p(w,h) = (4.883 + 2.68h^{0.529}) \cdot \left[1 - 0.19 \cdot \left(\frac{w - (1.764 + 3.426h^{0.78})}{(1.764 + 3.426h^{0.78})}\right)^1\right] \tag{6.9}$$

Turbulence Intensity Factor:

The wind turbulence intensity factor was found using a normal turbulence model [IEC61400-1, 2005, section 6.3.1.3]. The turbulence intensity factor is defined as:

$$T_I = \frac{\sigma_I}{w} \tag{6.10}$$

where the turbulence standard deviation is defined as

$$\sigma_I = I_{ref}(0.75w + b); b = 5.6m/s \tag{6.11}$$

I_{ref} is the expected value of the turbulence intensity at 15 m/s mean wind speed, and was set to 0.12 (Class C, [IEC61400-1, 2005]).

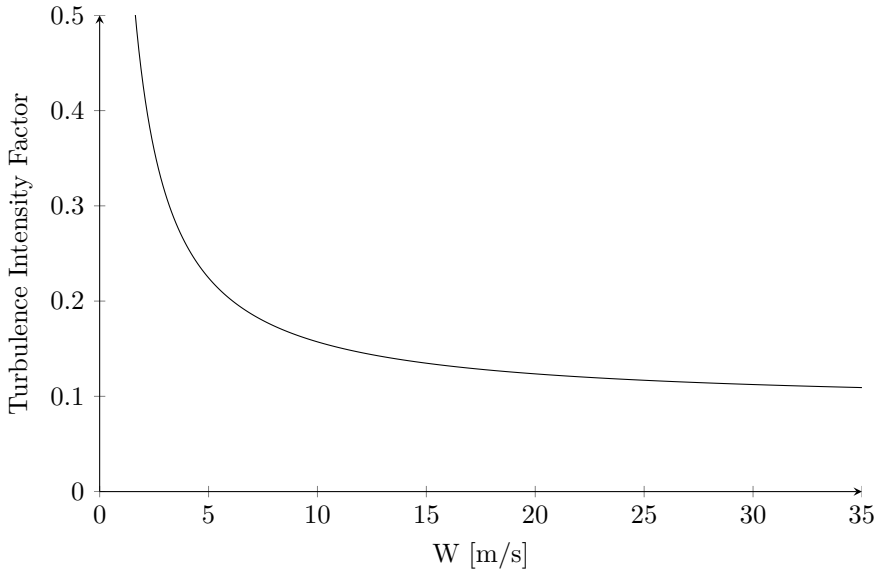

Figure 6.2: Turbulence Intensity Factor vs. Mean Wind Speed

Wind Shear:

Wind speeds were chosen from 3-31 m/s at hub height, H, with a resolution of 2 m/s, in accordance with [IEC61400-1, 2005, sec. 7.4]:

$$w(H) = 3 : 2 : 31 m/s \tag{6.12}$$

[Johannessen et al., 2001] assumes the wind speeds are defined at 10 m aswl, thus the wind speeds at 10 m aswl were needed to calculate H_s and T_p (The wind speeds were chosen at hub height because TDHMill uses hub height wind speed for its input). A power law wind shear with exponent 0.14 was assumed ([IEC61400-3, 2009, section 6.3]):

$$w(z = 10) = w(H) \cdot (z/H)^{0.14} \tag{6.13}$$

6.5.2 Short term sea states

The short term sea states are presented in Table 6.3.

Table 6.3: Short term Sea states

$w[m/s]$	$w_{10}[m/s]$	T_I	$H_s[m]$	$T_p[s]$
3	2.21	0.31	1.85	9.73
5	3.68	0.22	2.09	9.74
7	5.15	0.19	2.38	9.80
9	6.63	0.16	2.69	9.90
11	8.10	0.15	3.03	10.04
13	9.57	0.14	3.39	10.19
15	11.05	0.13	3.77	10.36
17	12.52	0.13	4.17	10.54
19	13.99	0.13	4.59	10.73
21	15.46	0.12	5.02	10.93
23	16.94	0.12	5.47	11.13
25	18.41	0.12	5.93	11.34
27	19.88	0.11	6.41	11.55
29	21.35	0.11	6.90	11.76
31	22.83	0.11	7.40	11.98

For each short term sea state, 10 1-hour simulations with different random seeds were run to reduce statistical uncertainty. The mean value of the fatigue damages were taken from these 10 simulations to represent the damage for that sea state. In the analyses the 3 parameter JONSWAP-spectra was used for the waves, and the Kaimal-spectra was used for the mean wind. Both waves and wind were attacking in global positive X-direction (west to east).

The rated wind speed is 11.3 m/s, while the wind turbine is parked for mean wind speeds above 25 m/s for safety.

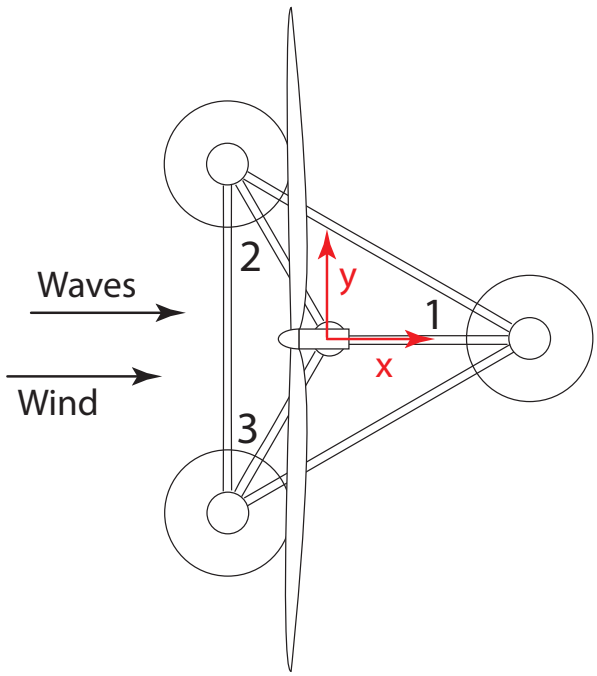

Figure 6.3: Incoming wave and wind direction, and brace plane definition

6.5.3 Weighting the Sea states

The long term distribution of stress ranges were obtained as the weighted average of the short term distributions. The short term sea states' fatigue damages were weighted and then summed to get the total fatigue damage. The mean wind speed distribution was discretized into 16 blocks. For each block, a sea state was established, with mean wind speed equal to the mean value of the respective block. A time domain analysis was done for each short term sea state, and for each time domain analysis, rainflow counting and fatigue damage calculation were carried out.

The total fatigue damage is equal to the sum of the accumulated fatigue damage in all short term sea states, F_{D_i}, multiplied with the probability, p_i of the respective short term sea state occurring:

$$D_{tot} = \sum_{i=1}^{16} F_{D_i} p_i \tag{6.14}$$

e.g. p_4 is equal to the area of the shaded block in Figure 6.4

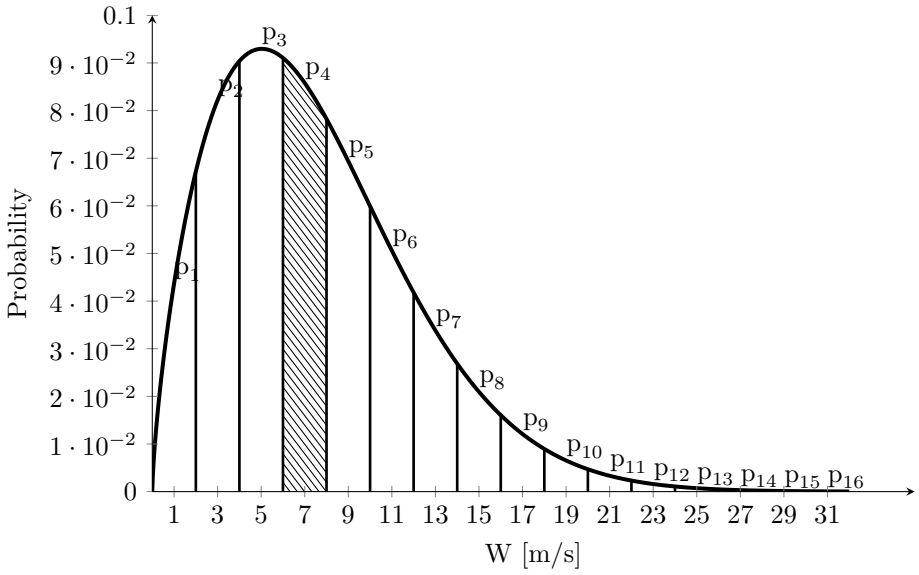

Figure 6.4: Weibull PDF for the wind speed

Table 6.4: Probabilities of sea states occurring. a and b are block limits

	a	b	Probability
p_1	0	2	0.0822
p_2	2	4	0.1621
p_3	4	6	0.1844
p_4	6	8	0.1708
p_5	8	10	0.1385
p_6	10	12	0.1014
p_7	12	14	0.068
p_8	14	16	0.0422
p_9	16	18	0.0245
p_{10}	18	20	0.0133
p_{11}	20	22	0.0068
p_{12}	22	24	0.0033
p_{13}	24	26	0.0015
p_{14}	26	28	0.0006
p_{15}	28	30	0.0003
p_{16}	30	32	0.0001
$\sum$			0.9999

The sum is almost identical to 1.0 because the PDF was cut at $W = 32$ m/s.

The fatigue damage for wind speeds 0-2 m/s was conservatively assumed to be identical to the case with wind speeds 2-4 m/s, and multiplied with the probability of wind speeds 0-2 m/s to occur, p_1. This sea state was not simulated because there is no thrust on the turbine at this mean wind speed range.

6.6 Results

The results for the fatigue damage and fatigue life are presented for Brace 1, Brace 2 and the chord. All results are presented with a DFF of 3.

The stress concentration factors for Brace 1 were heavily reduced when adding a horizontal bulkhead. The same could have been done for Brace 2. However, additional (complicated) stiffening was not attempted. Thus, Brace 2 was expected be the most critical member.

6.6.1 Fatigue Damage

There are three "brace-planes" considered in the fatigue analysis: brace plane 1, 2 and 3. It was expected that brace plane 1 would have the largest fatigue damage contribution, due to the incoming waves and wind direction.

The fatigue damage for all short term sea states for all members are presented below. The last figures (Figure 6.17, 6.18, 6.19) presents the **total damage**, D_{tot} for the members for three different planes.

Member definition:

1. B1 - Brace 1
2. B2 - Brace 2
3. C - Chord
4. B1C - Brace 1, chord side of weld
5. B2C - Brace 2, chord side of weld

Critical brace plane

Comparing Figure 6.17, 6.18, 6.19 it was confirmed that brace plane 1 was the most critical plane. However, for ROP 3 and 7, plane 2 was for some reason the most critical plane. This was unexpected, especially considering that brace plane 3 was found to be negligible compared to brace plane 1. It was expected that damage for brace plane 2 and 3 would be identical because of symmetry. This was not further investigated.

For all other ROPs other than 3 and 7, plane 1 was the critical brace plane. Below are presented plots of the fatigue damage for the three different planes for Brace 1. The same trend was observed for the other members as well.

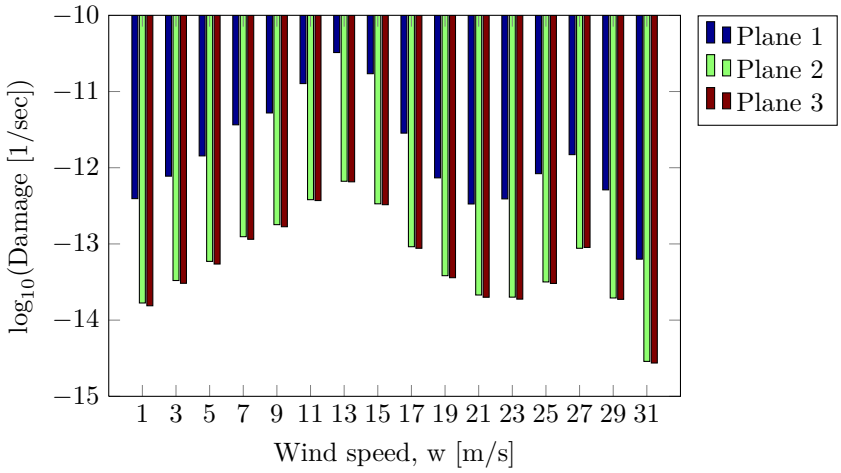

Figure 6.5: Planes: Damage for Brace 1, ROP 1. Notice that the fatigue damages for brace plane 2 and 3 are almost identical

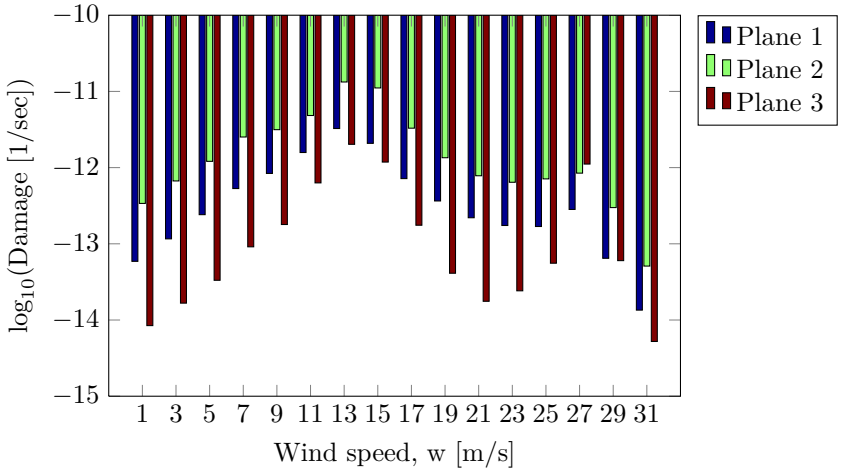

Figure 6.6: Planes: Damage for Brace 1, ROP 3. Notice that the fatigue damages for brace plane 2 and 3 are different

Fatigue damage as a function of wind speed w/o concerning p_i

The fatigue damages are presented as a function of wind speed for all members, without taking account for the probability of occurrence. These graphs are presented to be able to discuss the contribution for each short term sea state in a physical manner, without taking the probability into account.

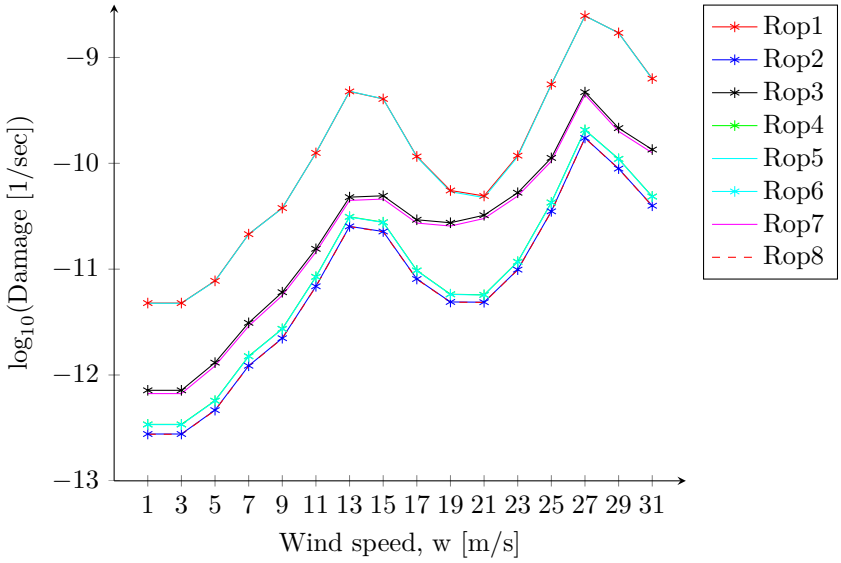

Figure 6.7: Damage all sea states, Brace 1

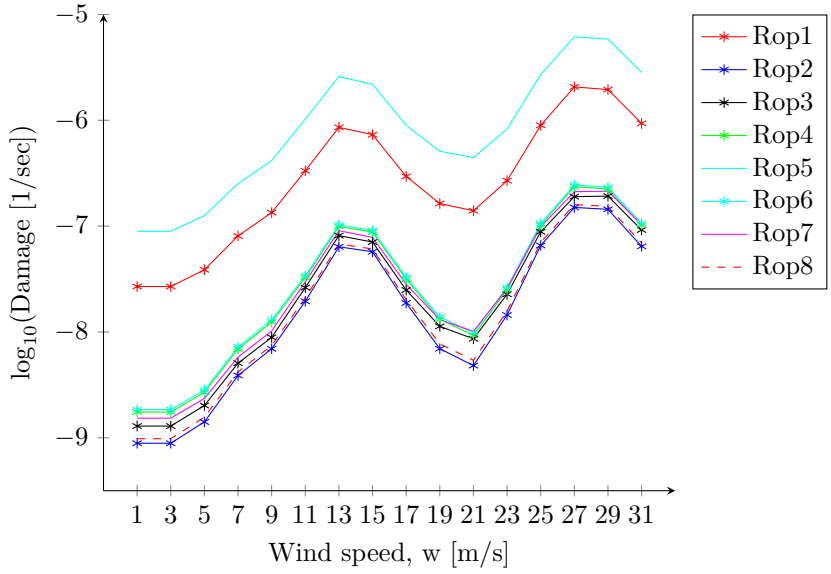

Figure 6.8: Damage all sea states, Brace 2

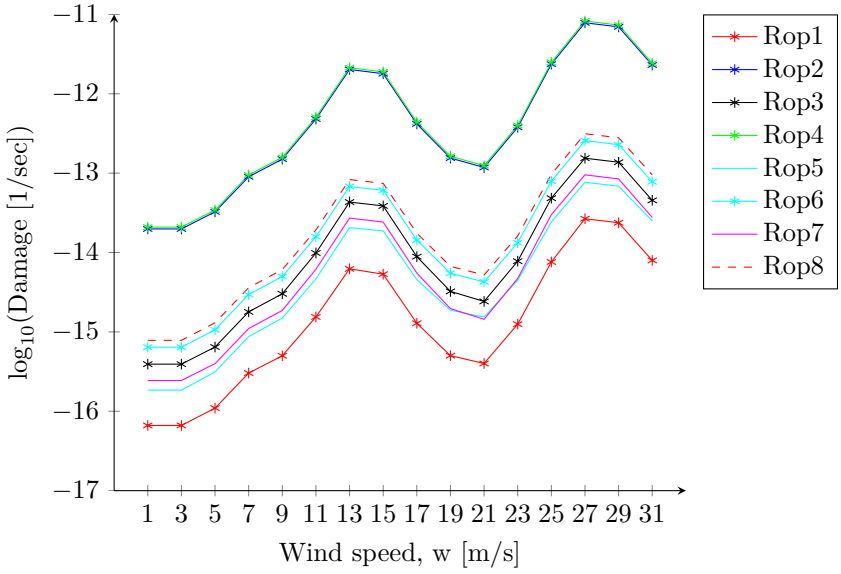

Figure 6.9: Damage all sea states, Chord

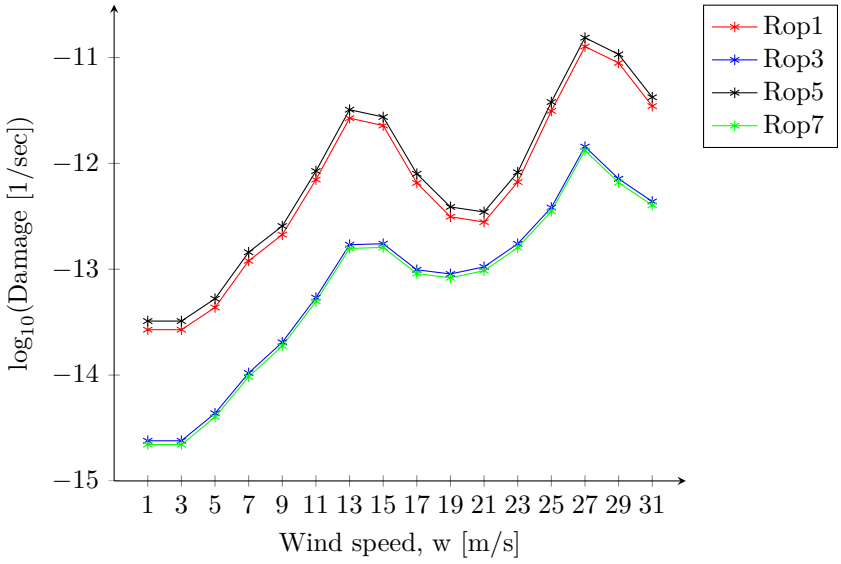

Figure 6.10: Damage all sea states, Brace 1, chord side of weld

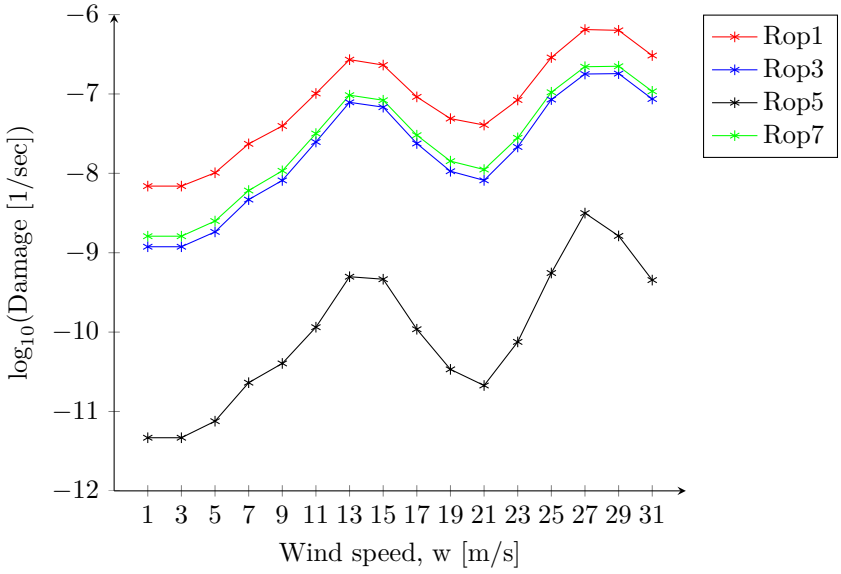

Figure 6.11: Damage all sea states, Brace 2, chord side of weld

Comments

The fatigue damage have a typical shape for all members, with two local maximums

and a local minimum. The higher wind speeds have the largest maximum.

- When the wind speed increases from 0-∼11.3 m/s, the damage increases due to an increasing thrust.
- Around the rated wind speed, 11.3 m/s, where the thrust has its highest value, there is a local maximum in the fatigue damage. From wind speeds ∼14-21 m/s the fatigue damage decreases because of the decreasing thrust, and then increases because of the increasing drag forces on the structure.
- At mean wind speeds above 25 m/s, sea states 14, 15 and 16 (see dots), the wind turbine is parked, and is thus letting all wind through. A drop in damage was expected at w = 27 m/s because of the total loss of thrust at sea state 14, and then from here increasing damage in sea state 15 and 16, because of increasing wind speeds (drag). However, from the plots there are still observed more damage than expected, and even decreasing damage for 15 and 16 compared to sea state 14.

Erroneous time simulations
It was later discovered that the time series for sea states 14, 15 and 16 were simulated in a non-physical manner. In reality, when the mean wind speeds are measured above 25 m/s over a certain time period, the wind turbine is parked. The turbine is then started again when the measured mean wind speeds over a certain time period are below 25 m/s. The dynamic response simulation method however, started and parked the turbine based on the instantaneous mean wind speed, and thus there is still thrust observed for the sea states with mean wind speed larger than 25 m/s. Consequently, sea state 14 shows (erroneously) a larger damage than sea state 13 because sea state 14's turbine is started every time the instantaneous mean wind speed reaches below 25 m/s. Sea state 15 and 16 (erroneously) show smaller damage than sea state 14 because the mean wind speeds are further away from the limit of 25 m/s, and thus the thrust observed is smaller. Ideally the simulations for sea state 14, 15 and 16, and perhaps lower sea states (because the turbine is parked every time the instantaneous mean wind speed reaches above 25 m/s) should be redone. However, because of limited time, the problem is only commented on. Hence, the simulation fault create conservative fatigue life answers.

Fatigue damage as a function of wind speed

The fatigue damages are presented as a function of wind speed for all members, taking the probability of occurrence into account. The presented fatigue damage values will of course decrease with a factor p_i for every $i'th$ sea state. This will be most evident for the fatigue damages for higher wind speeds, which will have their total contribution to total fatigue damage decreased the most. The shape of the fatigue damage curve is thus changed with a largest fatigue damage for wind speed around the rated wind speed.

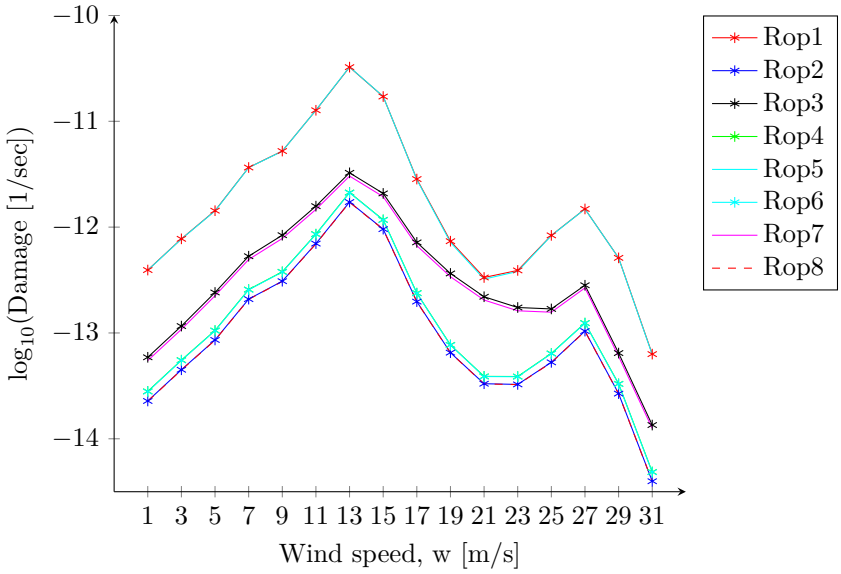

Figure 6.12: Damage all sea states, Brace 1

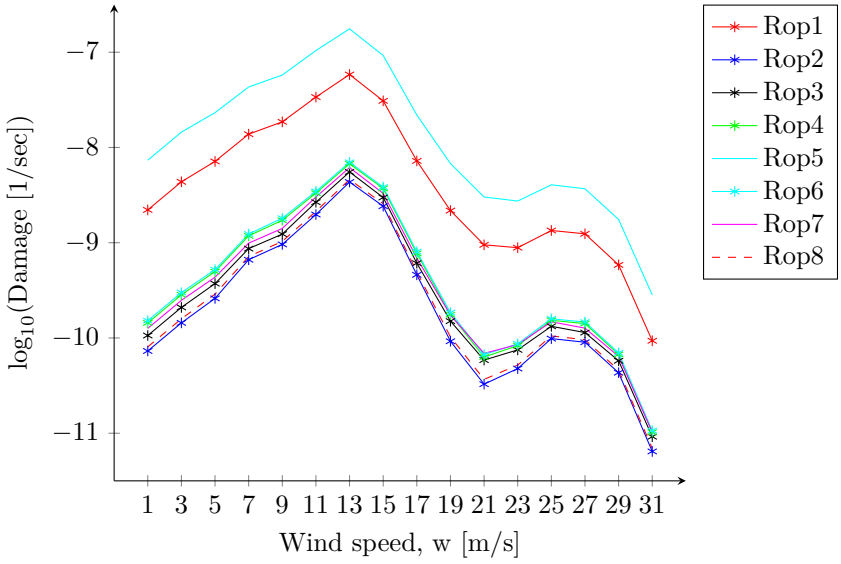

Figure 6.13: Damage all sea states, Brace 2

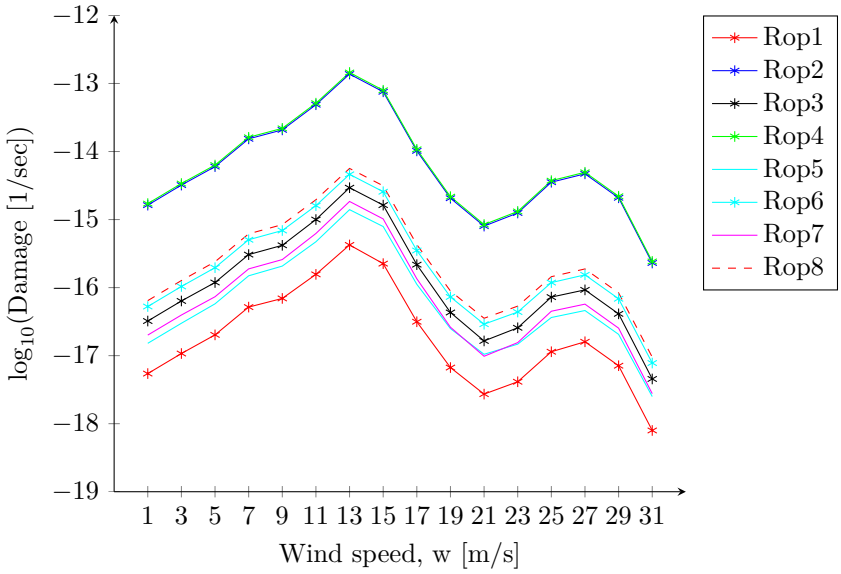

Figure 6.14: Damage all sea states, Chord

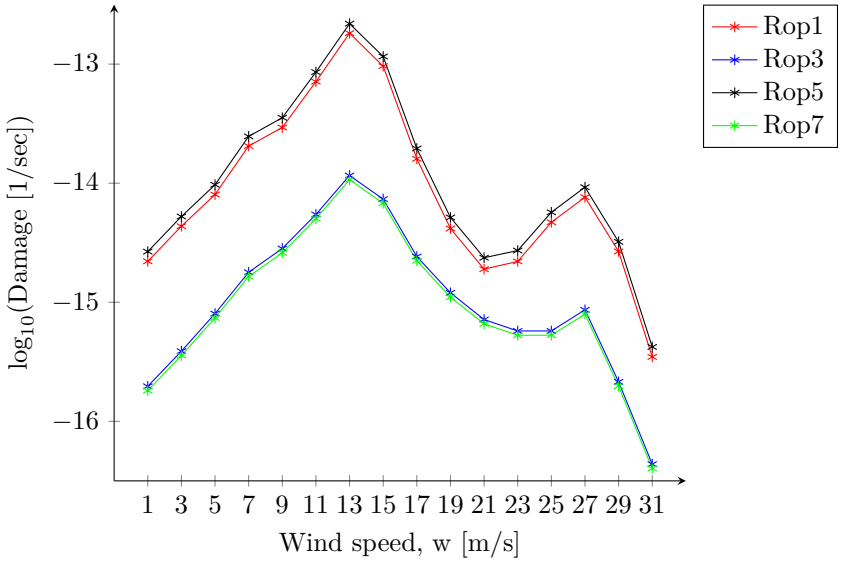

Figure 6.15: Damage all sea states, Brace 1, chord side of weld

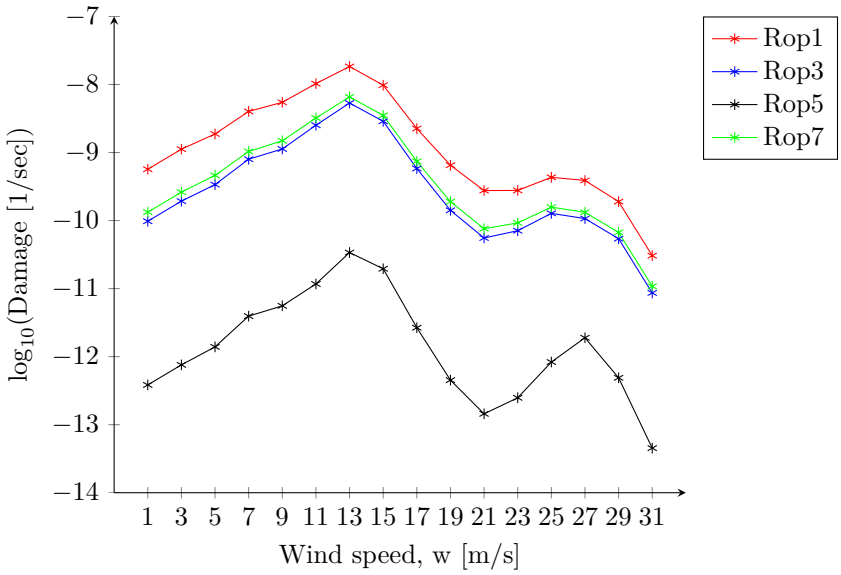

Figure 6.16: Damage all sea states, Brace 2, chord side of weld

ROP 1 and ROP 5, the crown toe and heel seem to be the most critical hot-spots, as one or both contribute to the largest fatigue damage. This does however not apply for the chord, where ROP 2 and ROP 4 are the most "critical" hot-spots.

Total fatigue damage, D_{tot}

Total fatigue damage for all members for all planes are presented. These values were calculated by taking the mean of the fatigue damage all short term sea states.

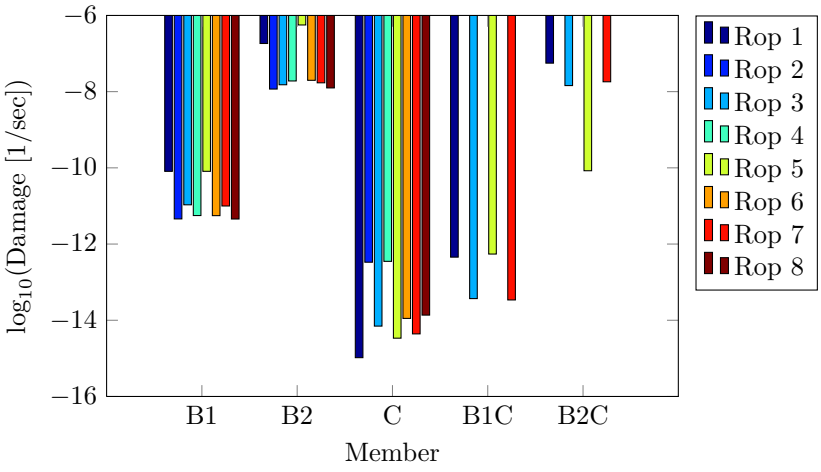

Figure 6.17: Total damage for all members, D_{tot}, brace plane 1

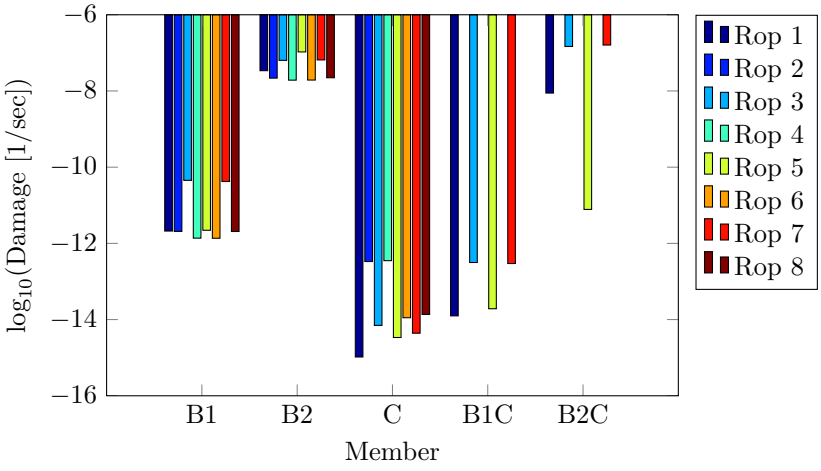

Figure 6.18: Total damage for all members, D_{tot}, brace plane 2

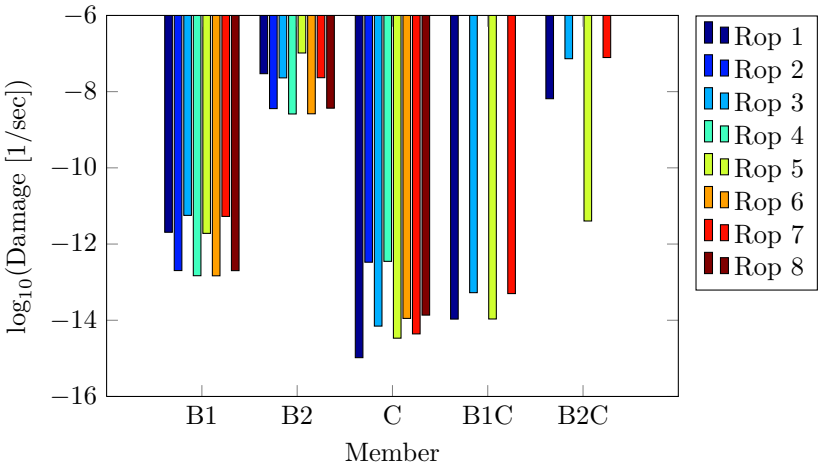

Figure 6.19: Total damage for all members, D_{tot}, brace plane 3

For Brace 1 and 2, the largest damage is seen at the brace side of the weld. The chord has a negligible damage contribution. Brace 2 is the most critical member.

6.6.2 Fatigue Life

Here the fatigue life for all members are presented in log-scale.

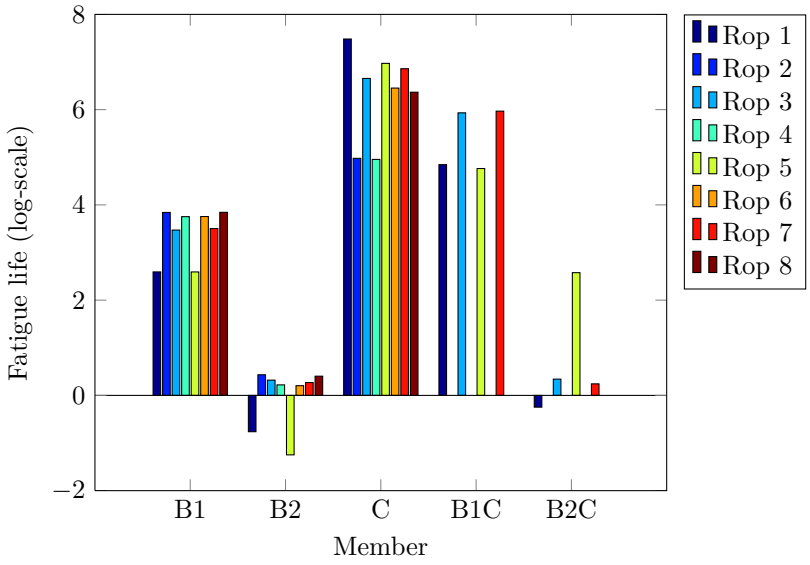

Figure 6.20: Fatigue life, plane 1

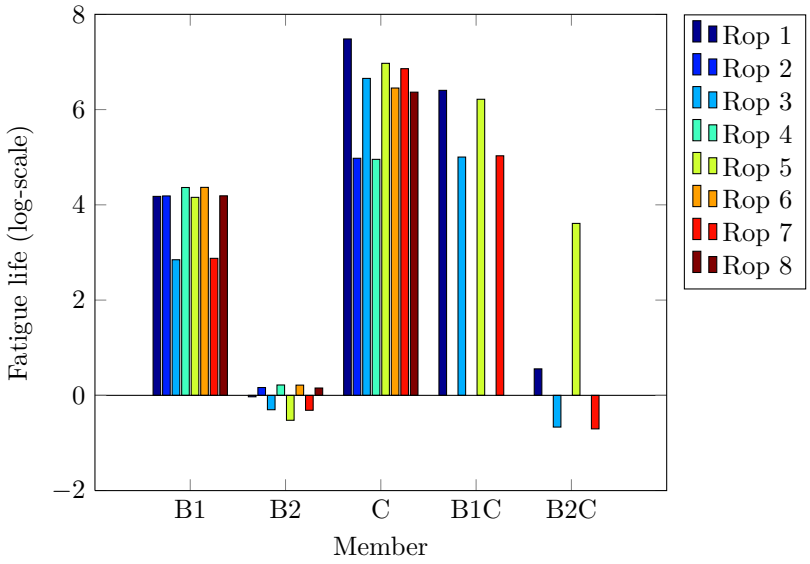

Figure 6.21: Fatigue life, plane 2

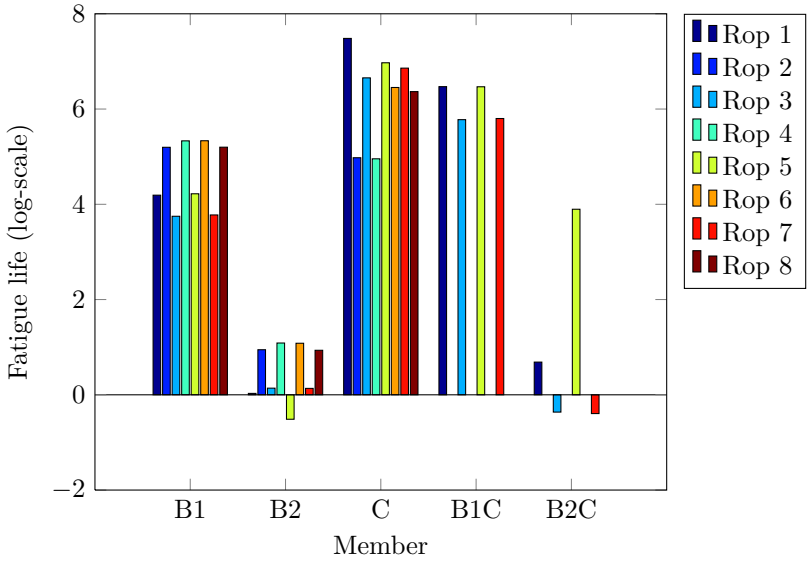

Figure 6.22: Fatigue life, plane 3

The fatigue life for all members for plane 1 are presented in Table 6.5.

Table 6.5: Fatigue Life plane 1 [years]

ROP	Brace 1	Brace 2	Chord	B1C	B2C
1	391	0.17	3.0E+07	7.0E+04	0.57
2	6941	2.71	9.5E+04		
3	2961	2.09	4.5E+06	8.6E+05	2.20
4	5663	1.66	9.0E+04		
5	391	0.06	9.4E+06	5.8E+04	377.62
6	5695	1.60	2.8E+06		
7	3178	1.86	7.2E+06	9.3E+05	1.75
8	6980	2.53	2.3E+06		

Comments

The fatigue damages were found largest for the hot spots at the brace side of the welds. Thus B1 is the most critical for Brace 1, and B2 most critical for Brace 2.

Brace 1 has a minimum lifetime of 391 years for ROP 1 and 5: the crown positions. These values satisfy the design requirement of 20 years. Brace 2 on the other hand has a critical life time of 0.06 years at ROP 5, the crown heel, followed by the crown toe with a life time of 0.17 years.

The critical ROPs were ROP 1 and 5 (crown toe and heel) for both Brace 1 and Brace 2. This is explained by the dominating axial and in-plane stresses in combination with the maximum stress concentrations for axial and in-plane action at ROP 1 and 5. These results show that Brace 2 needs modifications, perhaps in the same manner as was done for Brace 1, but maybe a more complicated solution because of the inclined member.

Remember that the final results were obtained after superposition of all load cases for all ROPs, respectively. The increase in fatigue life is thus a combined effect that can not be easily presented by looking at SCFs only. However, it is very clear that the fatigue life for Brace 1 with horizontal bulkhead is much larger than Brace 2 without bulkhead, mainly because of the higher SCF for Brace 2.

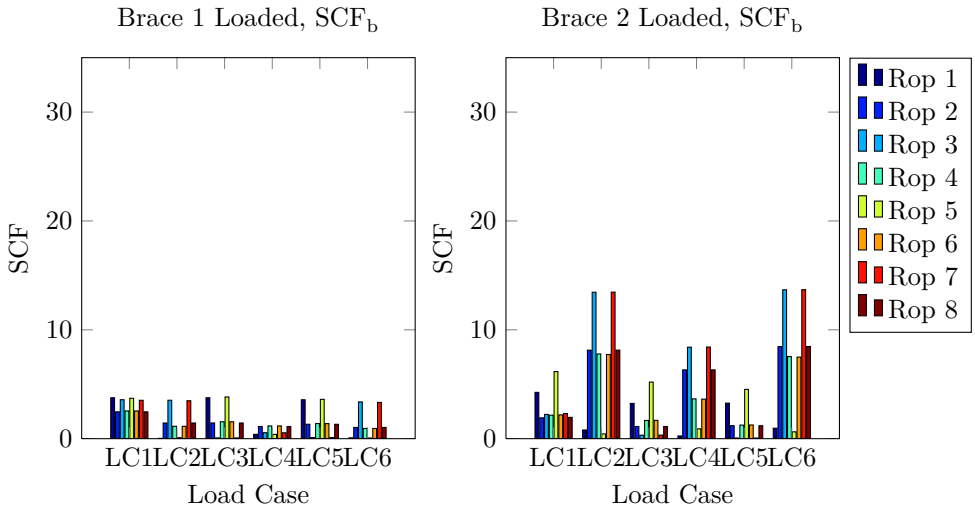

(a) Brace 1, Design 3 **(b)** Brace 2, Design 1

Figure 6.23: Comparison of SCFs

6.6.3 Force and Stress Contributers

The force and stress standard deviations give some indication of the most dominating contributions, for all short term sea states. The means of the standard deviations for the 10 simulations per sea state are presented. Brace 1 and 2 were considered.

Table 6.6: Standard deviation of forces and moments, Brace 1, Plane 1

S.St.	Fx [N]	Fy [N]	Fz [N]	Mx [Nm]	My [Nm]	Mz [Nm]
2	8.00E+04	3.15E+02	5.43E+03	4.17E+02	7.35E+04	6.69E+03
3	8.52E+04	3.69E+02	5.43E+03	4.93E+02	7.28E+04	7.90E+03
4	1.02E+05	5.10E+02	6.65E+03	7.04E+02	8.81E+04	1.09E+04
5	1.14E+05	7.32E+02	7.12E+03	1.08E+03	9.31E+04	1.58E+04
6	1.25E+05	1.11E+03	7.47E+03	1.69E+03	9.69E+04	2.40E+04
7	1.61E+05	2.07E+03	1.08E+04	2.26E+03	1.41E+05	3.69E+04
8	1.62E+05	1.79E+03	1.05E+04	1.96E+03	1.38E+05	3.70E+04
9	1.39E+05	1.29E+03	7.42E+03	1.48E+03	9.69E+04	2.75E+04
10	1.35E+05	1.09E+03	6.04E+03	1.30E+03	7.73E+04	2.38E+04
11	1.39E+05	1.06E+03	5.74E+03	1.30E+03	7.23E+04	2.37E+04
12	1.52E+05	1.26E+03	6.96E+03	1.60E+03	8.91E+04	2.78E+04
13	1.80E+05	1.72E+03	1.00E+04	2.34E+03	1.32E+05	3.77E+04
14	1.50E+06	1.75E+03	5.66E+04	2.59E+03	3.18E+05	3.46E+04
15	2.38E+05	3.61E+00	1.24E+04	1.58E+00	1.61E+05	6.45E+00
16	1.84E+05	1.16E-01	9.17E+03	1.09E-01	1.19E+05	4.02E-01

Table 6.7: Standard deviation of stresses for the critical hot-spot for the respective load case, Brace 1, Plane 1

Critical IF	25.4	315.95	336.16	0.021	0.063	0.059
ROP	B11	B13	B15	B14	B11	B13
S.St.	Fx [Pa]	Fy [Pa]	Fz [Pa]	Mx [Pa]	My [Pa]	Mz [Pa]
2	2.0E+06	9.9E+04	1.8E+06	8.8E+00	4.6E+03	3.9E+02
3	2.2E+06	1.2E+05	1.8E+06	1.0E+01	4.6E+03	4.7E+02
4	2.6E+06	1.6E+05	2.2E+06	1.5E+01	5.5E+03	6.4E+02
5	2.9E+06	2.3E+05	2.4E+06	2.3E+01	5.9E+03	9.3E+02
6	3.2E+06	3.5E+05	2.5E+06	3.6E+01	6.1E+03	1.4E+03
7	4.1E+06	6.5E+05	3.6E+06	4.8E+01	8.9E+03	2.2E+03
8	4.1E+06	5.7E+05	3.5E+06	4.1E+01	8.7E+03	2.2E+03
9	3.5E+06	4.1E+05	2.5E+06	3.1E+01	6.1E+03	1.6E+03
10	3.4E+06	3.4E+05	2.0E+06	2.7E+01	4.9E+03	1.4E+03
11	3.5E+06	3.4E+05	1.9E+06	2.7E+01	4.6E+03	1.4E+03
12	3.9E+06	4.0E+05	2.3E+06	3.4E+01	5.6E+03	1.6E+03
13	4.6E+06	5.4E+05	3.4E+06	4.9E+01	8.3E+03	2.2E+03
14	3.8E+07	5.5E+05	1.9E+07	5.4E+01	2.0E+04	2.0E+03
15	6.1E+06	1.1E+03	4.2E+06	3.3E-02	1.0E+04	3.8E-01
16	4.7E+06	3.7E+01	3.1E+06	2.3E-03	7.5E+03	2.4E-02

The axial force was expected to be the largest contributor, which is verified in Table

6.6. Fz is larger than Fy, probably because of the weight of the tower in combination with the moment created by the thrust. The same conclusion was drawn for My and Mz. Torsion moment, Mx, is the smallest contributor for moments.

Sea state 14, 15 and 16 have erroneous too large standard deviations. In sea state 14, 15 and 16 it is possible to identify the loss of thrust because of an "erroneous more and more parked turbine", in contrast to a correctly always parked turbine. The maximum stress contribution at the rated wind speed, and the decreasing thrust force and thus brace stresses for sea states 14, 15 and 16, emphasizes the importance of the wind turbine's impact on the fatigue life.

The stress contribution are largest for the axial force and the in-plane force (Fx and Fz), followed by Fy. This explains why the critical ROPs were at the crowns: the axial and in-plane actions are dominating, and have in addition large influence factors at ROP 1 and 5 (crowns). The moments give much smaller stress contributions than the forces. The main stress contributions are seen for ROP 1 and 5.

Table 6.8: Standard deviation of stresses for the critical hot-spot for the respective load case, Brace 2, Plane 1

Critical IF	28.76	1866.56	455.96	0.207	0.079	0.342
ROP	B21	C27	B25	C27	B25	C27
S.St.	Fx [Pa]	Fy [Pa]	Fz [Pa]	Mx [Pa]	My [Pa]	Mz [Pa]
2	2.0E+07	5.2E+05	3.6E+06	1.7E+02	5.0E+03	2.1E+03
3	2.0E+07	6.0E+05	4.2E+06	2.1E+02	5.0E+03	2.5E+03
4	2.4E+07	8.2E+05	6.3E+06	2.9E+02	5.9E+03	3.4E+03
5	2.5E+07	1.2E+06	8.1E+06	4.2E+02	6.1E+03	5.0E+03
6	2.6E+07	1.8E+06	8.9E+06	6.2E+02	6.2E+03	7.6E+03
7	3.8E+07	3.4E+06	1.2E+07	9.5E+02	9.2E+03	1.2E+04
8	3.8E+07	2.9E+06	1.2E+07	9.5E+02	9.0E+03	1.1E+04
9	2.7E+07	2.1E+06	8.4E+06	7.1E+02	6.4E+03	8.6E+03
10	2.2E+07	1.8E+06	5.7E+06	6.2E+02	5.1E+03	7.4E+03
11	2.1E+07	1.7E+06	4.7E+06	6.2E+02	4.7E+03	7.4E+03
12	2.5E+07	2.1E+06	6.2E+06	7.3E+02	5.9E+03	8.7E+03
13	3.7E+07	2.8E+06	1.0E+07	9.8E+02	8.9E+03	1.2E+04
14	7.2E+07	3.8E+06	3.1E+07	2.5E+02	1.6E+04	1.4E+03
15	4.5E+07	6.4E+03	1.4E+07	1.3E-01	1.1E+04	2.0E+00
16	3.4E+07	1.8E+02	8.7E+06	1.6E-02	7.9E+03	1.1E-01

The standard deviations of stresses seen for Brace 2 are up to 10 times larger than for Brace 1, meaning an increased damage by a factor of 1000 - 100000.

Standard deviation for forces for Brace 2 and a comparison with Brace 1 can be found in Appendix C.

Chapter 7

Conclusion

A stress concentration study and fatigue analysis were carried out for a column-brace connection. The connection was designed for a semi-submersible wind turbine. Three column-brace connection designs were analysed, and a final preliminary joint design was chosen.

The column-brace connection, or joint, is located at the centre column of the semi-submersible, connecting a wind turbine tower to a triangular semi-submersible floater. The joint has braces entering in pairs at three planes, meaning a total of six braces. The initial design included ring-stiffeners and three vertical bulkheads inside the column, which worked as both stiffening for the joint and support for the braces. No horizontal stiffening was added at this point, because it was believed that the axial forces would by far be the most dominating.

7.1 Stress Concentration Factors

The stress concentration factors were calculated using the Finite Element Method and DNV Recommended Practice. Only one of three planes was analysed due to symmetry. Two braces, Brace 1 (horizontal) and Brace 2 (inclined) are entering the joint at this plane.

For the initial design, the stress concentration factors generally were way too large, and peaked at a value of about 30 for out-of-plane action. This caused the fatigue damage for out-of-plane action to be dominating, although the out-of-plane forces were small. To deal with this problem, a second design was created. Additional horizontal bulkheads were added instead of the ring stiffeners, to increase the out-of-plane stiffness for the joint. This modification did not decrease the stress concentrations, and consequently a third design was created. For the third design, the horizontal bulkheads were removed, and instead a horizontal bulkhead at the brace centreline was added. This modification decreased the stress concentrations

by a maximum of over 90% for out-of-plane action. For in-plane-action, axial action and torsion, the reduction was not so significant, but an overall reduction was also seen for these cases in a range of 3-65%.

The modification was only carried out for Brace 1. Brace 2 still experienced too large stress concentrations - for out-of-plane action especially, with a maximum value of 20. There was no attempt at reducing the stress concentrations for brace 2.

Consequently, a maximum stress concentration factor was observed for Brace 2 with a value of 20 at the saddle (ROP 7). It is believed that these high stress concentrations are possible to reduce, adding horizontal bulkheads in a similar, but perhaps more complicated configuration. For Brace 1 the maximum stress concentration factor had a value of 3.83 at the crown (ROP 5).

7.2 Fatigue Life

The fatigue life was calculated based on the **stress concentration factors** and **force time series** from dynamic response analyses. A full long-term fatigue analysis was approximated. A northern North Sea joint-probability distribution of mean wind speed, expected significant wave height and expected peak spectral period for a given mean wind speed was considered. 16 sea states were chosen, and each sea state was simulated 10 times with different seed numbers. Every sea state was weighted with its probability of occurrence, and then all sea states were summed to get the total fatigue damage. The largest contribution to fatigue damage were found for mean wind speeds slightly higher and around the rated wind speed, 11.3 m/s. This result emphasizes the importance of the wind turbine's impact on the fatigue life. The largest stresses were observed for axial and in-plane action.

Brace plane 1 was expected to be the most critical plane for fatigue damage. This was confirmed for all read-out-points except 3 and 7. The critical fatigue damage was found for Brace 2, with a life time of 0.06 years. For Brace 1 the lowest life time was 391 years. The critical ROPs was ROP 1 and 5 (crown toe and heel) for both brace 1 and Brace 2. This is explained by the dominating axial forces in combination with the maximum stress concentrations for axial action at ROP 1 and 5.

The modification of Brace 1 with horizontal bulkheads as additional stiffening reduced the stress concentrations and increased the fatigue life from almost zero to 391 years. The same procedure can be carried out for Brace 2. It is believed that if modifications at a later stage are carried out for Brace 2, an adequate fatigue life of the column-brace connection can be achieved.

Chapter 8

Future work

- **Reduce SCFs.** Decreasing the stress concentrations are of high importance for increasing the fatigue life. Modifications to reduce SCFs are possible in many ways. More stiffening in form of bulkheads at the brace locations proved to be a very effective way to decrease the stress concentrations, and extra concern should be given brace 2, which at this point was concluded to be the most critical member. Other reduction methods include longitudinal and ring stiffeners, gusset plates etc. Outside stiffeners at e.g. the brace/chord intersection could improve the overall design.
- **Reduce overly stiffness.** The stiffness at some locations can become overly stiff and "hard-points" occur. To reduce this form of stress concentration, cut-out profiles could be created e.g. at the brace/chord intersection and at other occurring hot spots. This would create a smoother stress transition as described in e.g. [DNV, 2000], and thus lower the SCFs. Hopper knuckles and knee-plates are other possibilities. However, this is related to practical design at local details.
- **Find main parameter for full term fatigue analysis.** Sea states were chosen, assuming a joint-distribution of mean wind speed, W as the main parameter, while the expected significant wave height and spectral peak period given mean wind speed was used. A study should be carried out to identify the main parameter: W, H_s or T_p. A full long-term fatigue analysis and more time series should be carried out. Full long-term fatigue analysis is ideal for the fatigue analysis. The duration of the time series should also be longer to decrease the statistical uncertainty.
- **Apply different plate thickness** at different locations to optimize the design. A constant plate thickness of 30 mm was assumed. The thickness should be relative larger near the brace/chord intersection. The thickness should also be reduced to achieve a more reasonable design, since the fatigue life for brace 1 was conservative.

- **Parameter study for design optimization.** Check sensitivity to joint global stiffness, material thickness, brace positions, brace diameter, number/size of stiffeners, number of bulkheads. Check SCF sensitivity to small design changes. Chenyu Luan has also reported that the global joint design also was very sensitive to change.
- **Verify the global to local structure** method procedure to investigate that the joint is force balanced, and the importance of inertia effects.

Chapter 9

References

[ABS, 2005] (2005). GUIDANCE NOTES ON SPECTRAL-BASED FATIGUE ANALYSIS FOR FLOATING OFFSHORE STRUCTURES.

[Bard et al., 2012] Bard, J., Quesnel, L., and Hanssen (2012). HiPRWind. `http://www.hyperwind.eu/sites/default/files/HiPRWind_flyer.pdf`.

[Berge, 2006] Berge, S. (2006). *Fatigue and Fracture Design of Marine Structures II, Fatigue Design of Welded Structures*. Institutt for marin teknikk, IVT, NTNU.

[Brodtkorb et al., 2000] Brodtkorb, P., Johannesson, P., Lindgren, G., Rychlik, I., Rydén, J., and Sjö, E. (2000). WAFO - a Matlab toolbox for the analysis of random waves and loads. In *Proc. 10'th Int. Offshore and Polar Eng. Conf., ISOPE, Seattle, USA*, volume 3, pages 343–350.

[DeepC, 2010] DeepC (2010). *DeepC User Manual - Deep water coupled floater motion analysis*. DNV.

[DNV, 2000] DNV (2000). Fatigue Reliability of Old Semi-Submersibles. DNV HSE Health and Safety Executive.

[DNV-RP-C203, 2010] DNV-RP-C203 (2010). DNV-RP-C203, FATIGUE DESIGN OF OFFSHORE STEEL STRUCTURES.

[European Wind Energy Association, 2010] European Wind Energy Association (2010). Wind energy factsheets.

[Fricke, 2001] Fricke, W. (2001). Recommended Hot Spot Analysis Procedure for Structural Details of FPSOs and Ships Based on Round-Robin FE Analyses. volume VoL IV, pages pp. 89–96.

[GeniE, 2010] GeniE (2010). *GeniE User Manual - MODELLING OF PLATE/SHELL STRUCTURES*. DNV, 3. edition.

[HydroD, 2011] HydroD (2011). *HydroD - Wave Load & Stability Analysis of Fixed and Floating Structures*. Det Norske Veritas.

[IEC61400-1, 2005] IEC61400-1 (2005). NEK IEC 61400-1, Norwegian Electrotechinal Standard, Wind Turbines, Part 1: Design Requirements.

[IEC61400-3, 2009] IEC61400-3 (2009). NEK IEC 61400-3, Norwegian Electrotechinal Publication, Wind Turbines, Part 3: Design Requirements for Offshore Wind Turbines.

[Johannessen et al., 2001] Johannessen, K., Meling, T. S., and Haver, S. (2001). Joint Distribution for Wind and Waves in the Northern North Sea. *ISOPE*.

[Jonkman et al., 2009] Jonkman, J., Butterfield, S., Musial, W., and Scott, G. (2009). Definition of a 5-MW Reference Wind Turbine for Offshore System Development. 1617 Cole Boulevard, Golden, Colorado.

[Langen and Sigbjornsson, 1979] Langen, I. and Sigbjornsson, R. (1979). *Dynamisk Analyse av Konstruksjoner*. TAPIR.

[Luan, 2010] Luan, C. (2010). Dynamic Response Analysis of a Semi-Submersible Concept.

[Lygren, 2010] Lygren, J. E. (2010). Dynamic Response Analysis of a Tension-Leg Platform Wind Turbine.

[Minsaas and Steen, 2008] Minsaas, K. and Steen, S. (2008). *Naval Hydrodynamics Foil Theory*. Department of Marine Technology.

[Moan, 2003] Moan, T. (2003). *Finite Element Modelling and Analysis of Marine Structures*. Institutt for marin teknikk, IVT, NTNU.

[Moan et al., 2011] Moan, T., Klinger, A., Key Personnel at CeSos, Researchers at CeSOS, Wold, S. B., and Donnelly, J. (2011). CeSOS Annual Report 2011. NTNU - The Norwegian University of Science and Technology.

[NORSOK-N-001, 2010] NORSOK-N-001 (2010). NORSOK STANDARD N-001, Integrity of offshore structures.

[NORSOK-N-005, 1997] NORSOK-N-005 (1997). NORSOK STANDARD N-005, Condition Monitoring of Loadbearing Structures.

[Næss et al., 1985] Næss, A. A., Andersson, H., Moan, T., Berge, S., and et al. (1985). *Fatigue Handbook*. Tapir, NTNU.

[PrinciplePower, 2012] PrinciplePower (2012). WindFloat. `http://www.principlepowerinc.com/products/windfloat.html`.

[Riflex, 2008] Riflex (2008). *RIFLEX Theory Manual*, v3.6 edition.

[Riflex, 2010] Riflex (2010). *RIFLEX User Manual*, v3.6 rev. 8 edition.

[Ørjan Fredheim, 2011] Ørjan Fredheim (2011). Dynamic Response Analysis of a Semi-Submersible.

[Robertson and Jonkman, 2011] Robertson, A. N. and Jonkman, J. M. (2011). Loads Analysis of Several Offshore Floating Wind Turbine Concepts. National Renewable Energy Laboratory, Golden, CO, USA.

[Roddier et al., 2011] Roddier, D., Peiffer, A., Aubault, A., and Weinstein, J. (2011). A GENERIC 5 MW WINDFLOAT FOR NUMERICAL TOOL VALIDATION & COMPARISON AGAINST A GENERIC SPAR. Rotterdam, The Netherlands. Proceedings of the ASME.

[Simo, 2009] Simo (2009). *SIMO Theory Manual*. Marintek, 2. edition.

[Simo, 2010] Simo (2010). *SIMO User Manual*. MARINTEK, rev. 3 edition.

[Solberg, 2010] Solberg, T. (2010). Dynamic Response Analysis of a Spar Type Floating Wind Turbine.

[Wadam, 2011] Wadam (2011). *WADAM Theory Manual - Wave Analysis by Diffraction and Morison Theory*. DNV, 3 edition.

[WAFO-group, 2000] WAFO-group (2000). *WAFO - A Matlab Toolbox for Analysis of Random Waves and Loads - A Tutorial*. Math. Stat., Center for Math. Sci., Lund Univ.

[Wirsching et al., 1995] Wirsching, P. H., Paez, T. L., and Ortiz, K. (1995). *Random Vibrations, Theory and Practice*. A Wiley-Interscience Publication, John Wiley & Sons, Inc.

Appendix A

Comments

Matlab scripts, input and output-files and PATRAN-models were uploaded at DAIM. The ABAQUS databases were not uploaded.

Appendix B

SESAM

B.1 GeniE

GeniE is a Finite Element Modelling (FEM) program, used to define the geometry of a structure, and to create a panel model. The geometry is meshed to create a panel model, where each element represent a panel, and all panels together describe the entire wet surface. The panel model is exported to a T*.FEM-file.

More info about GeniE can be found in [GeniE, 2010].

B.2 HydroD

HydroD is an application which computes hydrostatics, stability, wave loads and motion response for offshore structures. HydroD make use of the DNV version of WAMIT, called WADAM. Morison and 3D potential theory are used in the wave loads calculations. The incident waves are modelled using Airy's linear wave theory. The T*.FEM-file exported from GeniE is used as input to HydroD. HydroD calculates RAO's, exciting forces and moments, added mass matrix, hydrostatic stiffness matrix and the potential damping matrix.

More info about HydroD and Wadam can be found in [HydroD, 2011] and [Wadam, 2011].

B.3 DeepC

DeepC is a program used to model floating configurations attached to the seabed with mooring lines, tension legs, risers etc. DeepC is using SIMO and RIFLEX to

do the non-linear time domain finite element simulations. DeepC uses input from HydroD/WADAM (G*.SIF).

B.3.1 SIMO

is a program for simulation of motions and station keeping behaviour of complex systems of floating vessels. The simulation is done in the time-domain to account for non-linear effects, ([Langen and Sigbjornsson, 1979]).

The semi-submersible is modelled as a large volume rigid body with 6 degrees of freedom. The rigid body and the mooring lines are coupled. To describe the system, the equation of motion can be written as

$$M\ddot{x} + C\dot{x} + D_1\dot{x} + D_2 f(\dot{x}) + K(x)x = q(t, x, \dot{x}) \tag{B.1}$$

The differential equation of motion is solved in SIMO using the Newmark β-predictor-corrector method, and the retardation function, [Simo, 2009].

B.3.2 RIFLEX

Riflex is a software made for modelling of flexible risers, but is also well suited for other slender structures like mooring and pipe lines - and also semi-submersible bracing. The program is based on a non-linear finite element formulation and does simulations of forces and motions in the time-domain.

More info about DeepC, SIMO and RIFLEX can be found in [DeepC, 2010], [Simo, 2010], [Simo, 2009], [Riflex, 2008] and [Riflex, 2010].

Appendix C

Standard deviation of forces and moments and stress

Table C.1: Standard deviation of forces and moments, brace 2, plane 1

S.t. Sea state	Fx [N]	Fy [N]	Fz [N]	Mx [Nm]	My [Nm]	Mz [Nm]
2	6.93E+05	2.76E+02	7.97E+03	8.45E+02	6.37E+04	6.10E+03
3	6.89E+05	3.21E+02	9.20E+03	1.00E+03	6.29E+04	7.21E+03
4	8.31E+05	4.38E+02	1.39E+04	1.39E+03	7.49E+04	9.95E+03
5	8.79E+05	6.25E+02	1.77E+04	2.01E+03	7.69E+04	1.45E+04
6	9.18E+05	9.58E+02	1.96E+04	2.99E+03	7.87E+04	2.23E+04
7	1.33E+06	1.80E+03	2.70E+04	4.57E+03	1.16E+05	3.39E+04
8	1.31E+06	1.58E+03	2.69E+04	4.59E+03	1.14E+05	3.36E+04
9	9.38E+05	1.12E+03	1.84E+04	3.44E+03	8.06E+04	2.50E+04
10	7.69E+05	9.48E+02	1.25E+04	3.01E+03	6.46E+04	2.17E+04
11	7.32E+05	9.31E+02	1.02E+04	3.01E+03	6.01E+04	2.17E+04
12	8.84E+05	1.10E+03	1.35E+04	3.52E+03	7.46E+04	2.55E+04
13	1.27E+06	1.52E+03	2.30E+04	4.72E+03	1.12E+05	3.48E+04
14	2.50E+06	2.02E+03	6.88E+04	1.20E+03	2.05E+05	4.09E+03
15	1.55E+06	3.44E+00	3.01E+04	6.23E-01	1.40E+05	5.93E+00
16	1.17E+06	9.77E-02	1.91E+04	7.62E-02	9.98E+04	3.27E-01

Table C.2: Standard deviation of forces and moments, STD(brace 1 / brace 2), plane 1

S.t. Sea state	Fx [N]	Fy [N]	Fz [N]	Mx [Nm]	My [Nm]	Mz [Nm]
2	1.2E-01	1.1E+00	6.8E-01	4.9E-01	1.2E+00	1.1E+00
3	1.2E-01	1.1E+00	5.9E-01	4.9E-01	1.2E+00	1.1E+00
4	1.2E-01	1.2E+00	4.8E-01	5.1E-01	1.2E+00	1.1E+00
5	1.3E-01	1.2E+00	4.0E-01	5.3E-01	1.2E+00	1.1E+00
6	1.4E-01	1.2E+00	3.8E-01	5.7E-01	1.2E+00	1.1E+00
7	1.2E-01	1.2E+00	4.0E-01	5.0E-01	1.2E+00	1.1E+00
8	1.2E-01	1.1E+00	3.9E-01	4.3E-01	1.2E+00	1.1E+00
9	1.5E-01	1.2E+00	4.0E-01	4.3E-01	1.2E+00	1.1E+00
10	1.8E-01	1.1E+00	4.8E-01	4.3E-01	1.2E+00	1.1E+00
11	1.9E-01	1.1E+00	5.6E-01	4.3E-01	1.2E+00	1.1E+00
12	1.7E-01	1.1E+00	5.2E-01	4.6E-01	1.2E+00	1.1E+00
13	1.4E-01	1.1E+00	4.4E-01	5.0E-01	1.2E+00	1.1E+00
14	6.0E-01	8.7E-01	8.2E-01	2.1E+00	1.6E+00	8.5E+00
15	1.5E-01	1.0E+00	4.1E-01	2.5E+00	1.2E+00	1.1E+00
16	1.6E-01	1.2E+00	4.8E-01	1.4E+00	1.2E+00	1.2E+00

Brace 2 seem to be exposed to larger forces in x and z directions than Brace 2 by a factor of approximately 10 for all wind speeds. Fy, My and Mz are very similar for all wind speeds, although a peak is seen at sea state 14. The larger forces in x and z direction is explained by the inclination: more vertical forces are distributed to the inclined bracing, and thus both Fx and Fz are increased because of the inclination.